Supplement of Atmos. Chem. Phys., 18, 16173–16211, 2018
https://doi.org/10.5194/acp-18-16173-2018-supplement

Atmospheric Chemistry and Physics
Open Access
EGU

Supplement of

TM5-FASST: a global atmospheric source–receptor model for rapid impact analysis of emission changes on air quality and short-lived climate pollutants

Rita Van Dingenen et al.

Correspondence to: Rita Van Dingenen (rita.van-dingenen@ec.europa.eu)

Supplemental information to:

TM5-FASST: a global atmospheric source-receptor model for rapid impact analysis of emission changes on air quality and short-lived climate pollutants

Table of Contents

S1 Supplemental information to Section 1 - Introduction

Table S1 Overview (non-exhaustive) of earlier studies based on TM5-FASST

	Scope	$PM_{2.5}$ and O_3 exposure detail	Climate metrics	Health impact	Crop impact
Kuylenstierna et al., 2011; The World Bank, The International Cryosphere Climate Initiative, 2013	Near-Term Climate protection and Clean Air Benefits: Actions for Controlling Short-Lived Climate Forcers	5 world regions	yes*	External assessment, TM5-FASST used for attribution by measure, by region based on $PM_{2.5}$	yes
Brauer et al., 2012; Cohen et al., 2017; Lim et al., 2012	Air pollution exposure assessment for Global Burden of Disease	Grid maps	no	External assessment based on TM5-FASST $PM_{2.5}$ and O_3 grid maps	no
Rao et al., 2016	A multi-model assessment of the co-benefits of climate mitigation for global air quality	Grid maps and World regions	no	Population exposure to $PM_{2.5}$ limit levels	no
Crippa et al., 2016	Retrospective analysis of European air quality policies versus hypothetical non-action	World regions	no	Change in statistical life expectancy	yes
OECD, 2016	The Economic Consequences of Air Pollution	Grid maps and World regions	no	External assessment based on TM5-FASST $PM_{2.5}$ and O_3 grid maps	yes
UNEP and CCAC, 2016	Integrated Assessment of Short-Lived Climate Pollutants for Latin America and the Caribbean	Grid maps	yes*	yes	yes
van Zelm et al., 2016	Regionalized characterisation factors for Life Cycle Analysis based on TM5-FASST source-receptors	FASST regions	no	yes	yes
Rao et al., 2017	Future air pollution in the Shared Socio-economic Pathways	Grid maps and World regions	no	Population exposure to $PM_{2.5}$ limit levels	No
Kitous et al., 2017	Global Energy and Climate Outlook 2017: How climate policies improve air quality	Grid maps and World regions	no	External based on TM5-FASST $PM_{2.5}$ and O_3 grid maps	yes

* In the 2 assessments where climate metrics were evaluated, the BC forcing was adjusted with a correction factor 3.6 relative to the default FASST BC forcing (see main text)

S2 Supplemental information to Section 2.1 –The native TM5 model

S2.1 Features of the native TM5 model

TM5-CTM is an off-line global transport and chemistry model (Huijnen et al., 2010; Krol et al., 2005) that mainly uses the ECMWF operational or re-analysed meteorological data. In this study the operational 12-hour IFS forecast product for the year 2001 has been utilized. We used the year 2000 of the 0.5x0.5 degree historical gridded anthropogenic emission data described by Lamarque et al. (2010) as the basis for our calculations. Components used were NO_x, NMVOC, NH_3, SO_2, OC, and BC, and gridding was done using RETRO and EDGAR-HYDE database. The choice for this reference emission dataset was motivated by the fact that this dataset was widely used as the 'handshake' between past- and future emission inventories in the activities informing the IPCC AR5 process.

Large scale biomass burning emissions of BC and POM are from (van der Werf et al., 2004); Organic aerosols are assumed to be emitted as primary following Dentener et al., (2006); dust and sea salt emission schemes are also from Dentener et al., (2006).

Model calculations were performed for 1 calendar year, with a spin-up of 6 months for the base-simulations, and 1 month for the perturbation simulations, justified by the fact that the perturbations were performed for components with lifetimes of hours to a few days (no simulations for CO and CH_4). TM5-CTM has a spatial global resolution of 6°×4° and a two-way zooming algorithm that allows regions (e.g. Europe, N. America, Africa, and Asia) to be resolved at a finer resolution of 1°×1°. To smooth the transition between the global 6°×4° region and the regional 1°×1° domain, a domain with a 3°×2° resolution has been added. The TM5 version used here has a vertical resolution of 25 layers, defined in a hybrid sigma-pressure coordinate system with a higher resolution in the boundary layer and around the tropopause. The height of the first layer is approximately 50 m.

TM5-CTM uses the first-moments "slopes" scheme for the advection calculations (Petersen et al., 1998; Russell and Lerner, 1981). The model transport has been extensively validated using ^{222}Rn and SF6 (Peters, 2004) and further validation was performed within the EVERGREEN Project (Bergamaschi et al., 2005).

Gas phase chemistry is calculated using the CBM-IV chemical mechanism (Gery et al., 1989a, 1989b) modified by Houweling et al. (1998), solved by means of the EBI method (Hertel et al., 1993). Dry deposition is calculated using the ECMWF surface characteristics and Wesely's resistance method (Ganzeveld and Lelieveld, 1995)

The inorganic aerosol compounds, sulphate (SO_4^{2-}), nitrate (NO_3^-) and ammonium (NH_4^+), are assumed internally mixed and in thermodynamical equilibrium, while black carbon (BC), particulate organic matter (POM), sea salt and dust are externally mixed. Sulphate, nitrate, ammonium, BC and POM are considered to be in the accumulation mode components and are considered only by mass. Sea salt and dust are described by two log-normal distributions, using two modes for each of the species: accumulation and coarse modes.

Wet deposition is the dominant removal process for most aerosols and therefore is a major source of uncertainty in aerosol modelling (Textor et al., 2006). Removal occurs in convective systems (convective precipitation) and in large-scale stratiform systems that are associated with weather fronts. The in-cloud removal rates, which depend on the precipitation rate are differentiated for convective and stratiform precipitation and are calculated following Guelle et al. (1998) and Jeuken et al. (2001). Aerosol below-cloud scavenging is parameterised according to Dana and Hales (1976).

The model results have been evaluated in model inter-comparison exercises (Textor et al., 2006), using in-situ, satellite and sun-photometer measurements (De Meij et al., 2006; Vignati et al., 2010), summarized in Table S2.1 below. We are aware of recent more accurate observational data have become available for the validation of the model since the validation studies listed in Table S2.1, in particular from satellite-based retrievals. However here we focus on the validation of FASST, using TM5 as a reference, and it is beyond the scope of this study to re-evaluate the TM5 model itself.

S2.2 Meteorological variability versus the use of a single meteorological year 2001

Although an in-depth quantification of the impact of meteorological variability on base concentrations and source-receptor matrices at climatological time scales (e.g. as in Andersson et al., 2007) was not feasible in the frame of this study, we evaluated for a limited ensemble of 5 meteorological years (2001 to 2005) the TM5 outcome at the model's coarsest resolution (6°x4°), using as input the same RCP year 2000 emission set. For 6 selected source regions (India, China, Europe, Germany, USA, Japan) the variability in the response to a -20% (SO_2 + NO_x + BC + POM) emission perturbation was evaluated as well. TM5 6°x4° concentration grid maps were re-gridded to 1°x1° and averaged over the FASST source regions to obtain regional area-weighted mean annual $PM_{2.5}$ and O_3 concentrations.

We find that the standard deviation on the regional pollutant concentrations for the 5-year ensemble varies between 1 and 23% for $PM_{2.5}$ (median value: 9%, see Fig. S2.2a) and between 0.4 and 4% for O_3 (median value: 2%, see Fig. S2.2b). The high variability for the European regions (in particular for $PM_{2.5}$) is partly linked to the smaller size of the defined source regions (the European Union is composed of 15 FASST source regions, while e.g. the USA, Brazil and China are represented by one single large region which tends to smooth out inter-annual variations), and partly due to the non-typical year 2003. The variability in annual mean ozone is much lower, due to its longer life-time and lower sensitivity to wet deposition. Excluding year 2003 from the ensemble results in a lower $PM_{2.5}$ variability over Europe – in particular for Great Britain (Fig. S2.2a). In this case, the relative standard deviation (over the 4 year ensemble) stays within 10% for 50 out of all FASST regions (median: 7%). Excluding 2003 does not significantly affect the O_3 inter-annual variability (Fig. 2.2b).

Regarding the representativeness of year 2001 in terms of absolute concentrations, Fig. S2.3 shows that in virtually all regions, the year 2001 $PM_{2.5}$ concentrations are lower than the 5-year ensemble mean with a median value of -10% for $PM_{2.5}$ and -1.6% for O_3. Excluding the year 2003, the $PM_{2.5}$ median bias between year 2001 and the 4-year average is -8% (-1.5% for O_3).

Inter-annual meteorological variability can also affect the emission response sensitivity within the source region as well as the long-range transport of pollutants between regions. Figure S2.4 shows for 5 selected source regions for which perturbation experiments are available at 6x4 resolution for the 5 years, that the variability in the perturbation response is of the same (relative) magnitude as the variability in the absolute concentrations. Regarding long range transport, Fig. S2.5 illustrates for 3 receptor regions (Germany, USA, Japan) the contribution of NO_x, SO_2, BC and POM emissions inside and outside the receptor region to $PM_{2.5}$ concentrations inside the receptor region. Note that the perturbation experiment did not include NH_3 emission perturbations, therefore the 'Other' fraction includes all contributions from direct NH_3 emissions (inside as well as outside the receptor region), plus NO_x, SO_2, BC and POM contributions not included in the displayed source regions. We

find that the relative share of the contributing source regions displays a lower inter-annual variability (typically between 2 and 6%) than the absolute contributions.

We note here that the ECMWF operational analysis used in this study is not ideal for assessing inter-annual variability, since the model system has changed during this period. More ideal would have been using re-analysis data, which is based on the same model and set-of assimilated data. Therefore, we consider the calculations above as an upper-limit estimate of inter-annual variability on source-receptor relationships.

S2.3 Impact of grid resolution on concentrations and source-receptor coefficients

The finer the model grid resolution, the better population exposure estimates can be obtained, however in practice model resolution is constrained by computational speed. Previous studies have evaluated the impact of grid resolution on modelled pollutant concentrations (Fenech et al., 2018; Li et al., 2016; Punger and West, 2013; Wild and Prather, 2006) .

The impact on population exposure of moving from coarse to fine grid resolution in TM5 is illustrated in Fig. S2.6 for all FASST regions. In particular population-weighted $PM_{2.5}$ (Fig S2.6a) is sensitive to the grid resolution and the impact of increasing resolution is highest for small regions and for regions with large coastal lines where a coarse grid resolution may include large portions of non-populated low-concentration ocean area. Extreme examples are Chile, the Philippines and Japan where passing from 6°x4° to 1°x1° results in an increase in population-weighted anthropogenic $PM_{2.5}$ with 400%, 100% and 110%, respectively, and passing from 3°x2° to 1°x1° with 147%, 41% and 60% respectively. For other countries the increase is more commonly in the order of 20% (from 6°x4° to 1°x1°) and 10% (from 3°x2° to 1°x1°).

Ozone concentrations are less sensitive to the grid resolution, and the impact of increasing grid size is generally to decrease the population-weighted-mean concentration inside the source region because of titration chemistry prevailing in more polluted conditions – except in most of the Southern Hemispheric countries where grid resolution increases the O_3 concentration (Fig. S2.6b). The impact of resolution is highest for regions like Japan and the Korea region (-19% and -30% respectively passing from 6°x4° to 1°x1°). For most regions, passing from 6°x4° to 1°x1° reduces O_3 exposure with 10% or less. Fig 2.7 shows for selected source region the resulting region-mean concentration for $PM_{2.5}$ (Fig. 2.7a) and O_3 (Fig. 2.7b). For comparison, we also include the 1°x1° population-weighted $PM_{2.5}$ concentration in Fig. S2.7a, after applying the sub-grid parameterisation accounting for the urban increment, described in section S4.

The impact of grid resolution on the within-region source-receptor coefficients can be significant, in particular for polluted regions where the coarse resolution includes ocean surface, like Japan. Table S2.3 shows as an example within-region and long-range SR coefficients for receptor regions Germany, USA and Japan. A higher grid resolution increases the within-region response and decreases the contribution of long–range transport (where the contribution of China to nearby Japan behaves as a within-region perturbation). In the case of Japan, the within-region $PM_{2.5}$ response magnitude increases with a factor of 3, and the sign of the within-region O_3 response is even reversed when passing from 6°x4° to higher resolution. Also over the USA, the population-weighted within-region response sensitivity upon NO_x perturbation increases with a factor of 5. Further, we find that in titration regimes, the magnitude of the O_3 response to NO_x emissions increases with resolution (i.e. ozone increases more when NO_x is reduced using a fine resolution) while the in-region ozone response is reduced in

non-titration regimes (India and China, Fig. 2.7d). These indicative results are in line with more detailed studies (e.g. Wild and Prather, 2006).

Table S2.1: Overview of validation studies of the chemistry-transport model TM5

Reference	Validation type	Major outcome
Van Dingenen et al. (2009)	TM5 regionally averaged monthly O_3 and O_3 metrics against observations (year 2000)	TM5 monthly O_3 and crop metrics generally within variability of observations in US, SE-Asia and Europe (except over-estimated AOT40 in Central Europe), underestimating monthly O_3 observations in India and Africa.
De Meij et al. (2006)	Comparison of AOD with AEROCOM and MODIS over Europe.	Underestimated of AERONET AOD values by 20–30%, high spatial correlation with MODIS. Column aerosol small dependency on emission inventory.
van Noije et al., 2006	Comparison of ensemble of models to multiple NO_2 satellite derived columns.	High spatial correlation of all models (including TM5) with satellite observations- large difference in retrievals precluded identification of systematic differences. Underestimate of NO_x retrieval in China and South Africa.
Dentener et al., 2006	Evaluation of ensemble of models over world regions.	In regions with observations, TM5 was one of the best performing models due to relatively high resolution. In other regions, larger deviations- in line with other models.
Shindell et al., 2008	Evaluation of CO, ozone, BC and Sulfate transport over the Arctic	Poor representation of reactive tracer transport by all models to 4 Arctic stations.
Brauer et al., 2016	$PM_{2.5}$ from worldwide-database of urban and rural stations.	Similar performance of TM5 with regard to satellite derived surface PM

Table S2.2 Definition of TM5- FASST master zoom areas, source regions and individual countries included

MASTER 1°x1° ZOOM WINDOW		FASST SOURCE REGIONS IN ZOOM	COUNTRIES IN FASST REGION	COUNTRIES ISO CODE
AFR	AFRICA	EAF	Eastern Africa	CAF TCD SDN ETH SOM KEN UGA COD RWA TZA MDG ERI DJI COM BDI BID MUS REU SYC SDS SOL
		NOA	Morocco, Tunisia, Libya and Algeria	MAR DZA ESH TUN LBY SAH
		SAF	Southern Africa (excl. RSA)	AGO NAM ZMB BWA ZWE MOZ MWI MYT
		WAF	West Africa	COG CNQ GAB GIN CMR NGA NER MLI BEN GHA BFA CIV SEN GMB GNB SLE LBR STP CPV SHN TGO GNQ MRT
AUS	AUSTRALIA	AUS	Australia	AUS
		NZL	New Zealand	NZL
EAS	EAST ASIA	CHN	China, Hong Kong and Macao	CHN HKG MAC
		COR	South Korea	KOR
		JPN	Japan	JPN
		MON	Mongolia and North Korea	MNG PRK
		TWN	Taiwan	TWN

(continues on next page)

Table S2.2 Cont'd

MASTER 1°x1° ZOOM WINDOW		FASST SOURCE REGIONS IN ZOOM	COUNTRIES IN FASST REGION	COUNTRIES ISO CODE
MASTER 1°x1° ZOOM WINDOW		FASST SOURCE REGIONS IN ZOOM	COUNTRIES IN FASST REGION	COUNTRIES ISO CODE
EUR	EUROPE	AUT	Austria, Slovenia and Liechtenstein	AUT SVN LIE
		BGR	Bulgaria	BGR
		BLX	Belgium, Luxemburg and Netherlands	BEL LUX NLD
		CHE	Switzerland	CHE
		ESP	Spain and Portugal	ESP PRT GIB
		FIN	Finland	FIN
		FRA	France and Andorra	FRA AND
		GBR	Great Britain and Ireland	GBR IRL GGY IMN JEY
		GRC	Greece and Cyprus	GRC CYP
		HUN	Hungary	HUN
		ITA	Italy, Malta, San Marino and Monaco	ITA VAT SMR MCO MLT
		NOR	Norway, Iceland and Svalbard	NOR ISL SJM
		POL	Poland and Baltic states	POL EST LVA LTU
		RCEU	Serbia, Montenegro, Macedonia and Albania (Rest of Central Europe)	SCG MKD HRV BIH ALB SRB MNE
		RCZ	Czech Republic and Slovakia	CZE SVK
		GER	Germany	DEU
		ROM	Romania	ROU
		SWE	Sweden and Denmark	SWE DNK FRO

(continues on next page)

Table S2.2 Cont'd

MASTER 1°x1° ZOOM WINDOW		FASST SOURCE REGIONS IN ZOOM	COUNTRIES IN FASST REGION	COUNTRIES ISO CODE
MAM	CENTRAL AMERICA	MEX	Mexico	MEX
		RCAM	Central America and Caribbean	PAN NIC HND GTM SLV ANT KNA LCA VCT TTO TCA VIR BLZ AIA ATG ABW BHS BRB VGB CYM DMA CUB DOM GRD GLP HTI JAM MTQ MSR PRI CRI
MEA	MIDDLE EAST	EGY	Egypt	EGY
		GLF	Gulf states	BHR IRQ KWT OMN QAT SAU ARE YEM IRN
		MEME	Israel, Jordan, Lebanon, Palestine Territories and Syria (Near East)	ISR JOR PSE LBN SYR PSX
		TUR	Turkey	TUR
NAM	NORTH AMERICA	CAN	Canada and Greenland	CAN GRL
		USA	United States	USA SPM BMU

Table S2.2 Cont'd

MASTER 1°x1° ZOOM WINDOW		FASST SOURCE REGIONS IN ZOOM	COUNTRIES IN FASST REGION	COUNTRIES ISO CODE
MASTER 1°x1° ZOOM WINDOW		FASST SOURCE REGIONS IN ZOOM	COUNTRIES IN FASST REGION	COUNTRIES ISO CODE
RSA	SOUTH AFRICA	RSA	Republic of South Africa, Swaziland and Lesotho	ZAF SWZ LSO
RUS	FORMER SOVIET UNION	KAZ	Kazachstan	KAZ
		RIS	Rest of former Soviet Union	KGZ TKM UZB TJK
		RUE	Eastern part of Russia	RUE
		RUS	Russia, Armenia, Georgia and Azerbeijan	RUS ARM GEO AZE
		UKR	Ukraine, Belarus and Moldovia	BLR MDA UKR
SAM	SOUTH AMERICA	ARG	Argentina, Falklands and Uruguay	ARG FLK URY
		BRA	Brazil	BRA
		CHL	Chile	CHL
		RSAM	Rest South America	BOL COL ECU GUF GUY PER SUR VEN PRY PRA
SAS	SOUTH ASIA	NDE	India, Maldives and Sri Lanka	IND LKA MDV
		RSAS	Rest of South Asia	AFG BGD BTN NPL PAK
SEA	SOUTHEAST ASIA	IDN	Indonesia and East Timor	IDN TLS
		MYS	Malaysia, Singapore and Brunei	MYS SGP BRN
		PHL	Philippines	PHL
		RSEA	Cambodia, Laos and Myanmar	KHM LAO MMR
		THA	Thailand	THA
		VNM	Vietnam	VNM
PAC	PACIFIC	PAC	Pacific Islands and Papua New Guinea	FJI NCL SLB VUT FSM GUM KIR MHL NRU MNP PLW NFK TKL ASM COK PYF NIU PCN TON TUV WLF WSM PNG

Table S2.3 Population-weighted mean annual $PM_{2.5}$ and O_3 responses to a 20% emission reduction in (NO_x, SO_2, BC, POM) for TM5 6°x4° and 1°x1° model resolution for selected source and receptor regions

	$dPM_{2.5}$ (µg/m³)		dO_3 (ppb)	
	1°x1°	6°x4°	1°x1°	6°x4°
Source region:	Receptor region: Germany			
Europe	-1.4	-1.2	1.1	0.8
USA	-0.009	-0.013	-0.10	-0.12
China	-0.005	-0.005	-0.048	-0.052
Source region:	Receptor region: USA			
USA	-1.1	-0.8	1.0	0.2
China	-0.004	-0.005	-0.066	-0.068
Europe	0.000	-0.001	-0.013	-0.015
Source region:	Receptor region: Japan			
Japan	-1.3	-0.3	1.1	-0.3
USA	-0.001	-0.001	-0.066	-0.078
China	-0.18	-0.16	-0.26	-0.31
Europe	-0.003	-0.003	-0.030	-0.038

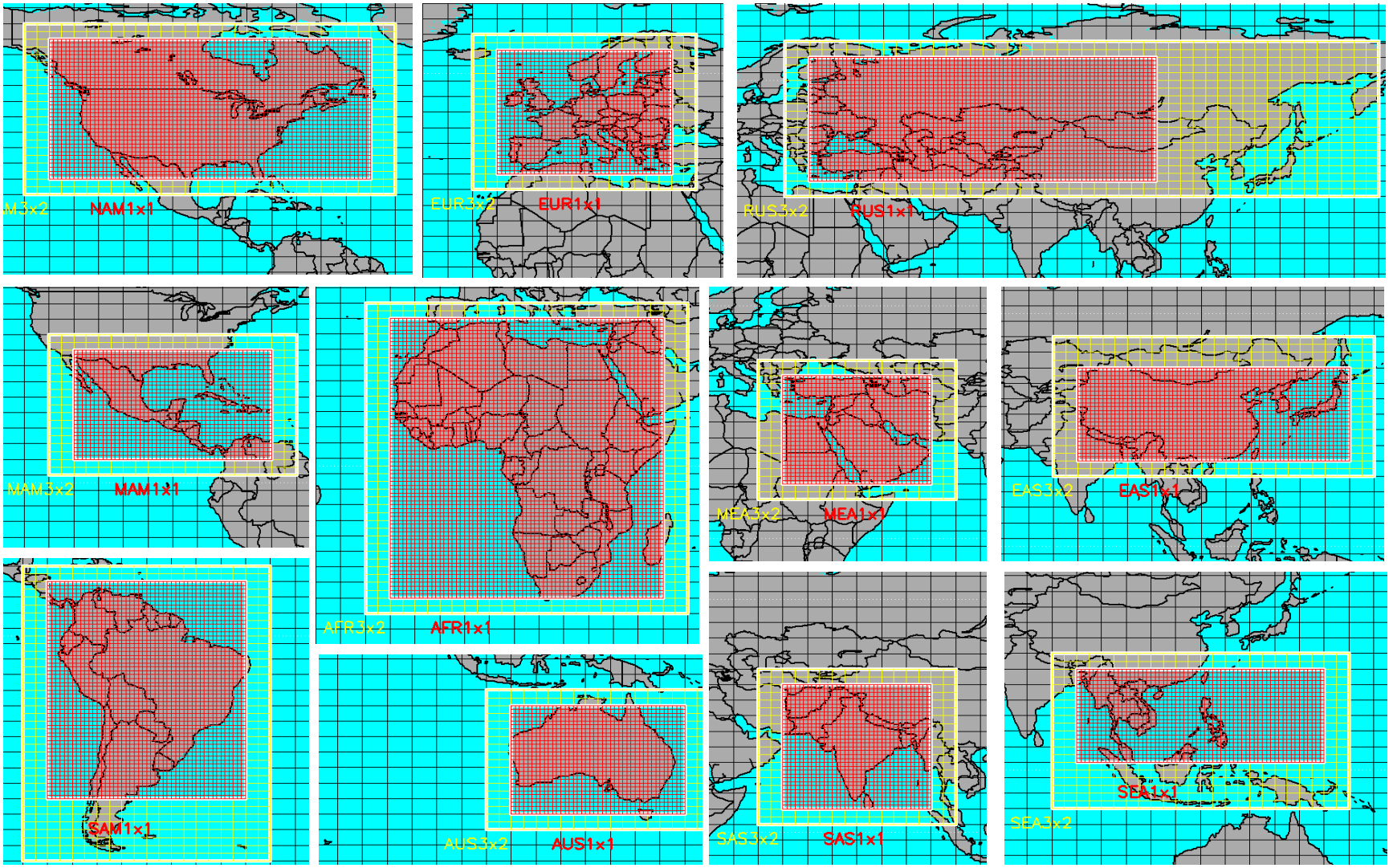

Figure S2.1 Definition of the high-resolution master zoom regions. Populated areas are covered with 1°x1° resolution, the remainder of the continents with 3°x2°, oceans with 6°x4°. Not shown: PAC , RSA

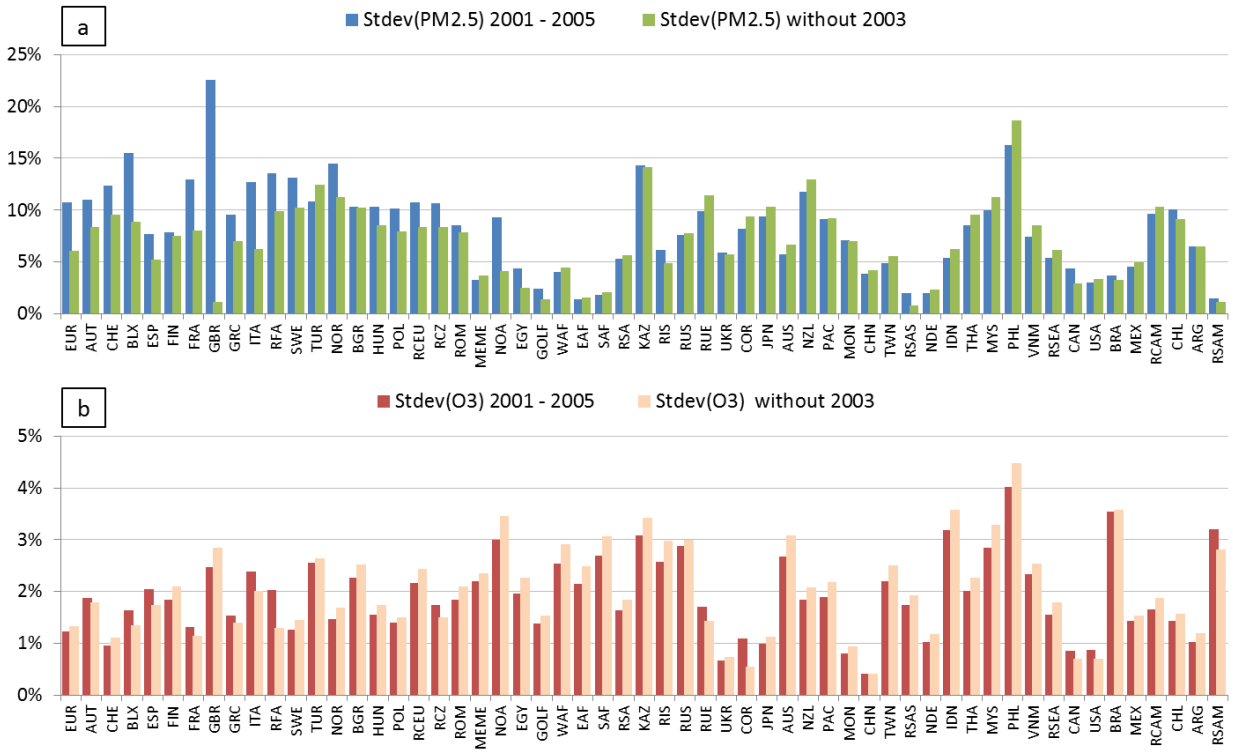

Figure S2.2: TM5 6°x4° regional annual mean $PM_{2.5}$ (upper panel) and ozone (lower panel) standard deviation for an ensemble of meteorological years, using RCP year 2000 emissions. Each panel shows the relative standard deviation (stdev/ensemble mean) for the 5 year ensemble (2001 – 2005) as well as for the 4 year ensemble, excluding the a-typical year 2003.

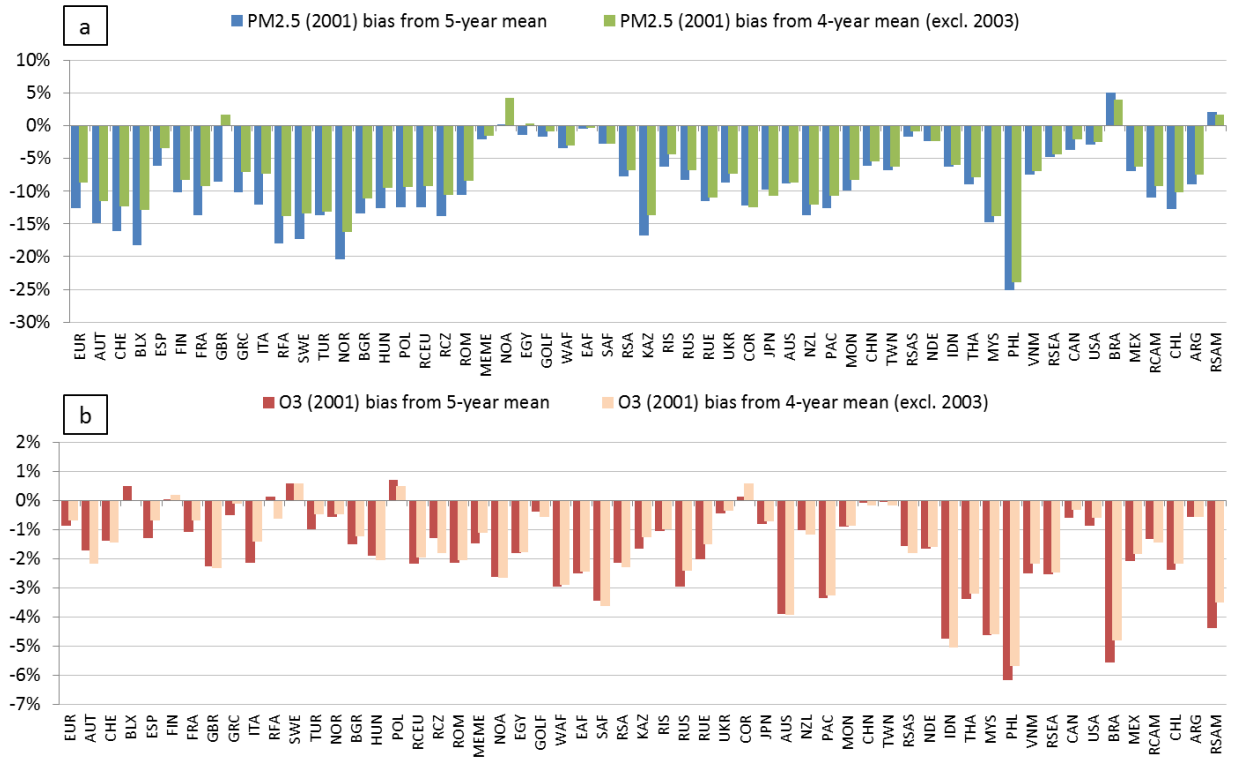

Figure S2.3: TM5 6°x4° regional annual mean $PM_{2.5}$ (upper panel) and ozone (lower panel) year 2001 bias versus an ensemble of meteorological years, using RCP year 2000 emissions. Each panel shows the relative deviation (year 2001/ensemble mean) for the 5 year ensemble (2001 – 2005) as well as for the 4 year ensemble, excluding the a-typical year 2003.

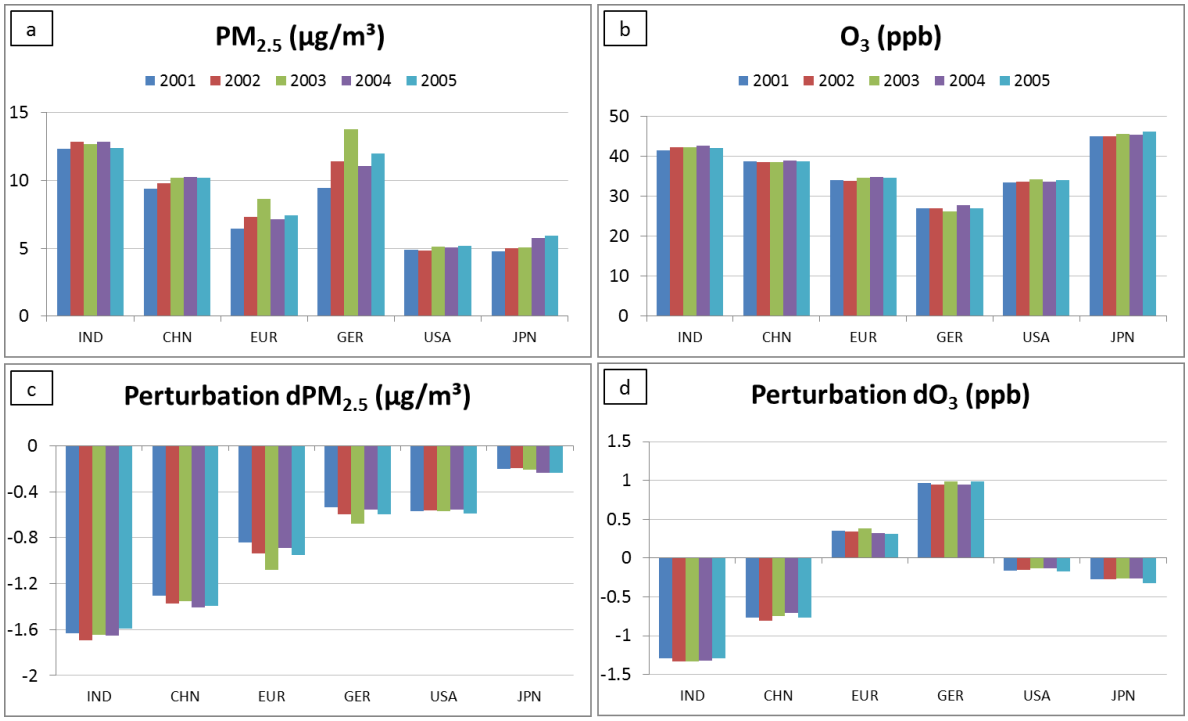

Figure S2.4: Regional annual mean (upper panels) and within-region response upon -20% emission perturbation of (NO_x + SO_2 + BC + POM) (lower panels) for $PM_{2.5}$ (a,c) and O_3 (b,d) for 5 consecutive meteorological years (2001 – 2005), from TM5 6°x4° resolution and RCP year 2000 emissions

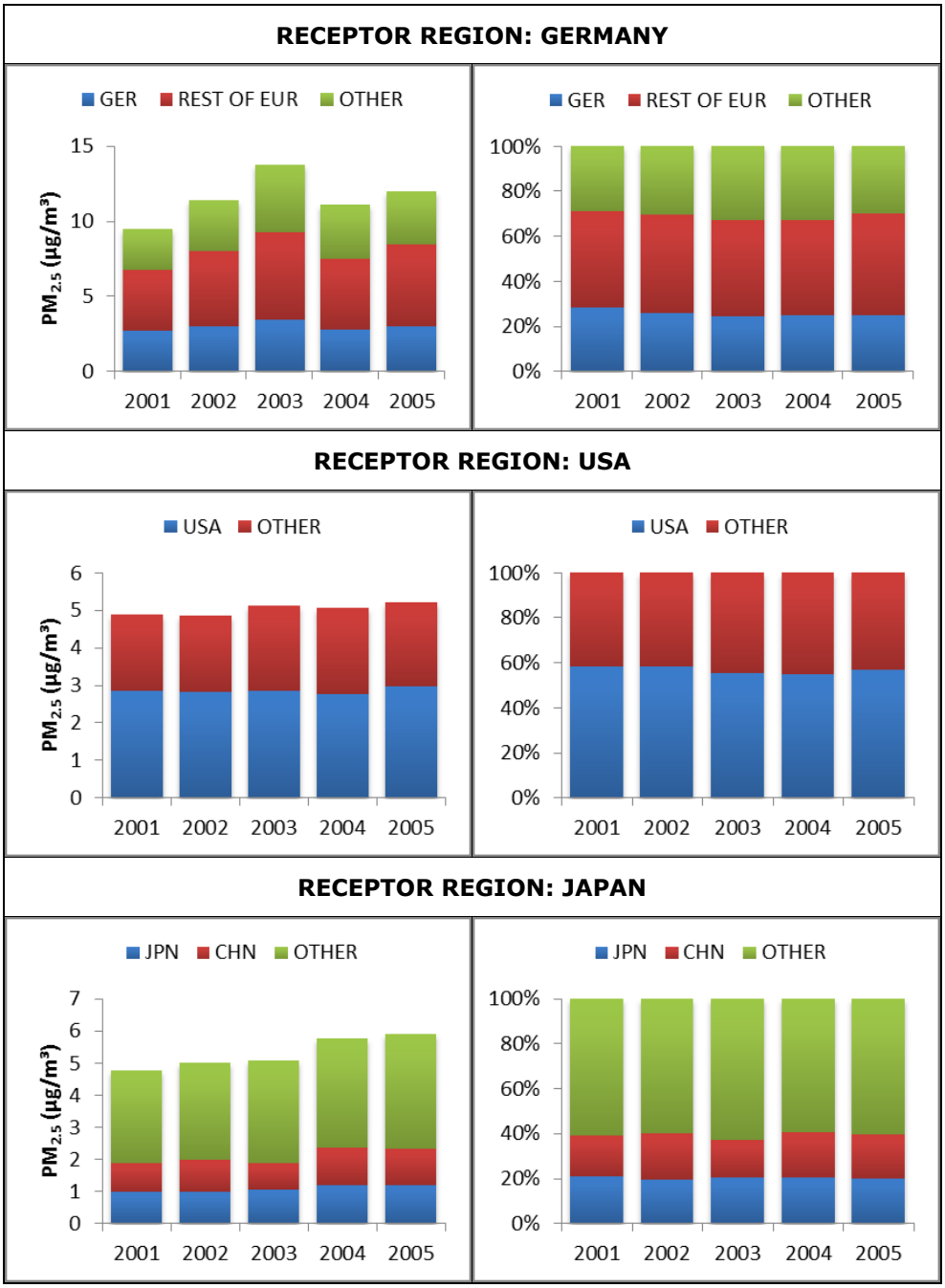

Figure S2.5: Inter-annual variability in local and long-range transported contributions of NO_x, SO_2, BC and POM from within to regional anthropogenic $PM_{2.5}$. Left: absolute concentrations; Right: relative shares. The blue section represents the contribution from emissions within the receptor region itself; the other sections are from major contributing external regions and the rest of the world. 'Other' includes rest of the world transported contributions from NO_x, SO_2, BC and POM as well the contribution from directly emitted NH_3 inside and outside the receptor region.

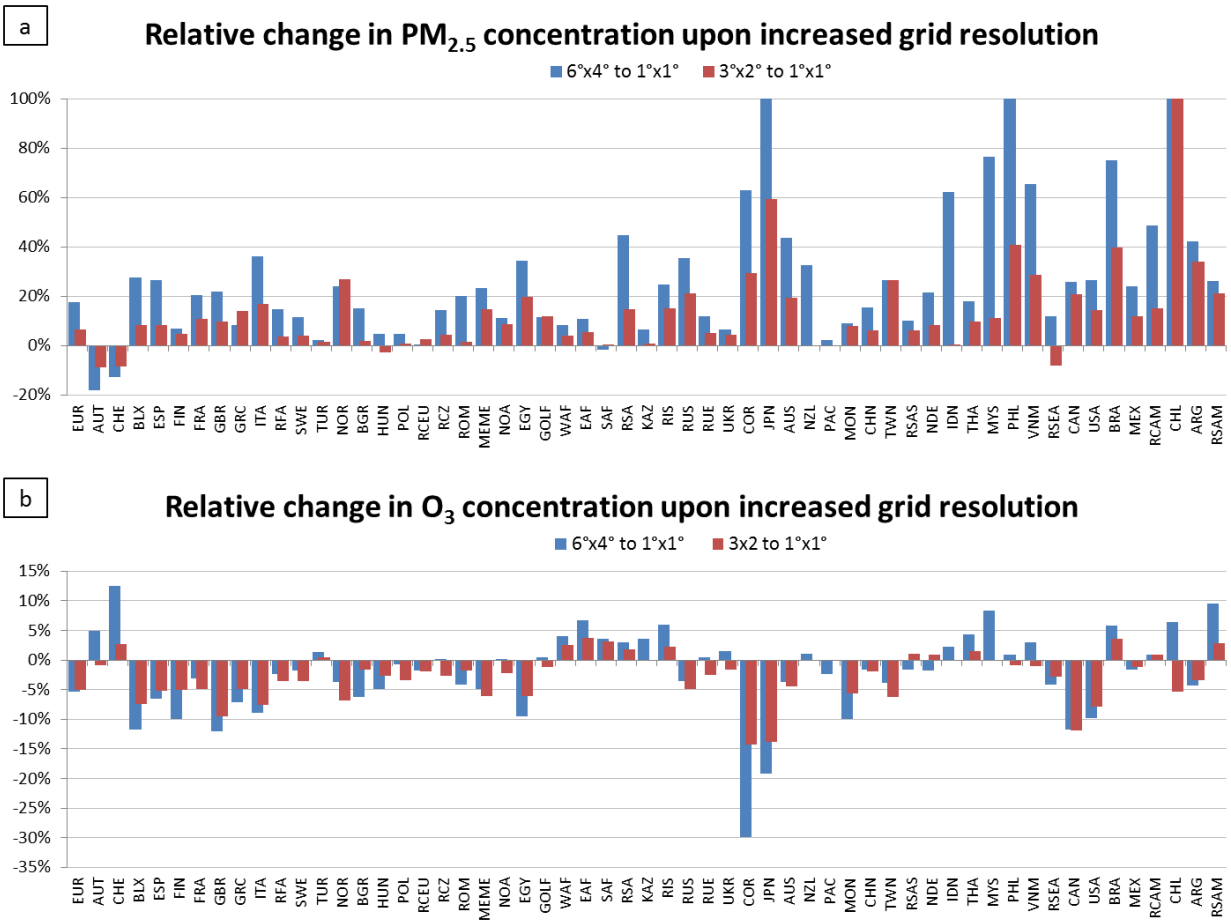

Figure S2.6: TM5 computed relative change in regional annual population-weighted mean $PM_{2.5}$ (a) and O_3 (b) concentrations when passing from coarse to fine grid resolution. Blue bars: $(C_{1x1}-C_{6x4})/C_{6x4}$ Red bars: $(C_{1x1}-C_{3x2})/C_{3x2}$

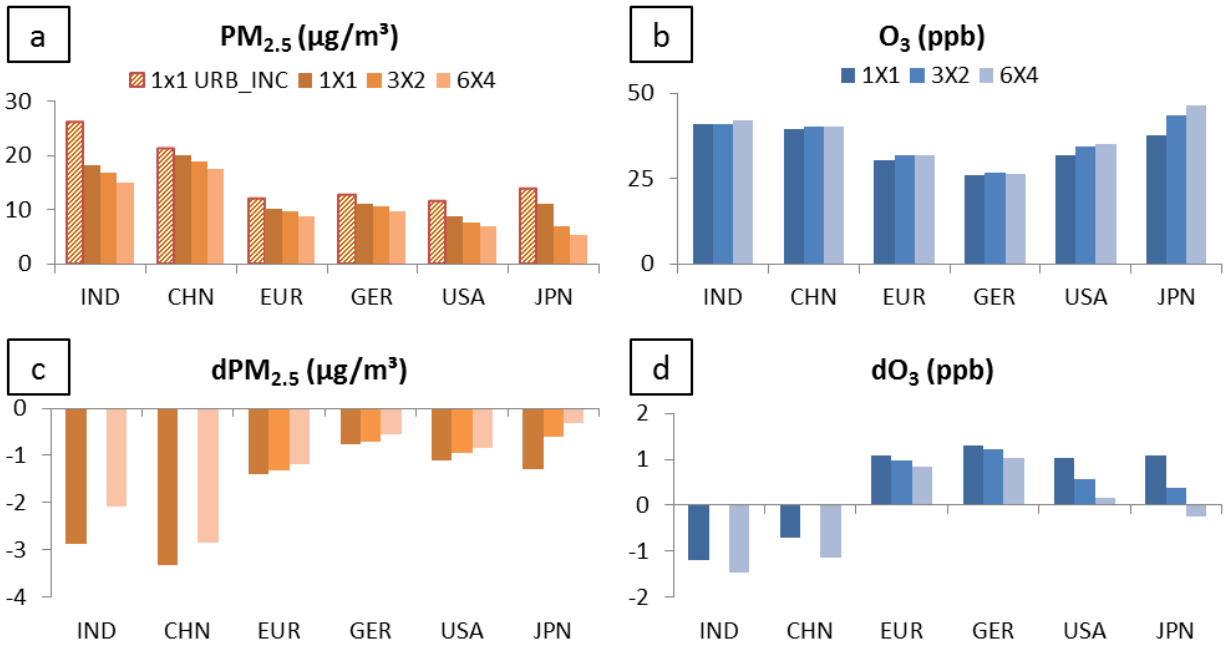

Figure S2.7: Population-weighted regional annual mean (upper panels) and within-region response upon -20% emission perturbation of (NO_x + SO_2 + BC + POM) (lower panels) for $PM_{2.5}$ (a,c) and O_3 (b,d) for the 3 TM5 grid resolutions (6°x4°, 3°x2° and 1°x1°, see Fig. S2.1). Panel (a) includes as well the 1°x1° 'urban incremented' $PM_{2.5}$ concentration, by applying the sub-grid parameterization described in section S4.1 of this SI. The 3°x2° perturbation experiments are not available for India (IND) and China (CHN).

S3 Supplemental information to Section 2.3 - Air pollutants source-receptor relations

S3.1 CH_4 – O_3 source-receptor relations from HTAP1 perturbation experiments:

CH_4 emissions lead to a change in CH4 concentrations with a perturbation response time of about 12 years. In order to avoid expensive transient computations, HTAP1 simulations SR1 and SR2 with prescribed fixed CH4 concentrations (1760 ppb and 1408 ppb, see Dentener et al., 2010) were used to establish CH4 – O_3 response sensitivities. Previous transient modeling studies have shown that a change in steady-state CH_4 abundance can be traced back to a sustained change in emissions, but the relation is not linear because an increase in CH_4 emissions removes an additional fraction of atmospheric OH (the major sink for CH_4) and prolongs the lifetime of CH_4 (Fiore et al., 2002, 2008; Prather et al., 2001).

In a steady-state situation, the CH4 concentration is the result of balanced sources and sinks. In the HTAP1 experiments, keeping all other emissions constant, the change in the amount of CH4 loss (mainly by OH oxidation with a lifetime of ca. 9 years, neglecting loss to soils and stratosphere with lifetimes of ca.160 and 120 years respectively (Prather et al., 2001)) under the prescribed change in CH4 abundance should therefore be balanced by an equal and opposite source which we consider as an "effective emission". The amount of CH4 oxidized by OH in one year being diagnosed by the model, the resulting difference between the reference and perturbation experiment of -77 Tg sets the balancing "effective" emission rate to 77Tg/yr, which is then used to normalize the resulting O_3 and O_3 metrics response to a CH4 emission change.

The same perturbation experiments also allow us to establish the CH4 self-feedback factor F describing the relation between a change in emission and the change in resulting steady-state concentration:

$$\frac{C_2}{C_1} = \left(\frac{E_2}{E_1}\right)^F \qquad \text{(S3.1)}$$

With CH4 concentrations prescribed, CH4 emissions were not included in the SR1 and SR2 experiments. The feedback factor F is derived from model-diagnosed respective CH4 burdens (B) and total lifetimes (LT) as follows (Fiore et al., 2009; Wild and Prather, 2000):

$$F=1/(1-s) \qquad \text{(S3.2)}$$

$$s = \partial\ln(LT) / \partial\ln(B) \qquad \text{(S3.3)}$$

TM5 returns s = 0.33 which can be compared to a range of values between 0.25-and 0.31 in IPCC-TAR (Prather et al., 2001, Table 4.2) , resulting in a TM5-inherent calculated feedback factor F=1.5. This factor can be used to estimate the corresponding SR2-SR1 change in CH_4 emission in a second way. From Eq. S3.1 we find that a 20% decrease in CH_4 abundance corresponds to a 14% decrease in total CH_4 emissions. Kirschke et al. (2013) estimate total CH_4 emissions in the 2000s in the range 550 – 680 Tg yr^{-1} from which we obtain an estimated emission change between the HTAP SR1 and SR2 experiments in the range 77 – 95 Tg yr^{-1}, in line with our steady-state loss-balancing approach.

Table S3 Overview of additional perturbation experiments for selected regions, in addition to the 20% perturbation for the standard source-receptor simulations (empty cells: not available)

			Emission perturbation magnitude relative to base simulation			
Source region	Simulation code	Compounds perturbed	-80%	-50%	+50%	+100%
EUR MASTER ZOOM REGION	P1'	$SO_2 + NO_x$	X			X
	P3'	NO_x	X	X	X	X
	P5'	NO_x+NMVOC	X			X
	P4'	NH_3+NMVOC	X			X
	P2'	SO_2	X			X
GERMANY	P1'	$SO_2 + NO_x$	X			X
	P3'	NO_x	X	X	X	X
	P4'	NH_3+NMVOC	X			X
	P2'	SO_2	X			X
USA	P1'	$SO_2 + NO_x$	X			X
	P3'	NO_x	X	X	X	X
	P5'	NO_x+NMVOC	X			X
	P4'	NH_3+NMVOC	X			X
	P2'	SO_2	X			X
CHINA	P3'	NO_x	X	X	X	X
	P5'	NO_x+NMVOC	X			X
	P4'	NH_3+NMVOC	X			X
	P2'	SO_2	X			X
JAPAN	P1'	$SO_2 + NO_x$	X			X
	P3'	NO_x	X	X	X	X
	P4'	NH_3+NMVOC	X			X
	P2'	SO_2	X			X
INDIA	P3'	NO_x	X	X	X	X
	P5'	NO_x+NMVOC	X			X
	P4'	NH_3+NMVOC	X			X
	P2'	SO_2	X			X

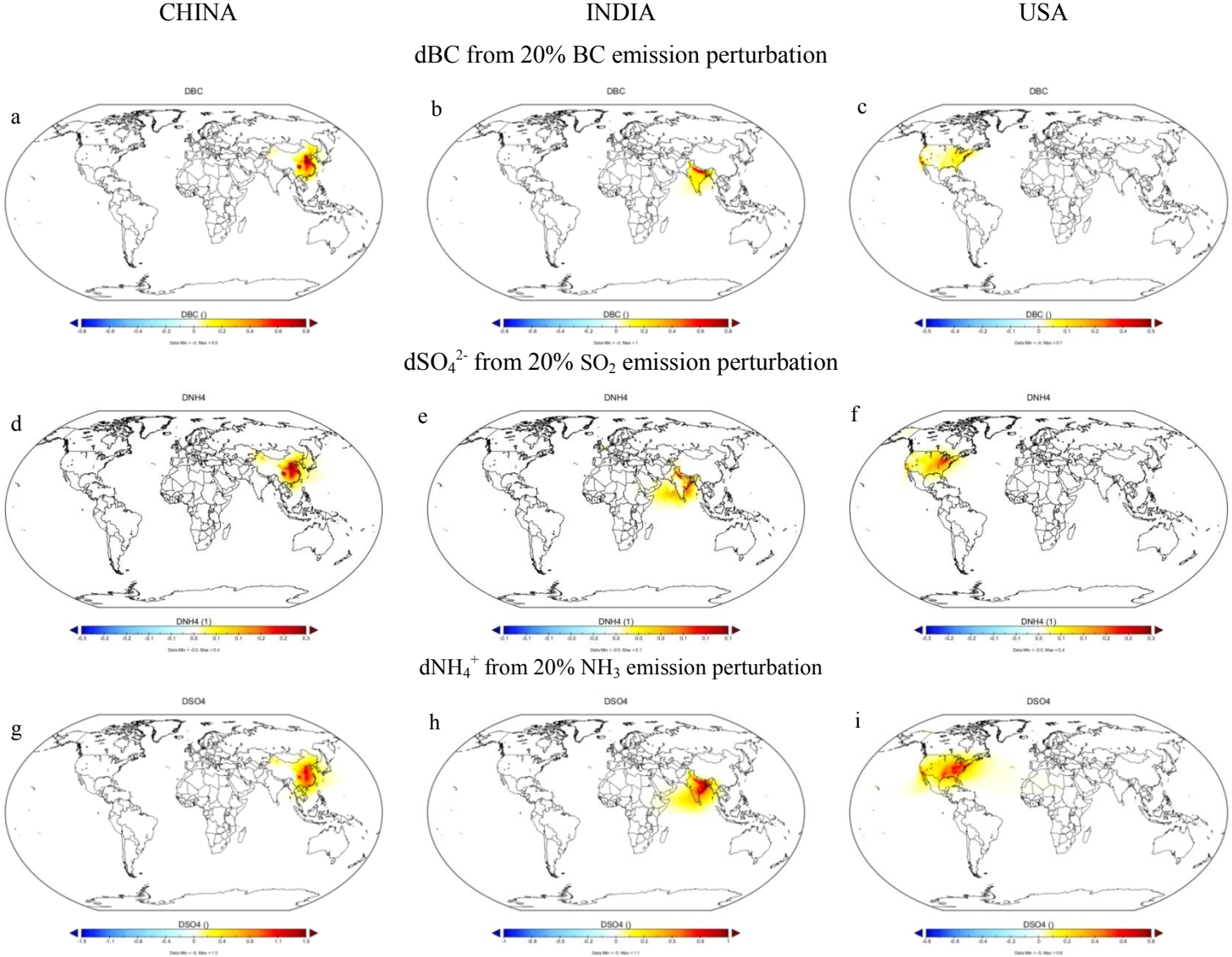

Figure S3.1 Decrease in annual mean surface BC (a to c), SO_4^{-2} (d to f) and NH_4^+ (g to i) response for a 20% decrease in year 2000 emissions of selected precursors from source regions China, India and USA respectively

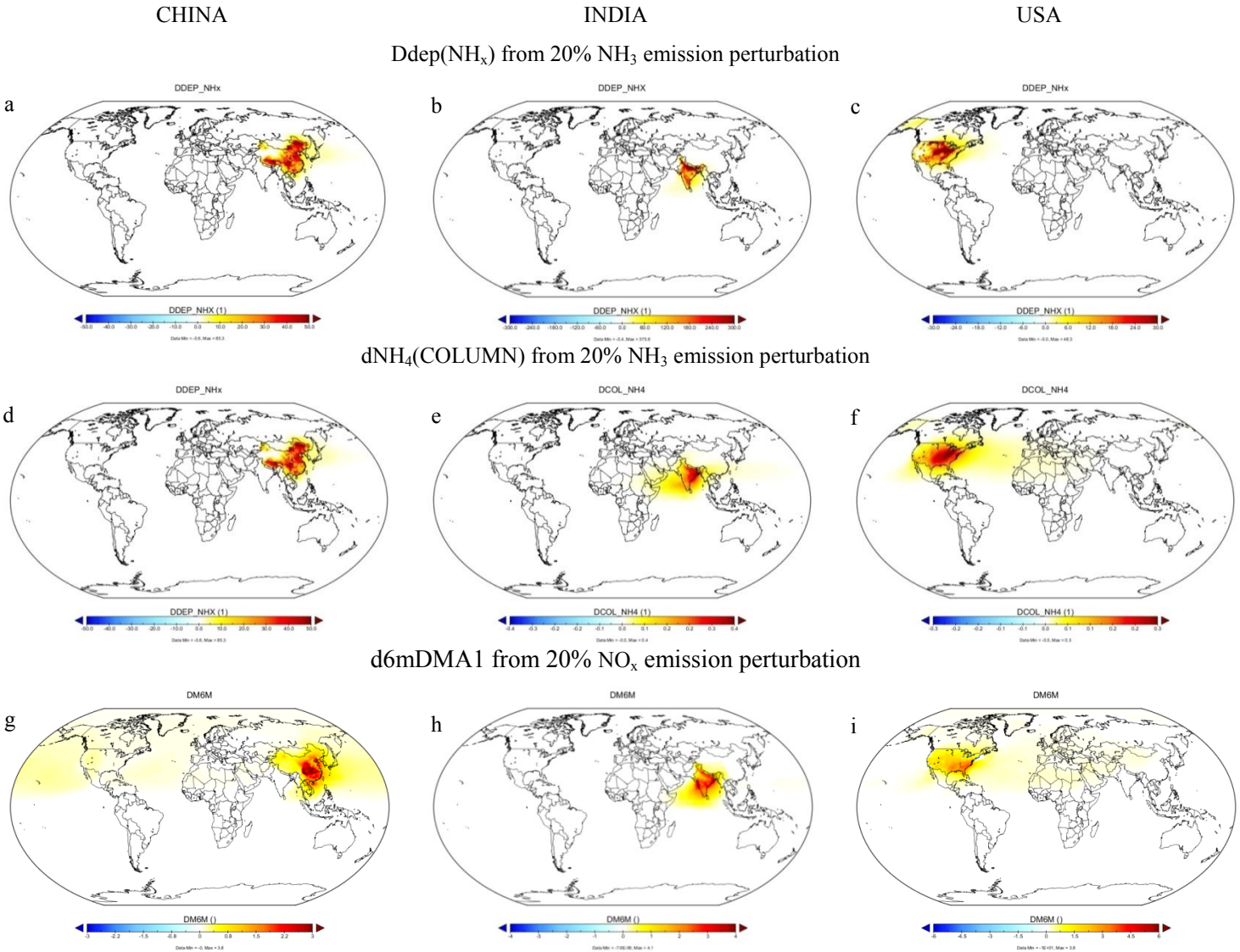

Figure S3.2 Decrease in annual deposition (a to c) , total column burden (d to f) and ozone exposure metric 6mDMA1 (g to i) response for a 20% decrease in year 2000 emissions of NH_3 (a to f) and NO_x (g to i) from source regions China, India and USA respectively

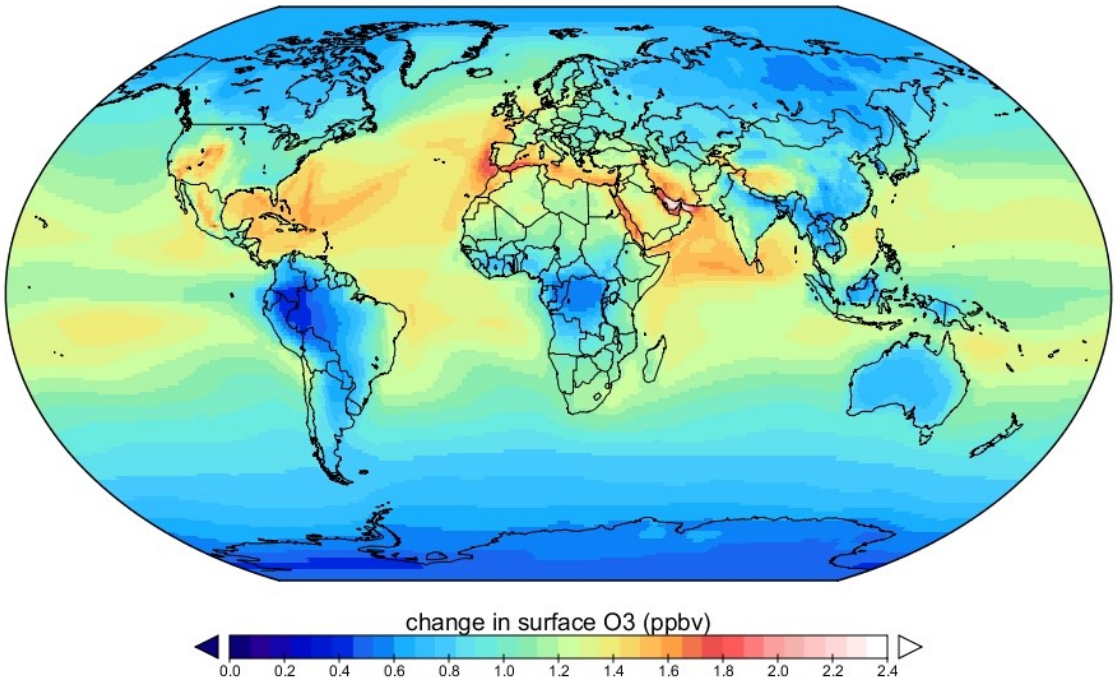

Figure S3.3 Decrease in annual mean surface O_3 for a 20% decrease in year 2000 CH_4 concentration, i.e. 1760 to 1408 ppb (TF-HTAP1 SR1-SR2 scenarios)

S4 Supplemental information to Section 2.4 – $PM_{2.5}$ adjustments in urban regions for health impact evaluation

S4.1 Methodology for the calculation of the urban increment adjustment factor for primary $PM_{2.5}$

Previous studies have developed methodologies to calculate the so-called urban increment for some European cities (Amann et al., 2007), but at present no globally applicable simple method is available. Therefore, within TM5-FASST a parameterization was developed to adjust the gridcell area-averaged $PM_{2.5}$ concentration to a more appropriate population-averaged urban background concentration, accounting for the sub-grid gradient in population distribution and pollutant concentrations. The urban increment correction will be applied to primary $PM_{2.5}$ only, as secondary $PM_{2.5}$ species (sulphate and nitrate) are formed from chemical conversion mechanisms over larger time and spatial scales, i.e. secondary $PM_{2.5}$ species are expected to be more homogeneously mixed over the native gridcell. It has to be noted that exposure to O_3 in urban areas will rather be overestimated using the gridcell average, because of O_3 titration inside traffic-dominated areas. Sub-grid effects on O_3 and NO_x are currently not taken into account in our approach.

In brief, the method relies on high spatial resolution population statistics from which the urban area fraction and urban population fraction inside each native 1°x1° gridcell are calculated. TM5-FASST has the choice of 2 families of population datasets, listed in Table S5.1.

The CIESIN Global Population of the World (GWPv3) set has the advantage of very high resolution, but lacks projected data beyond 2015[1]. The GEA - UN dataset (provided via personal communication by S. Rao, 2009) has a more limited spatial resolution but contains projections until 2100 in decadal steps from 2010 onwards. Further, the GEA - UN dataset contains already information on the urban population fraction, whereas the CIESIN dataset provides only count and density, and needs further assumptions and processing to derive the urban population.

Defining the urban area and population fraction:

The CIESIN dataset was used to label a sub-grid as 'urban' if the population density exceeds 600/km², and 'rural' otherwise. The urban area fraction (f_{UA}) is then the number of urban sub-grids per native gridcell divided by 576, the total number of sub-grids. The urban population fraction (f_{UP}) is defined as the fraction of the population within the 1°x1° gridcell which resides in the urban-flagged sub-grids.

The GEA population data set provides the urban population fraction g_{UP} within each subgridcell. For each 1°x1° gridcell, we define the urban area fraction f_{UA} and urban population fraction f_{UP} as follows:

$$f_{UA} = \frac{\sum_{i=1}^{64} g_{UP,i} A_i}{\sum_{i=1}^{64} A_i}$$

$$f_{UP} = \frac{\sum_{i=1}^{64} g_{UP,i} POP_i}{\sum_{i=1}^{64} POP_i}$$

Where i runs over all 64 population subgrids, with A_i the surface area and POP_i the population number in a subgridcell. The urban area fraction is estimated as the area-weighted average urban population fraction over the

[1] Since 2017 an update to GWPv4 is available with projection to 2020, accessible at https://earthdata.nasa.gov/.

64 sub-grids. This method is less accurate than the CIESIN method and tends to overestimate the urban area fraction and, hence, to smooth out emission and concentration gradients.

Urban increment parameterisation development

We first assume that only a fraction of emitted primary BC and POM is incremented in urban areas, namely only BC and POM emitted from residential and road transport sectors:

$PM_{2.5,inc} = SO_4 + NO_3 + NH_4 + (1\text{-}k_{BC})\ BC + (1\text{-}k_{POM})\ POM + INCR(k_{BC}\ BC + k_{POM}\ POM)$

with SO_4, NO_3, NH_3, BC and POM the 1°x1° gridcell average values resulting from TM5 or TM5-FASST; k_{BC} (k_{POM}) = fraction of (residential + transport) BC (POM) emissions in the total BC (POM) emissions within the 1°x1° gridcell respectively and *INCR* the urban increment factor.

We assume that black carbon anthropogenic emissions E_{BC} in the native gridcell with area A are divided between the urban and rural areas according to their corresponding population fraction. In this way fraction $f_{UP}.E_{BC}$ is emitted from area $f_{UA}.A$ and, to ensure mass conservation, the remaining fraction $(1- f_{UP})E_{BC}$ is emitted from area $(1- f_{UA})A$.

Assuming steady-state conditions and neglecting the incoming concentration of BC from neighbouring gridcells, the 1°x1° grid-average BC concentration can be written as: $C_{BC,1x1} = \frac{E_{BC}}{\lambda}$, with λ the ventilation factor. We assume that this definition of factor λ is also valid for the urban and rural parts of the gridcell, i.e., it is equivalent with the hypothesis that mixing layer height and wind speed are the same. Hence, the steady-state concentration in the urban sub-area can be written as: $C_{BC} = \frac{f_{UP}}{f_{UA}} \cdot \frac{E_{BC}}{\lambda}$ for the urban contribution and $C_{BC} = \frac{(1-f_{UP})}{(1-f_{UA})} \cdot \frac{E_{BC}}{\lambda}$ for the rural fraction. The ventilation factor λ, including an implicit correction factor for the non-zero background concentration in neighbouring cells, is obtained from the explicitly modelled gridcell concentration $C_{BC,TM5}$ as $\lambda = \frac{E_{BC}}{C_{BC,TM5}}$. Hence, the urban enhanced BC concentration within a gridcell is estimated from

$$C_{BC,URB} = \frac{f_{UP}}{f_{UA}} \cdot C_{BC,TM5} \qquad [4.1]$$

From the constraint that $f_{UA} \cdot C_{URB} + (1-f_{UA}) \cdot C_{RUR} = C_{TM5}$ the remaining rural fraction is given by

$$C_{BC,RUR} = \frac{(1-f_{UP})}{(1-f_{UA})} \cdot C_{BC,TM5} \qquad [4.2]$$

In order to avoid potential artificial spikes in urban concentrations when occasionally a very small fraction of the native gridcell contains a very large fraction of the population, empirical bounds are applied on the adjustment factors: rural primary BC and POM should not be lower than 0.5 times the TM5 grid average, and urban primary BC and POM should not exceed the rural concentration by a factor 5.

The population-weighted concentration is calculated as

$$C_{BC,TM5}^{pop} = f_{up} C_{BC,URB} + (1 - f_{up}) C_{BC,RUR} \qquad [4.3]$$

Substituting $C_{BC,URB}$ and $C_{BC,RUR}$ with equations 4.1 and 4.2, we obtain the population-weighted concentration expressed as a correction factor to be applied on the original 1°x1° gridcell mean concentration:

$$C^{pop}_{BC,TM5} = INCR \cdot C^{area}_{BC,TM5} \quad [4.4]$$

Where

$$INCR = \left[\frac{(f_{UP})^2}{f_{UA}} + \frac{(1-f_{UP})^2}{1-f_{UA}}\right] \quad [4.5]$$

The analogous process is done for primary anthropogenic organic carbon (POM). All secondary components (sulphates, nitrates) and primary natural PM (mineral dust, sea-salt) are assumed to be distributed uniformly over the native 1°x1° gridcell.

Obviously the highest correction factor is found when a large fraction of the population is concentrated in a small urban area inside the gridcell, generating a high sub-grid gradient. Conversely, large urban agglomerations where the urban population is covering most of the native gridcell do not lead to a large correction factor. In other words, the correction factor will be highest for spatially limited and isolated urban settlements within rural surroundings.

Table S4.2 gives regional population-weighted increment factors for BC and POM based on the baseline simulations performed with TM5 for the year 2000, i.e. using year 2000 population (CIESIN GWPv3) and RCP year 2000 gridded emissions.

S4.2 Comparison of TM5-FASST urban incremented $PM_{2.5}$ with observations

We use the year 2010 0.1°x0.1° resolution global satellite product from the Dalhousie University Atmospheric Composition Analysis group (available at http://fizz.phys.dal.ca/~atmos/martin/?page_id=140), which includes ground-based observations via a Geographically Weighted Regression, while mineral dust and seasalt have been removed, as described in van Donkelaar et al. (2016).

The high-resolution satellite data (SAT) contain the sub-grid population and concentration gradients that we try to simulate with parametrization described above. Creating a SAT population-weighted average at 1°x1° resolution makes it possible to evaluate the TM5-FASST native and urban-incremented 1°x1° output. We convert the 0.1°x0.1° SAT resolution to the 2.5'x2.5' resolution of the CIESIN (year 2000) population dataset i.e. 24 sub-grid cells for each 1°x1° cell, to be overlaid with the satellite dataset. FASST $PM_{2.5}$ 1°x1° grid maps are calculated from the HTAP2 year 2010 emission inventory, includig the GFED v3 biomass burning emission inventor (REF). To remain consistent with the SAT product, residual water at 35% has been included. Fig. S4.1 shows global gridmaps of FASST and SAT $PM_{2.5}$ with dust and sea salt removed), and with the sub-grid increment included in the FASST result.

We evaluate both FASST native and urban incremented 1°x1°grid cell concentrations, using the parameterization described in the previous section. We calculate the following 1°x1° grid mean concentrations from the 2.5'x2.5' SAT $PM_{2.5}$ and population sub-grid cells

$$SAT_{AREA} = \frac{1}{24}\sum_{i=1}^{24} PM_{2.5,i}$$

$$SAT_{POP} = \frac{\sum_{i=1}^{24} PM_{2.5,i} \cdot POP_i}{\sum_{i=1}^{24} POP_i}$$

SAT_{AREA} is the equivalent of the native FASST 1°x1° grid cell concentration, while SAT_{POP} represents the population-weighted mean 1°x1° concentration considering sub-grid gradients, to be compared with the FASST urban-incremented value, hereafter referred to as incremented concentrations. Regional and global mean population exposure to $PM_{2.5}$ (Table S4.3) is calculated using population-weighing on the 1°x1° grid cells, for both native (area-mean) and incremented concentrations.

Table S4.3and Fig. S4.2 show that for all regions, except for MEA (Mediterranean + Middle East), we find an over-all good agreement in regional mean $PM_{2.5}$ exposure between FASST and SAT, both for the native and incremented values. Figure S4.3 shows the absolute regional-mean increment in $PM_{2.5}$ exposure. We find that applying the FASST sub-grid parameterization increases global mean exposure with 1.4 μg m^{-3} (FASST), versus an increase of 1.1 from SAT, corresponding to a global population-weighted mean 5% increase for both methods. The FASST urban increment parameterization generates a regional-mean increase in $PM_{2.5}$ exposure from 0.6 μg/m³ (Latin America) to 3.4 μg/m³ (Russia and former Soviet Union states). In Europe and North-America the regional increase is around 1μg/m³. Except for East-Asia and Latin America, the regional FASST increment exceeds the SAT value. SAT regional increments range between 0.3 μg/m³ for Russia and former Soviet Union states and 1.8 μg/m³ in East-Asia. Although we don't find a direct correlation between the SAT and FASST computed increments, it is encouraging that without applying any fitting procedure, and using two completely different approaches, increments from FASST and SAT are in the same order of magnitude.

Figs. S4.4 (Europe and North-America), S4.5 (China and India) and S4.6 (Africa and Latin America) show a detailed grid-to-grid comparison for selected key regions between native and incremented FASST on the one hand and SAT_{POP} on the other. In general, individual grid cells are reproduced within a factor of two. The FASST increment parameterization slightly improves the correspondence with SAT_{POP} compared to the native data except for China where the native concentrations already exceed SAT_{POP}. Although an agreement at grid cell level is not the ambition of FASST, these results indicate that our crude approach is roughly performing, but that a more sophisticated approach in the urban increment may be warranted.

Finally, seen the large uncertainties on absolute $PM_{2.5}$ concentrations, one may wonder if the implementation of an urban increment parameterization is worth the effort. A FASST RCP2000 analysis of global mortalities with and without the generic urban increment factors (given in Table S4.2) shows that the global 5% increase in $PM_{2.5}$ exposure due to the urban increment accounts for an increase in total mortality numbers with 14% when dry $PM_{2.5}$ is considered, and with 11% when $PM_{2.5}$ is humidified at 35% RH. The difference is due to the threshold in the exposure-response functions (see section S5 in this SI). In areas where the native grid concentration is just below threshold, a small increase in $PM_{2.5}$ will have a strong response in mortalities while areas with native 1°x1° concentrations above the threshold will respond more proportional to the subgrid increment. Including hygroscopic growth at 35% from the onset reduces the cases where native resolution $PM_{2.5}$ remains below the threshold which explains the lower impact of the subgrid increment factor

Table S4.1 Population datasets properties

Name	Source	Metrics used	Resolution	Nr. of sub-grid per TM5 1°x1° gridcell	Years available
CIESIN[1]	University of Columbia	Population density Population count	2.5'x2.5'	24x24 sub-grids	1990, 2000, 2005
GEA[2]	United Nations population division	Population count Urban population count	7.5'x7.5'	8x8 sub-grids	2000, 2005, 2010, 2020, 2030, … , 2100

[1] CIESIN, 2005

[2] Riahi et al., 2012

Table S4.2 Regional urban increment factors for primary $PM_{2.5}$ from RCP emissions and population for the year 2000.

CNTRY	BC URB INCR FACTOR	POM URB INCR FACTOR	CNTRY	BC URB INCR FACTOR	POM URB INCR FACTOR
ESP	2.46	1.56	RUE	1.75	1.18
AUS	2.44	1.54	RFA	1.73	1.43
RUS	2.43	1.83	MYS	1.72	1.64
GRC	2.36	1.71	CHE	1.72	1.18
EGY	2.34	1.88	BRA	1.69	1.5
RIS	2.28	2.08	NOR	1.64	1.17
CHL	2.15	1.93	ARG	1.63	1.41
TWN	2.13	2.23	POL	1.61	1.33
FRA	2.12	1.36	RCAM	1.57	1.3
UKR	2.07	1.76	HUN	1.56	1.23
CAN	2.05	1.77	RCZ	1.49	1.22
GOLF	2.03	1.59	JPN	1.46	1.65
MEME	2.02	1.71	BGR	1.38	1.12
RSA	2	1.73	NOA	1.34	1.55
USA	2	1.65	TUR	1.34	1.2
NDE	2	1.75	ROM	1.3	1.15
ITA	2	1.49	WAF	1.2	1.15
NZL	1.98	1.5	MON	1.19	1.3
FIN	1.98	1.44	IDN	1.13	1.09
KAZ	1.94	1.49	RCEU	1.11	1.04
MEX	1.93	1.63	PHL	1.08	1.17
RSAS	1.91	1.72	SAF	1.07	1.03
AUT	1.9	1.3	EAF	1.06	1.04
COR	1.9	1.88	VNM	1	1.09
RSAM	1.89	1.51	RSEA	1	1.03
BLX	1.84	1.54	THA	1	1.05
GBR	1.82	1.51	CHN	1	1.14
SWE	1.78	1.3	PAC	1	1

Table S4.3 Year 2010 regional population-weighted mean $PM_{2.5}$ concentrations, based on 0.1°x0.1° satellite + ground based product (van Donkelaar et al., 2016), and FASST averages based on 1°x1° grid cell-mean (NATIVE) and urban incremented (URB-INCR).

MASTER	SAT_{AREA} (µg/m³)	FASST NATIVE (µg/m³)	SAT_{POP} (µg/m³)	FASST URB-INCR (µg/m³)	SAT incr. factor	FASST incr. factor
EUR	11.3	9.9	11.9	11.0	5%	11%
MEA	9.9	19.0	10.2	19.9	4%	5%
AFR	11.4	9.9	11.8	10.8	4%	9%
RUS	14.4	9.6	14.7	13.0	2%	35%
EAS	37.2	47.9	39.0	49.1	5%	3%
SAS+SEA	32.6	33.9	33.8	36.0	4%	6%
NAM	7.4	8.6	8.2	9.5	11%	10%
SAM	7.7	11.4	8.5	12.0	10%	5%
GLOBAL	23.9	27.6	25.0	29.0	5%	5%

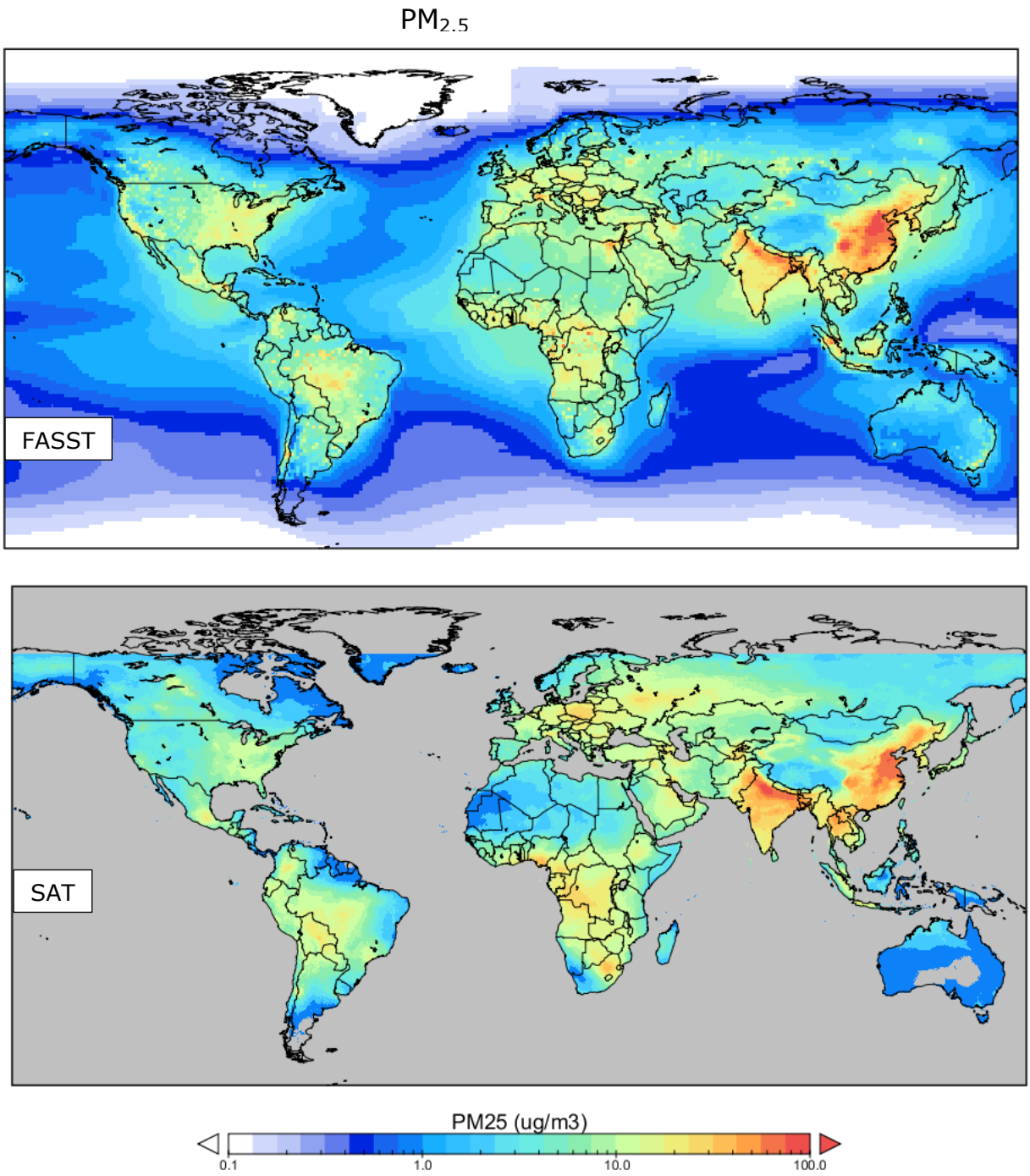

Figure S4.1 FASST(1°x1°) and SAT $PM_{2.5}$ (0.1°x0.1°) at 35% RH for the year 2010 (dust and seasalt removed). FASST based on HTAP2 year 2010 emission inventory + GFED v3 biomass burning emissions. SAT product (van Donkelaar et al., 2016). .

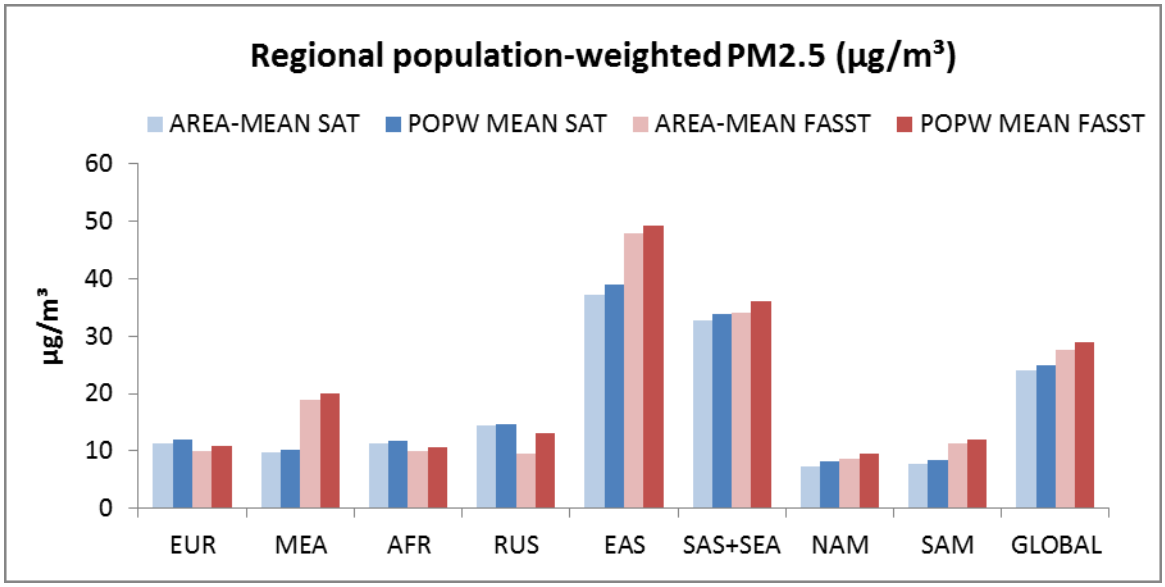

Figure S4.2 Population-weighted regional mean $PM_{2.5}$ from FASST and SAT, from native grid cell concentrations (AREA MEAN) and from incremented exposure accounting for sub-grid gradients (POPW MEAN).

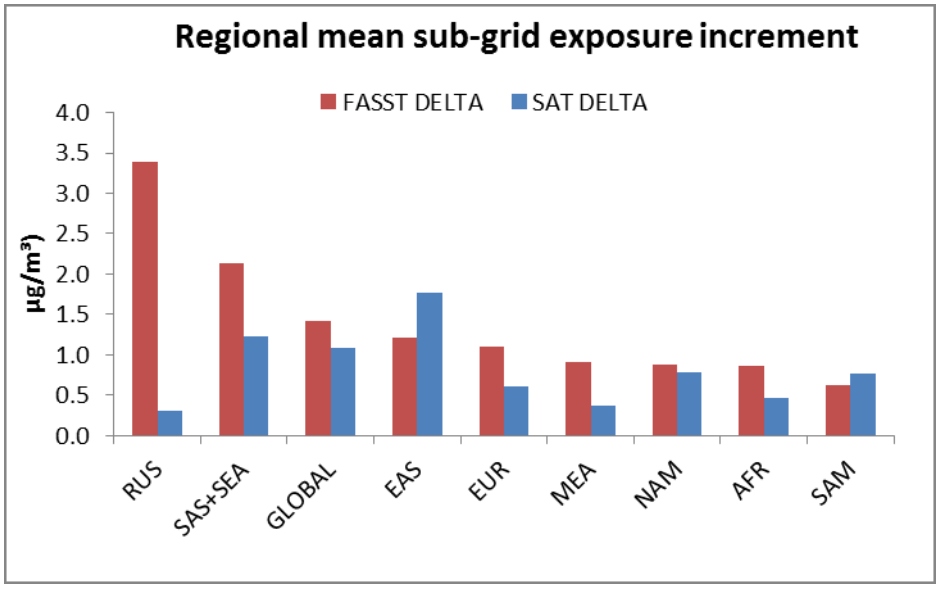

Figure S4.3 Population weighted regional mean difference between native and incremented $PM_{2.5}$ from FASST (red) and the SAT product (blue).

SAT: POP-weighted; FASST: Native grid cell **SAT: POP-weighted; FASST: Incremented**

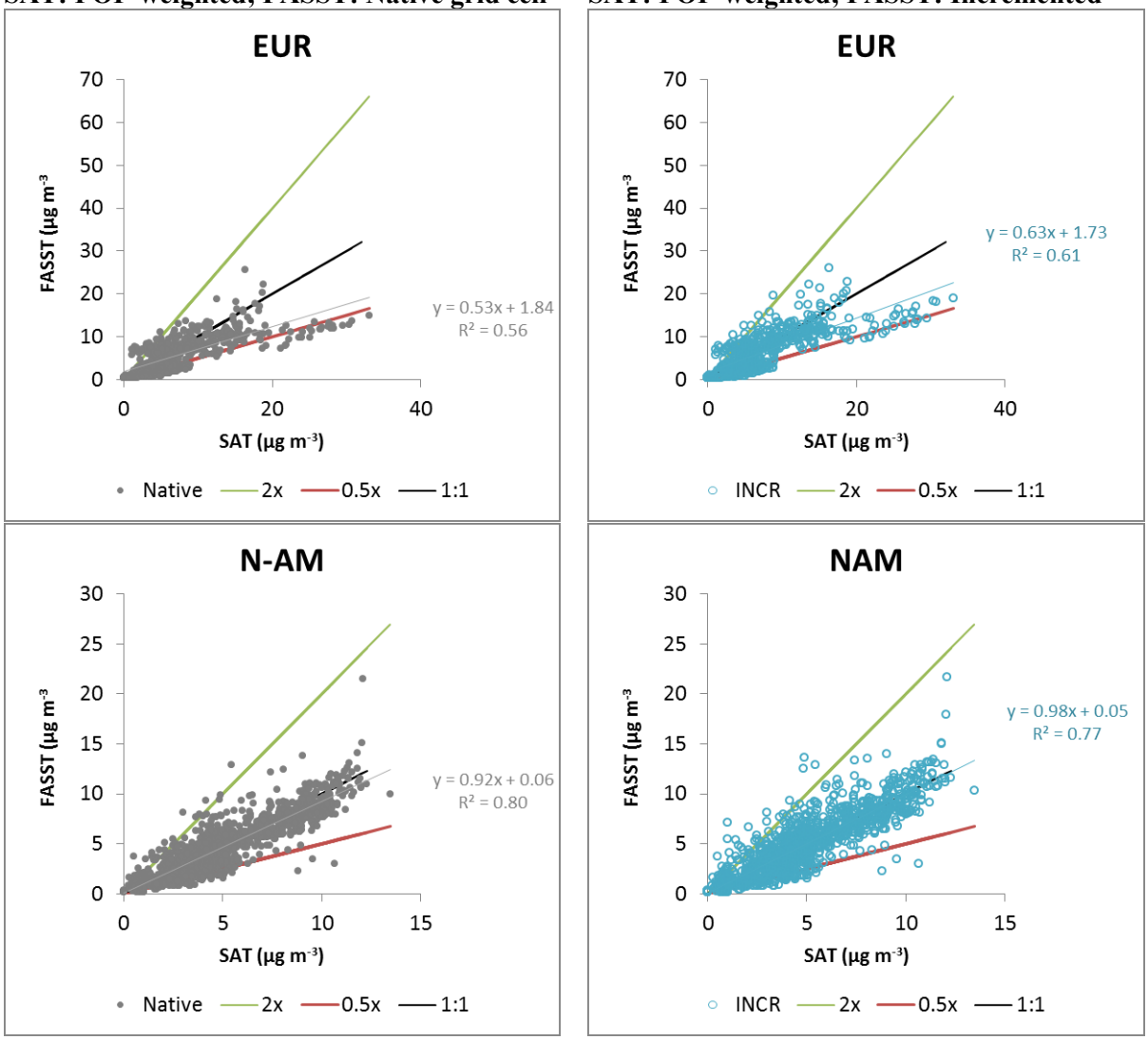

Figure S4.4 Scatterplot of single 1°x1° native (left panels) and urban incremented (right panels) FASST $PM_{2.5}$ concentrations versus satellite product. The latter was obtained as population-weighted mean of the original 0.1°x0.1° resolution, averaged to 1°x1°. Upper panels: European zoom region, lower panels: North-America

SAT: POP-weighted ;FASST: Native grid cell **SAT: POP-weighted; FASST: Incremented**

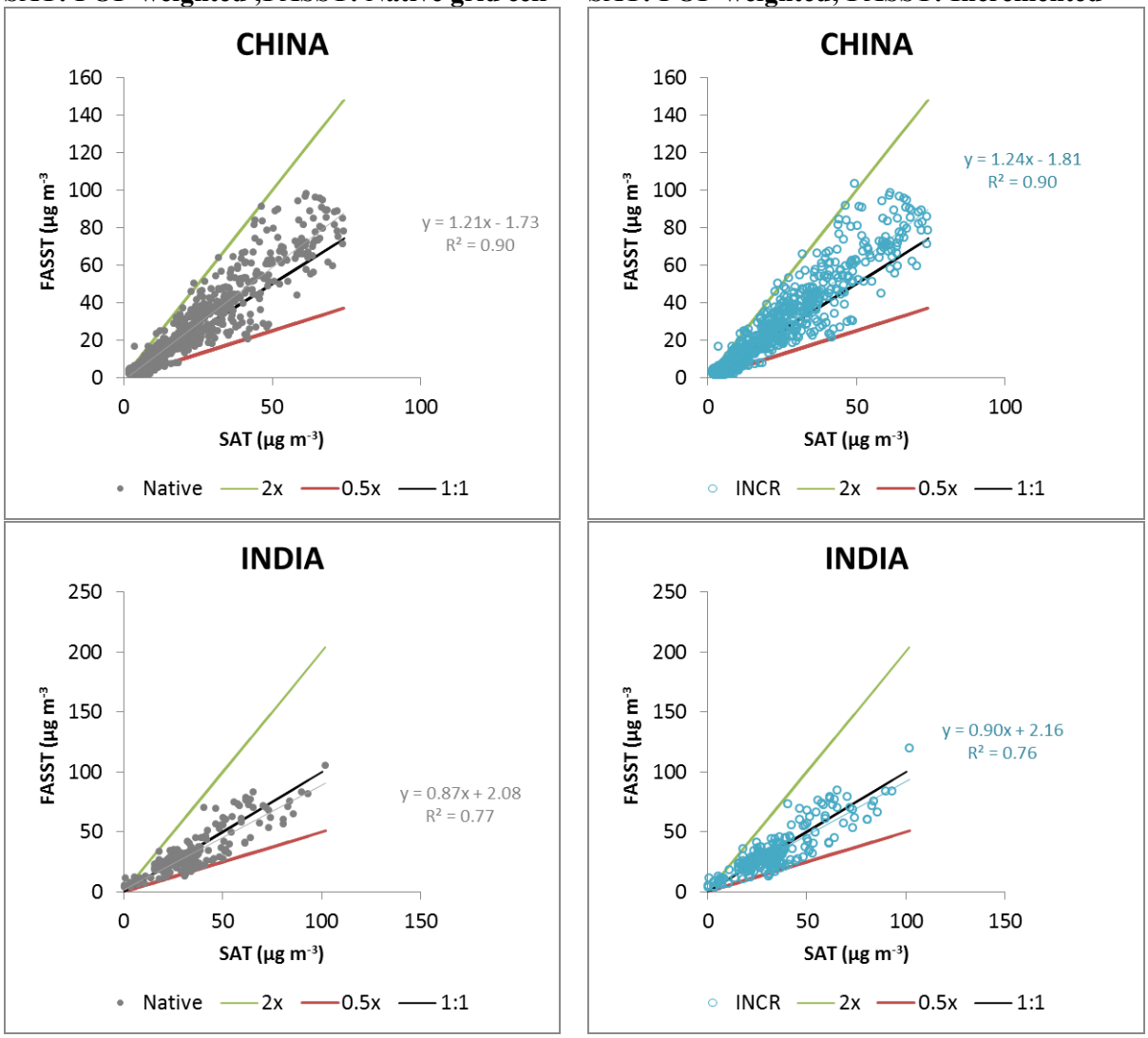

Figure S4.5 as Fig. S4.4, now for China and India

SAT: POP-weighted ;FASST: Native grid cell **SAT: POP-weighted; FASST: Incremented**

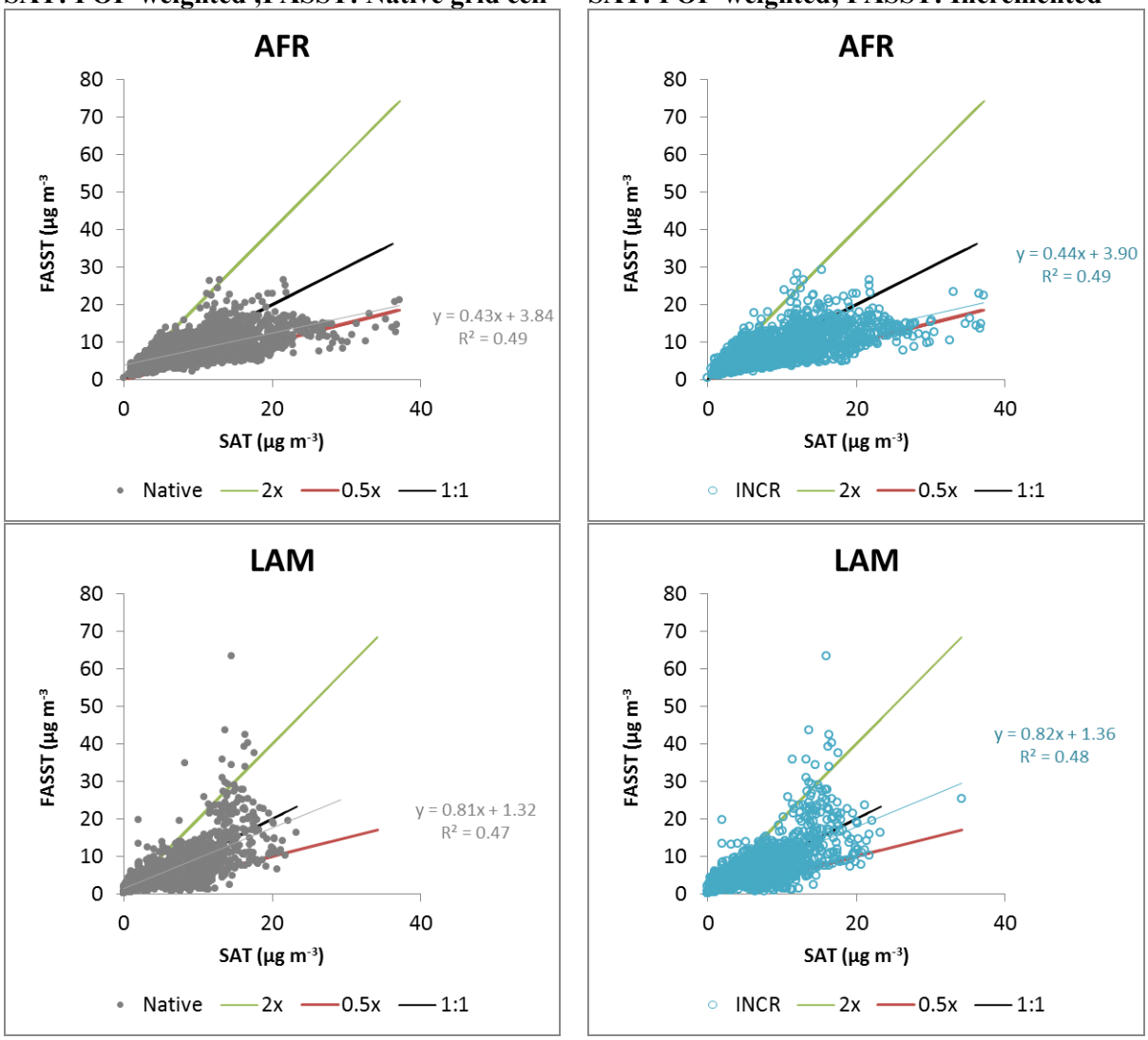

Figure S4.6 as Fig. S4.4, now for Africa and Latina America

S5 Supplemental information to Section 2.5 – Health impacts

S5.1 Calculation of premature mortalities from ambient $PM_{2.5}$ and O_3

TM5-FASST currently includes two approaches from the literature to evaluate RRs for $PM_{2.5}$: the first one follows methodology and outcomes of the American Cancer Society (ACS) study (Krewski et al., 2009; Pope et al., 2002) based on a log-linear exposure response function $RR = \exp^{\beta\Delta}PM_{2.5}$ where β is the concentration–response factor (CRF; i.e., the estimated slope of the log-linear relation between concentration and mortality) and $\Delta PM_{2.5}$ is the change in concentration. The fraction of the disease burden attributable to $PM_{2.5}$ as a risk factor, the attributable fraction (AF), is defined as

$$AF = \frac{RR - 1}{RR} = 1 - exp(-\beta \Delta PM2.5)$$

A 10 μg/m^3 increase in $PM_{2.5}$ (concentration range, 5.8–22.2 μg/m^3) was associated with 13% (95% CI, 10–16%), and 14% (95% CI, 6–23%) increases in cardiopulmonary (CP) and lung cancer (LC) mortality, corresponding to β (for a 1 μg/m³ increase in $PM_{2.5}$) of 0.01213 and 0.01284 for CP and LC respectively. We also include an evaluation based on total non-accidental mortality with a RR per 10μg/m³ of 6.2% (95% CI, 4.0-8.3%) (Hoek et al., 2013).

The second methodology uses age-averaged Integrated Exposure-Response functions (IER) developed by Burnett et al. (2014), and first applied in e.g. the Global Burden of Disease study (Lim et al., 2012). IERs expand epidemiological studies on the long-term effects of ambient $PM_{2.5}$ exposure to higher concentration ranges than the one available from the ACS study, making use of health impact studies for smoking and second-hand smoking. This tends to flatten off the RR function at high $PM_{2.5}$ concentration levels compared to the traditionally-used log-lin function which, extrapolated outside the concentration range where the health impacts were determined, would lead to unrealistically high mortality fractions attributed to air pollution. The RR functions are given by:

$$RR(PM2.5) = 1 + \alpha\left[1 - e^{-\gamma(PM2.5 - zcf)^{\delta}}\right] \quad \text{for } PM2.5 > zcf$$

$$RR = 1 \quad \text{for } PM2.5 \leq zcf$$

where *zcf* is the counterfactual concentration (theoretical minimum-risk exposure, assumed by Burnett et al. (2014) to have a uniform distribution between 5.8 and 8.8. We used the age-averaged values for parameters α, γ, δ and *zcf* reported by Burnett *et al.* (2014) for 1000 simulations (IHME, 2011) to generate a look-up table of cause-specific RRs as a function of $PM_{2.5}$, where for each $PM_{2.5}$ value the mean (of 1000) RRs was used as central value, and the 95% CI as uncertainty range. Alternatively, we fitted a set of α, γ, δ and *zcf* parameters to the IER functional shapes based on the generated ($PM_{2.5}$, RR) look-up table. This was done by generating an array of $PM_{2.5}$ values between 0 and 300μg/m³ and calculating for each value 1000 RRs using the corresponding 1000 function parameter sets, from which we derive for each $PM_{2.5}$ value the median and 95% RR. Next we make a fitting of the resulting median and 95% CI RR($PM_{2.5}$), using the proposed functional shape for the IER functions.

$$RR(PM_{2.5}) = 1 + \alpha\left[1 - e^{-\gamma(PM2.5 - zcf)^{\delta}}\right]$$

The generated RR ($PM_{2.5}$) and best fit analytical functions are shown in Fig. S5, and the corresponding parameter values are given in Table S5.1.

The inclusion of a theoretical minimum risk exposure level (*zcf*) in the $PM_{2.5}$ exposure-response functions is motivated by the lowest prevailing concentration at which an increased risk was observed in the ACS cohort studies. Burnett et al. (2014) argue that zero exposure is not a practical counterfactual level because it is impossible to achieve even in pristine environments, implicitly indicating that their exposure-response curves strictly apply to total $PM_{2.5}$, including the natural components (mineral dust, sea-salt). In impact assessment studies, evaluating the difference between two anthropogenic emission scenarios (under otherwise identical natural background conditions) is often more relevant than evaluating absolute impacts for a single scenario. Therefore, TM5-FASST includes the option to customize the value of *zcf*, both in the IER as the log-linear shaped functions. In practice, we recommend to use *zcf* =0 when evaluating anthropogenic emissions only. Because of the non-linear IER functions, Δmortalities between 2 scenarios (S1, S2) with population-weighted $PM_{2.5}$ concentrations PM_{S1} and PM_{S2} respectively are evaluated as *Mort*(PM_{S2}) – *Mort*(PM_{S1}), and not as *Mort* (PM_{S2}-PM_{S1}).

WHO (2013) recommends both a log-linear and IER approach for long-term mortality from $PM_{2.5}$ exposure, with the log-linear RR referring to total (non-accidental) mortalities rather than the 2 specific causes (CP and LC) in the Krewski et al. (2009) approach. The WHO recommendations however refer specifically to European impact assessments. We deem that the attribution of mortalities to air pollution, as a fraction of total mortalities, rather than attributed to specific diseases, induces large uncertainties in other world regions because of different relative contributions of pollution-related diseases to total mortality.

For O_3 exposure, $RR = e^{\beta(\Delta M6M)}$, β is the concentration–response factor, and RR = 1.040 [95% confidence interval (CI): 1.013, 1.067] for a 10 ppb increase in 6mDMA1 according to Jerrett et al. (2009). We apply a default counterfactual concentration of 33.3 ppbV, the minimum 6mDMA1 exposure level in the Jerrett et al. (2009) epidemiological study.

The coefficients in the IER functions used in the GBD assessments have been recently updated due to methodological improvements in the curve fitting, leading to generally higher RR and mortality estimates (Cohen et al.,2017; Forouzanfar et al., 2016). In particular, the theoretical minimum risk exposure level was assigned a uniform distribution of 2.4–5.9 μg/m^3 for $PM_{2.5}$, bounded by the minimum and fifth percentiles of exposure distributions from outdoor air pollution cohort studies. Further, a recent health impact assessment (Malley et al., 2017), using updated RR estimate and exposure parameters from the epidemiological study by Turner et al. (2016), estimates 1.04–1.23 million respiratory deaths in adults attributable to O_3 exposure, compared with 0.40–0.55 million respiratory deaths attributable to O_3 exposure based on the earlier (Jerrett et al., 2009) risk estimate and parameters. These updates have not been included in the current version of TM5-FASST.

Health impacts from exposure to other pollutants (NO_2, SO_2 for example) are currently not being evaluated in TM5-FASST-v0 although the model output does provide population-weighted mean concentrations of NO_x and SO_2.

S5.2 Sources for population statistics

We use high-resolution population grid maps up to 2100 that were prepared for the Global Energy Assessment (GEA, 2012), based on the Medium Fertility variant of UN population projections (UN DESA, 2009). Year 2030 population distribution by age class, which are required to establish the age classes ≥30 and <5 years are

obtained from the United Nations Population Division (2015) Revision. Alternatively the high-resolution Gridded Population of the World V3 (CIESIN, 2005) can be used for scenario years between 2000 and 2015.

S5.3 Baseline mortality rates for relevant causes of death

Cause-specific base mortalities from stroke, ischemic heart disease (IHD), chronic obstructive pulmonary disease (COPD), acute lower respiratory illness diseases (ALRI) and lung cancer (LC) are obtained from WHO (2008)[2]

Cause-specific base mortalities for the year 2005 are taken from the WHO ICD-10 update (WHO, 2012) for individual countries where available, or back-calculated from 14 WHO regional average mortalities when not available. Projections until 2030 are taken from WHO Global Health estimates[3]. In the tool, mortalities for the year 2005 are used for scenario years up till 2005, and mortalities for the year 2030 are used for scenario years 2030 and beyond. Intermediate years are interpolated.

[2] http://www.who.int/healthinfo/global_burden_disease/cod_2008_sources_methods.pdf

[3] http://www.who.int/healthinfo/global_burden_disease/en/

Table S5 IER fitted function parameters (parameters have been fitted to a range up to 300 µg/m³)

	COPD	LC	ALRI	STROKE	IHD
			MEDIAN		
α	58.99	54.61	1.98	1.03	0.83
β	0.00031	0.00034	0.00259	0.02002	0.07101
δ	0.67	0.74	1.24	1.07	0.55
zcf	7.58	6.91	6.79	8.80	6.86
			2.5%ile		
α	28.91	12.54	1.61	1.35	1.02
β	0.00015	0.00013	0.01025	0.02064	0.05557
δ	0.83	1.02	0.81	0.49	0.40
zcf	8.19	7.24	13.84	10.91	9.62
			97.5%ile		
α	120.48	23.51	2.82	1.41	1.21
β	0.00028	0.00169	0.00083	0.01469	0.01283
δ	0.63	0.67	1.50	1.26	1.09
zcf	6.02	6.56	1.50	7.21	1.97

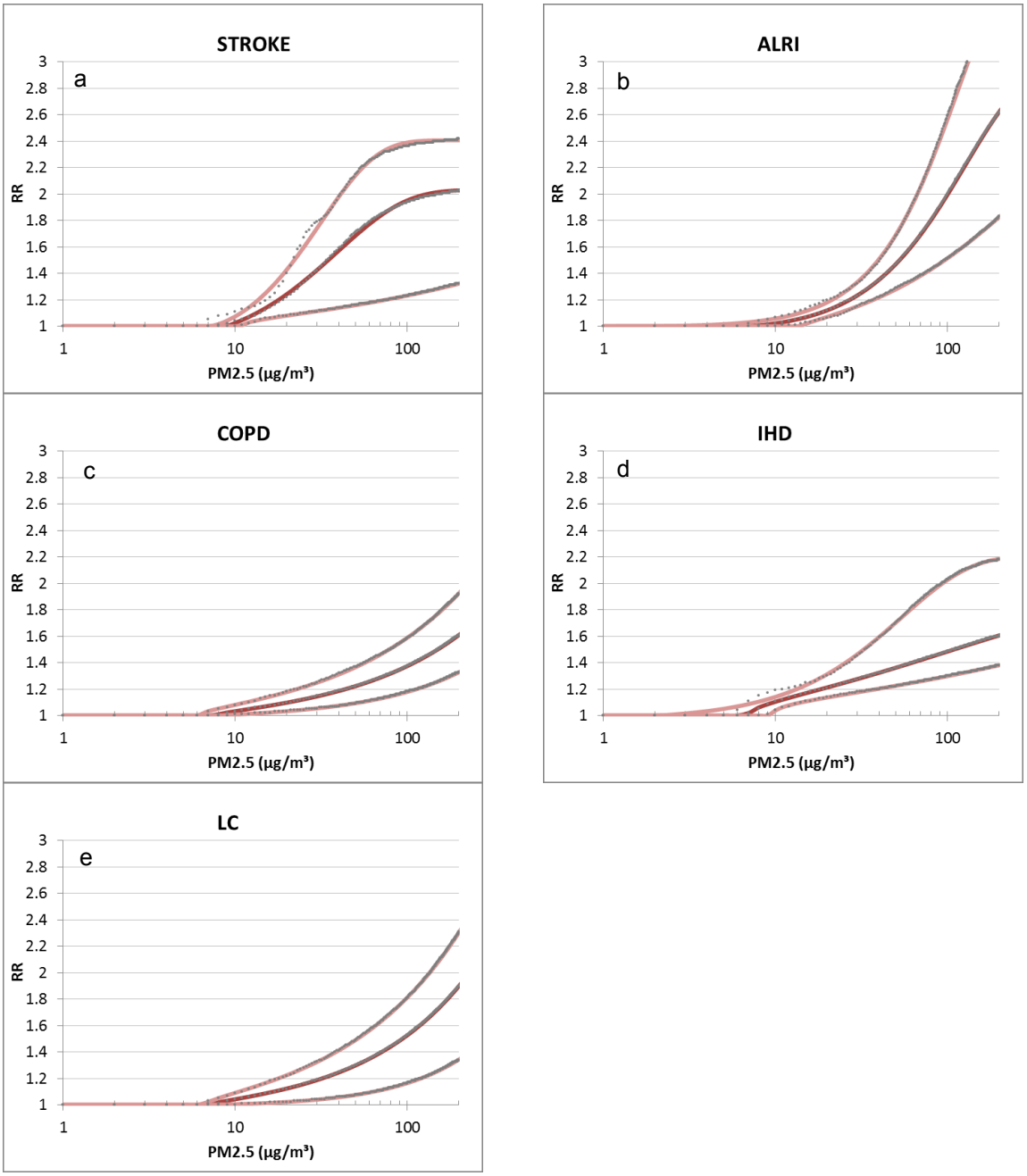

Figure S5.1: Dashed line: Median and 95% CI of the relative risk (RR) as a function of exposure to $PM_{2.5}$ from 1000 Monte Carlo samples provided by Burnett et al. (2014). Red lines: fitted curves for all-age IER functions for 5 mortality causes, using the parameters listed in Table S6.1 (this work). (a): Stroke, (b): Acute Lower Respiratory Airways Infections (c) Chronic Obstructive Pulmonary Disease (d) Ischaemic Heart Disease (e) Lung Cancer

S6 Supplemental information to Section 2.7 – Climate metrics

S6.1 calculation of aerosol optical properties and radiative forcing in TM5

Direct radiative forcing:

The broadband aerosol optical properties were determined in two steps: first, the spectral optical properties in the wavelength region between 0.2 μm and 5 μm were calculated on the basis of Mie theory. Only the short-to-infrared wave spectrum 0.2-5 μm has been considered, since the anthropogenic aerosols are most efficient in scattering and absorbing the solar radiation in the submicron size range. In a second step, these spectral quantities were weighted by the extra-terrestrial solar flux (Wehrli, 1985), and averaged over the applied wavelength intervals of the Off-line Radiative Transfer Model (ORTM).

TM5 determines aerosol mass, and does not provide information about particle size distributions or particle densities, so assumptions were made about these properties for the Mie calculations (Table S6.1). We assume a lognormal size distribution with a geometric mean radius r_g of 0.05 μm for inorganics and OC, a geometric standard deviation σ_g of 1.8 for sulphate and 2.0 for OC, and a particle density of 1600 kg.m^{-3} and 1200 kg.m^{-3} respectively. The optical properties of inorganics, which mainly scatter shortwave radiation, are reasonably well known compared with other types of aerosols (Li et al., 2001). Wavelength-dependent complex refractive indices for sulphate were taken from Toon et al. (1976). The same values were assumed for organic carbon (Lund Myhre and Nielsen, 2004; Sloane, 1983). The geometric mean radius for BC particles is assumed to be 0.0118 mm with a sigma of 2.0 and a particle density of 1800 kg.m^{-3} (Penner et al., 1998). For the BC refractive indices, the values from Fenn et al. (1985) were applied. We assume externally mixed aerosols and calculate the forcing separately for each component. The total aerosol forcing is obtained by summing up these contributions.

The aerosol water content is calculated assuming equilibrium between aerosol particles and atmospheric water vapour pressure at each location. The modification of aerosol specific extinction due to relative humidity of the ambient air is considered using a simple approximation adapted from the data given by Nemesure et al. (1995). For relative humidities (RH) below 80%, the specific extinction is enhanced by a factor of RH*0.04, assuming a minimum RH of 25%. For RH exceeding 80%, the specific extinction increases exponentially with RH. The factor 9.9 is reached for RH = 100%. Exponential growth is assumed for hygroscopic aerosols (ammonium salts and organic carbon). Black carbon (here assumed to be externally mixed) is assumed to be mostly hydrophobic and its specific extinction increases only linearly with RH. Single scattering albedo and the asymmetry factor are assumed to be independent of RH. This approach might result in a small overestimation of the shortwave radiative forcing of scattering aerosols, because with increasing relative humidity forward scattering is increased and backscattering in space direction reduced (asymmetry factor increased).

Indirect forcing:

The cloud droplet number concentrations (*CDNC*) were calculated using the following set of equations from Boucher and Lohmann (1995), separating continental and maritime clouds:

$$CDNC_{cont}^{St} = 10^{2.24+0.257log(m_{SO_4})} \quad [S6.1]$$

$$CDNC_{cont}^{Cu} = 10^{2.54+0.186log(m_{SO_4})} \quad [S6.2]$$

$$CDNC_{ocean} = 10^{2.06+0.48log(m_{SO_4})} \quad [S6.3]$$

Following Boucher and Lohmann (1995), the cloud droplet effective radius is calculated from the mean volume cloud droplet radius:

$$r_e = 1.1\left(\frac{l\rho_{air}}{(4/3)\pi\rho_{water}CDNC}\right)^{1/3} \quad [S6.4]$$

Where l = cloud liquid water content, ρ_{air} = air density, ρ_{water} = water density

S6.2 Secondary forcing feedbacks of O_3 precursors on CH_4 and background O_3

Emissions of short-lived species (NO_x, NMVOC, CO, SO_2) influence the atmospheric OH burden and therefore the CH_4 atmospheric lifetime, which in turn contributes to long-term change in CH4 and background ozone. Hence, the total forcing contribution from O_3 precursors consists of a short-term direct contribution from immediate O_3 formation (S-O_3), and secondary contributions from CH_4 (I-CH4) and a long-term feedback from this CH_4 on background O_3 (M-O_3).

We apply the formulation by (Fiore et al., 2009; Prather et al., 2001; West et al., 2007) to calculate the secondary change in steady-state CH_4 from SLS emissions, using the TM5 perturbation experiments for FASST (see section S3). TM5 diagnoses the CH_4 loss by oxidation for reference and perturbation run (where the emissions of SLS are decreased with -20%), from which we calculate the CH_4 oxidation lifetime ratio between reference and perturbation:

$$\frac{LT_P}{LT_{Ref}} = \frac{CH4\_ox_P}{CH4\_ox_{Ref}} \quad [S6.5]$$

Where LT is the CH4 lifetime against loss by OH oxidation, and $CH4\_ox$ = the amount (Tg) of CH4 oxidized.

The new steady-state methane concentration M due to the changing lifetime from perturbation experiment P, induced by O_3 precursor emissions follows from (Fiore et al., 2008, 2009; Wild and Prather, 2000):

$M = M_0 \times \left(\frac{LT_P}{LT_{ref}}\right)^F$ where $M_0 = 1760$ ppb, the reference CH_4 concentration and F = 1.5, determined from the HTAP1 CH4 perturbation experiments, as described in section S3.

The change in CH_4 forcing (I-CH4) associated with the change to the new steady-state concentration is obtained from IPCC AR5 equations:

$$\Delta F = \alpha\left(\sqrt{M} - \sqrt{M_0}\right) - \left(f(M, N_0) - f(M_0, N_0)\right) \quad [S6.6]$$

$$f(M, N) = 0.47ln[1 + 2.01 \times 10^{-5}(MN)^{0.75} + 5.31 \times 10^{-15}M(MN)^{1.52}] \quad [S6.7]$$

Where M, M_0 = CH_4 concentration in ppb, N_0 = N_2O (=320 ppb) [S6.8]

The associated long-term O_3 forcing (M-O_3) per Tg precursor emitted is obtained by scaling linearly the change in O_3 forcing obtained in the HTAP1 CH_4 perturbation simulation (SR2–SR1), with the change in CH_4 obtained above, and normalizing by the precursor emission change (Fiore et al., 2009)

$$\Delta F = \frac{\Delta F_{O3}[SR2-SR1]}{M_{SR2}-M_{SR1}}(M - M_0) \quad [S6.8]$$

The response of CH_4 and O_3 forcing to CO emission changes (for which no regional TM5-FASST perturbation model simulations were performed) was taken from the SR5 simulations performed for the HTAP1 assessment using the average forcing efficiency for North America, Europe, South-Asia and East-ia from(Fry et al., 2012). For regions not covered by the HTAP1 regions, the HTAP1 rest-of-the-world forcing efficiency was used.

The resulting region-to-globe emission-based forcing efficiencies are given in Tables S6.2 to S6.5 for aerosols, CO, CH_4 and other O_3 precursors respectively.

Table S6.1 Parameters of aerosol log-normal size distributions

	r_g (μm)	σ_g	Density (kg m^{-3})	Refr. index real	Refr. index imaginary
Inorganic	0.05	1.8	1600	1.53	1.0×10^{-7}
BC	0.0118	2.0	1800	1.75	4.4×10^{-1}
OC	0.05	2.0	1200	1.53	1.0×10^{-7}

S6.3 Tables with emission-based forcing efficiencies by source region in TM5-FASST

Table S6.2 Regional emission-to-global forcing efficiencies for aerosol precursors (no feedback on O_3 included). Emission strengths are expressed in component mass (SO_2, NO_2, BC, POM, NH_3)

		DIRECT					INDIRECT
FASST REGION	FASST CODE	W/m^2/Tg SO_2	W/m^2/Tg NO_x	W/m^2/Tg BC	W/m^2/Tg POM	W/m^2/Tg NH_3	W/m^2/Tg SO_2
N-AFR	NOA	-7.38E-03	-8.13E-04	5.32E-02	-1.28E-02	-0.00426	-7.19E-03
W-AFR	WAF	-6.74E-03	-2.91E-04	3.02E-02	-1.01E-02	-0.00242	-1.14E-02
E-AFR	EAF	-9.41E-03	-9.07E-04	3.22E-02	-9.92E-03	-0.00473	-1.69E-02
S-AFR	SAF	-8.74E-03	-1.21E-03	3.07E-02	-1.10E-02	-0.00495	-2.57E-02
REP. S. AFR	RSA	-4.03E-03	-4.24E-04	1.64E-02	-5.55E-03	-2.32E-03	-1.98E-02
AUSTRALIA	AUS	-4.20E-03	-1.03E-04	2.02E-02	-6.63E-03	-2.18E-03	-2.06E-02
NZL	NZL	-1.84E-03	-1.03E-04	8.12E-03	-2.84E-03	-1.25E-03	-2.42E-02
S KOREA	COR	-1.66E-03	-6.80E-05	1.20E-02	-4.69E-03	-3.14E-03	-3.36E-03
JAPAN	JPN	-1.45E-03	-9.75E-05	9.59E-03	-2.85E-03	-1.16E-03	-4.25E-03
MON+N KOREA	MON	-1.89E-03	-4.48E-04	1.47E-02	-5.24E-03	-1.77E-03	-3.70E-03
CHINA	CHN	-2.18E-03	-4.41E-04	1.67E-02	-4.93E-03	-2.24E-03	-4.90E-03
TWN	TWN	-2.48E-03	-3.75E-05	8.51E-03	-3.14E-03	-2.13E-03	-6.94E-03
AUT+SLV	AUT	-3.23E-03	-3.66E-04	2.45E-02	-6.03E-03	-2.21E-03	-3.03E-03
SWITZERLAND	CHE	-3.15E-03	-3.73E-04	2.39E-02	-5.74E-03	-2.70E-03	-3.07E-03
BE+NL+LUX	BLX	-1.63E-03	-3.43E-04	1.36E-02	-3.72E-03	-2.46E-03	-2.14E-03
SP+POR	ESP	-5.06E-03	-4.68E-04	2.82E-02	-8.58E-03	-3.25E-03	-5.31E-03
FIN	FIN	-1.38E-03	-1.18E-04	1.84E-02	-3.33E-03	-1.40E-03	-1.35E-03
FRA	FRA	-2.75E-03	-3.91E-04	1.87E-02	-5.56E-03	-1.88E-03	-3.30E-03
GBR+IRL	GBR	-1.52E-03	-1.70E-04	1.21E-02	-3.66E-03	-1.82E-03	-3.45E-03
GRC+CYP	GRC	-4.66E-03	-8.43E-04	3.87E-02	-9.11E-03	-2.64E-03	-3.91E-03
ITA+MLT	ITA	-3.97E-03	-5.40E-04	2.88E-02	-7.93E-03	-2.37E-03	-3.42E-03
GER	RFA	-2.16E-03	-4.24E-04	1.72E-02	-4.38E-03	-2.33E-03	-2.46E-03
SWE+DK	SWE	-1.47E-03	-3.77E-04	1.53E-02	-3.56E-03	-1.15E-03	-1.80E-03
NORWAY	NOR	-1.47E-03	-2.16E-04	1.67E-02	-3.07E-03	-6.27E-04	-4.59E-03
BULGARIA	BGR	-3.90E-03	-7.18E-04	3.27E-02	-7.59E-03	-2.36E-03	-3.13E-03
HUN	HUN	-2.91E-03	-3.39E-04	2.35E-02	-5.39E-03	-2.23E-03	-2.88E-03
POL+BALTIC	POL	-1.96E-03	-2.01E-04	1.75E-02	-3.66E-03	-1.66E-03	-2.47E-03
REST OF C EUR	RCEU	-3.58E-03	-6.60E-04	3.07E-02	-7.30E-03	-1.69E-03	-3.23E-03
CZ+SLK	RCZ	-2.47E-03	-3.13E-04	2.14E-02	-4.90E-03	-2.46E-03	-2.63E-03
ROM	ROM	-3.13E-03	-4.83E-04	2.47E-02	-5.84E-03	-2.02E-03	-2.61E-03
MEX	MEX	-6.35E-03	-3.03E-04	1.97E-02	-7.89E-03	-3.36E-03	-1.38E-02
REST OF C AM	RCAM	-3.93E-03	-3.96E-04	1.53E-02	-6.57E-03	-1.90E-03	-1.01E-02
MIDDLE EAST	MEME	-4.83E-03	-1.49E-03	4.29E-02	-9.49E-03	-3.33E-03	-4.70E-03
EGY	EGY	-5.73E-03	-5.21E-04	5.64E-02	-1.21E-02	-2.93E-03	-6.05E-03
GULF REGION	GLF	-7.14E-03	-1.49E-03	4.40E-02	-1.08E-02	-1.61E-03	-7.80E-03

(continues on next page)

Table S6.2 Cont'd

		DIRECT					INDIRECT
FASST REGION	FASST CODE	$W/m^2/Tg$ SO_2	$W/m^2/Tg$ NO_x	$W/m^2/Tg$ BC	$W/m^2/Tg$ POM	$W/m^2/Tg$ NH_3	$W/m^2/Tg$ SO_2
TUR	TUR	-4.76E-03	-4.83E-04	3.55E-02	-8.01E-03	-2.92E-03	-4.18E-03
CANADA	CAN	-1.80E-03	-2.87E-04	1.96E-02	-3.35E-03	-1.91E-03	-4.16E-03
USA	USA	-2.84E-03	-1.33E-04	1.69E-02	-5.55E-03	-2.67E-03	-5.79E-03
PAC	PAC	-3.25E-03	-1.03E-04	9.01E-03	-2.72E-03	-1.44E-03	-1.74E-02
KAZ	KAZ	-2.31E-03	-4.89E-04	2.90E-02	-4.36E-03	-2.15E-03	-4.14E-03
FRMR USSR AS	RIS	-2.83E-03	-2.56E-04	2.79E-02	-4.93E-03	-2.51E-03	-4.50E-03
RUS-EUR	RUS	-2.47E-03	-2.10E-04	2.44E-02	-4.24E-03	-1.76E-03	-3.22E-03
RUS-ASIA	RUE	-2.15E-03	-7.52E-04	2.58E-02	-3.91E-03	-1.12E-03	-3.90E-03
UKR	UKR	-2.78E-03	-3.61E-04	2.33E-02	-5.04E-03	-1.92E-03	-3.07E-03
BRAZIL	BRA	-5.21E-03	-1.77E-04	2.00E-02	-7.40E-03	-1.58E-03	-1.30E-02
CHL	CHL	-4.88E-03	-4.26E-04	2.15E-02	-6.74E-03	-1.66E-03	-2.38E-02
ARG	ARG	-8.75E-04	-4.26E-04	1.32E-02	-4.51E-03	-8.03E-04	-1.52E-02
REST OF S AM	RSAM	-5.31E-03	-9.85E-05	1.50E-02	-5.10E-03	-1.57E-03	-1.31E-02
REST OF S AS	RSAS	-6.46E-03	-1.41E-04	3.02E-02	-9.09E-03	-1.73E-03	-8.34E-03
INDIA	NDE	-6.29E-03	-1.41E-04	2.61E-02	-9.37E-03	-1.59E-03	-9.66E-03
INDON	IDN	-3.65E-03	-4.41E-04	1.17E-02	-4.35E-03	-6.19E-04	-1.89E-02
THAIL	THA	-3.78E-03	-4.41E-04	1.45E-02	-5.37E-03	-1.08E-03	-1.19E-02
MALYS	MYS	-3.14E-03	-4.41E-04	1.32E-02	-5.02E-03	-1.16E-03	-2.63E-02
PHIL	PHL	-2.64E-03	-4.41E-04	8.79E-03	-3.44E-03	-1.47E-03	-1.56E-02
VTNAM	VNM	-2.90E-03	-4.41E-04	1.30E-02	-5.02E-03	-1.19E-03	-1.13E-02
REST OF EAS	RSEA	-6.16E-03	-4.41E-04	1.81E-02	-7.83E-03	-1.14E-03	-1.40E-02
SHIP	SHIP	-2.32E-03	-8.95E-05	1.26E-02	-2.06E-03	0.00E+00	-9.38E-03

Table S6.3: Global response in radiative forcing due to emissions of CO by including the short and long-term feedback on CH_4 and O_3. S-O_3: short-term O_3 contribution M-O_3: long term O_3 forcing feedback via CH_4 lifetime I-CH_4: long-term feedback on CH_4 via CH_4 lifetime

	CO forcing (W/m²/Tg CO)		
	S-O_3	M-O_3	I-CH_4
North-America	2.85E-05	3.61E-05	8.78E-05
Europe	1.84E-05	3.95E-05	9.62E-05
South Asia	3.94E-05	4.25E-05	1.04E-04
East Asia	3.15E-05	4.27E-05	1.04E-04
Rest of the World	1.91E-04	5.10E-05	1.24E-04

Table S6.4: Global response in radiative forcing to CH_4 emissions, including the long-term feedback on O_3

	CH_4 forcing (W/m²/Tg CH_4)	
	Direct CH_4	O_3 feedback
Globe	1.79E-03	7.16E-04

Table S6.5 Global response in radiative forcing due to regional emissions of short-lived O_3 precursors - including the long-term feedback on CH_4 and O_3. S-O_3: short-term O_3 contribution M-O_3: long term O_3 forcing feedback via CH_4 lifetime I-CH_4: long-term feedback on CH_4 via CH_4 lifetime.

	Forcing (W/m²/Tg NO_2)			Forcing (W/m²/Tg NMVOC)			Forcing (W/m²/Tg SO_2)		
	S-O_3	M-O_3	I-CH_4	S-O_3	M-O_3	I-CH_4	S-O_3	M-O_3	I-CH_4
NOA	1.20E-03	-7.63E-04	-1.86E-03	2.32E-04	1.34E-04	3.26E-04	-1.29E-04	1.28E-05	3.11E-05
WAF	1.42E-03	-9.95E-04	-2.43E-03	2.04E-04	1.26E-04	3.06E-04	-9.05E-05	1.42E-05	3.45E-05
EAF	1.28E-03	-7.96E-04	-1.94E-03	1.90E-04	1.15E-04	2.81E-04	-6.89E-05	1.68E-05	4.09E-05
SAF	1.35E-03	-7.86E-04	-1.92E-03	1.51E-04	1.24E-04	3.02E-04	-1.65E-04	2.41E-05	5.88E-05
RSA	1.27E-03	-6.99E-04	-1.70E-03	3.93E-04	3.56E-05	8.66E-05	-9.92E-05	2.33E-05	5.67E-05
AUS	2.80E-03	-1.48E-03	-3.61E-03	2.55E-04	1.40E-04	3.40E-04	-6.01E-05	1.54E-05	3.75E-05
NZL	2.95E-03	-1.95E-03	-4.77E-03	8.45E-05	1.96E-04	4.76E-04	-6.01E-05	4.11E-07	1.00E-06
COR	3.02E-04	-1.75E-04	-4.26E-04	2.92E-04	3.01E-05	7.33E-05	-2.36E-05	2.33E-06	5.68E-06
JPN	4.64E-04	-2.55E-04	-6.22E-04	2.23E-04	1.16E-04	2.82E-04	-2.18E-05	2.04E-06	4.96E-06
MON	5.36E-04	-2.89E-04	-7.03E-04	2.77E-04	2.02E-04	4.92E-04	-2.25E-05	1.10E-06	2.69E-06
CHN	8.31E-04	-3.66E-04	-8.91E-04	2.11E-04	1.16E-04	2.82E-04	-2.22E-05	4.73E-05	1.15E-04
TWN	1.12E-03	-5.46E-04	-1.33E-03	3.49E-04	7.88E-05	1.92E-04	-4.08E-05	1.40E-06	3.41E-06
AUT	2.54E-04	-1.60E-04	-3.89E-04	2.19E-04	1.12E-04	2.74E-04	-4.23E-05	7.20E-07	1.75E-06
CHE	3.36E-04	-1.89E-04	-4.60E-04	2.22E-04	1.18E-04	2.86E-04	-2.65E-05	1.27E-07	3.10E-07
BLX	8.16E-05	-7.31E-05	-1.78E-04	2.01E-04	1.20E-04	2.91E-04	-1.76E-05	4.66E-07	1.14E-06
ESP	4.89E-04	-3.01E-04	-7.32E-04	2.22E-04	1.14E-04	2.77E-04	-6.54E-05	1.56E-05	3.80E-05
FIN	1.57E-04	-1.40E-04	-3.40E-04	1.60E-04	1.18E-04	2.87E-04	-1.30E-05	1.69E-07	4.13E-07
FRA	2.46E-04	-1.59E-04	-3.87E-04	2.14E-04	1.15E-04	2.79E-04	-3.69E-05	2.50E-06	6.09E-06
GBR	7.17E-05	-8.03E-05	-1.95E-04	2.01E-04	1.22E-04	2.96E-04	-1.69E-05	2.63E-06	6.40E-06
GRC	4.74E-04	-2.87E-04	-7.00E-04	2.70E-04	4.62E-05	1.13E-04	-7.23E-05	5.13E-06	1.25E-05
ITA	3.58E-04	-2.04E-04	-4.97E-04	2.46E-04	8.61E-05	2.10E-04	-5.68E-05	5.76E-06	1.40E-05
RFA	1.29E-04	-9.65E-05	-2.35E-04	1.98E-04	1.17E-04	2.84E-04	-2.28E-05	1.82E-06	4.44E-06
SWE	1.94E-04	-1.60E-04	-3.90E-04	1.60E-04	1.17E-04	2.84E-04	-1.17E-05	2.12E-07	5.16E-07
NOR	4.20E-04	-3.01E-04	-7.33E-04	1.35E-04	1.03E-04	2.50E-04	-1.38E-05	9.75E-07	2.37E-06
BGR	3.63E-04	-2.24E-04	-5.46E-04	2.39E-04	9.99E-05	2.43E-04	-5.05E-05	6.36E-06	1.55E-05
HUN	2.14E-04	-1.42E-04	-3.46E-04	2.07E-04	1.17E-04	2.84E-04	-3.39E-05	1.95E-06	4.75E-06
POL	1.67E-04	-1.20E-04	-2.92E-04	1.93E-04	1.10E-04	2.67E-04	-2.16E-05	4.41E-06	1.07E-05
RCEU	4.17E-04	-2.47E-04	-6.02E-04	2.00E-04	1.24E-04	3.01E-04	-4.56E-05	6.86E-06	1.67E-05
RCZ	1.72E-04	-1.21E-04	-2.95E-04	2.05E-04	1.09E-04	2.66E-04	-2.78E-05	1.27E-06	3.10E-06
ROM	2.52E-04	-1.44E-04	-3.51E-04	2.15E-04	1.17E-04	2.86E-04	-3.63E-05	2.16E-06	5.26E-06
EUR	2.37E-04	-1.59E-04	-3.87E-04	2.01E-04	1.54E-05	3.74E-05	-3.98E-05	5.90E-05	1.44E-04
MEX	1.67E-03	-8.98E-04	-2.19E-03	2.38E-04	1.17E-04	2.84E-04	-9.34E-05	3.15E-05	7.67E-05
RCAM	2.12E-03	-1.22E-03	-2.97E-03	2.08E-04	1.43E-04	3.49E-04	-5.67E-05	5.69E-06	1.39E-05
MEME	5.71E-04	-3.17E-04	-7.72E-04	2.73E-04	1.00E-04	2.44E-04	-1.06E-04	1.05E-05	2.55E-05
EGY	7.14E-04	-4.89E-04	-1.19E-03	3.28E-04	6.19E-05	1.51E-04	-1.13E-04	7.85E-06	1.91E-05
GOLF	1.28E-03	-7.11E-04	-1.73E-03	2.03E-04	1.47E-04	3.59E-04	-1.18E-04	7.70E-05	1.87E-04
TUR	5.69E-04	-3.07E-04	-7.48E-04	2.53E-04	1.01E-04	2.46E-04	-8.00E-05	1.52E-05	3.71E-05
CAN	4.83E-04	-2.85E-04	-6.94E-04	1.39E-04	1.32E-04	3.22E-04	-3.13E-05	8.27E-06	2.01E-05
USA	4.72E-04	-2.39E-04	-5.81E-04	2.35E-04	1.09E-04	2.66E-04	-5.73E-05	8.43E-05	2.05E-04
PAC	4.91E-03	-2.33E-03	-5.69E-03	1.50E-04	1.96E-04	4.77E-04	-4.21E-05	3.75E-07	9.13E-07

Table continues on next page

Table S6.5 – Cont'd

	Forcing (W/m²/Tg NO_2)			Forcing (W/m²/Tg NMVOC)			Forcing (W/m²/Tg SO_2)		
	S-O_3	M-O_3	I-CH_4	S-O_3	M-O_3	I-CH_4	S-O_3	M-O_3	I-CH_4
KAZ	6.52E-04	-3.36E-04	-8.18E-04	1.57E-04	1.22E-04	2.98E-04	-2.56E-05	5.21E-06	1.27E-05
RIS	7.94E-04	-3.66E-04	-8.93E-04	2.12E-04	1.35E-04	3.28E-04	-4.48E-05	1.48E-06	3.61E-06
RUS	2.93E-04	-1.97E-04	-4.80E-04	1.80E-04	1.26E-04	3.07E-04	-2.16E-05	1.02E-05	2.49E-05
RUE	6.96E-04	-4.02E-04	-9.80E-04	1.11E-04	1.24E-04	3.01E-04	-3.42E-05	5.25E-06	1.28E-05
UKR	2.56E-04	-1.66E-04	-4.04E-04	2.08E-04	1.24E-04	3.03E-04	-3.50E-05	6.48E-06	1.58E-05
BRA	2.84E-03	-1.30E-03	-3.16E-03	8.43E-05	1.41E-04	3.43E-04	-6.90E-05	1.45E-05	3.54E-05
CHL	2.13E-03	-1.30E-03	-3.18E-03	3.06E-04	7.81E-05	1.90E-04	-1.14E-04	1.14E-05	2.77E-05
ARG	2.95E-03	-1.44E-03	-3.52E-03	1.10E-04	1.58E-04	3.84E-04	-1.14E-04	1.93E-06	4.71E-06
RSAM	2.79E-03	-1.52E-03	-3.71E-03	1.33E-04	1.44E-04	3.50E-04	-6.78E-05	7.48E-06	1.82E-05
RSAS	1.20E-03	-5.60E-04	-1.36E-03	2.22E-04	1.32E-04	3.21E-04	-5.08E-05	7.69E-06	1.87E-05
NDE	1.18E-03	-5.97E-04	-1.45E-03	2.59E-04	1.31E-04	3.18E-04	-5.08E-05	4.27E-05	1.04E-04
IDN	2.23E-03	-1.25E-03	-3.05E-03	2.19E-04	1.57E-04	3.83E-04	-4.21E-05	1.01E-05	2.46E-05
THA	1.90E-03	-9.83E-04	-2.40E-03	2.22E-04	1.37E-04	3.33E-04	-4.21E-05	4.81E-06	1.17E-05
MYS	2.23E-03	-1.18E-03	-2.87E-03	2.54E-04	1.47E-04	3.59E-04	-4.21E-05	2.36E-06	5.76E-06
PHL	2.29E-03	-1.07E-03	-2.61E-03	3.57E-04	1.57E-04	3.82E-04	-4.21E-05	6.33E-06	1.54E-05
VNM	2.03E-03	-1.04E-03	-2.53E-03	2.14E-04	1.60E-04	3.91E-04	-4.21E-05	9.48E-07	2.31E-06
RSEA	1.40E-03	-8.07E-04	-1.97E-03	1.48E-04	1.40E-04	3.41E-04	-4.21E-05	8.35E-07	2.03E-06
SHIP	1.40E-03	-8.46E-04	-2.06E-03	0.00E+00	0.00E+00	0.00E+00	-2.87E-05	3.64E-05	8.87E-05
AIR	4.25E-03	-1.14E-03	-2.77E-03	0.00E+00	0.00E+00	0.00E+00	0.00E+00	0.00E+00	0.00E+00

Table S6.6 Year 2000 global anthropogenic forcing (W/m²) by component from TM5-FASST, versus values reported in AR5 (1750 – 2011). Large scale forest fires have not been included.

		CH_4	BC $PM_{2.5}$	OC $PM_{2.5}$	O_3 (SS)	O_3 (PM)	NO_3 $PM_{2.5}$	SO_4 $PM_{2.5}$	INDIR	TOT
CH_4	AR5	0.641				0.24				0.88
	FASST	*0.500*				*0.20*				*0.70*
CO	AR5	0.072			0.075					0.15
	FASST	*0.083*			*0.074*	*0.034*				*0.19*
NMVOC	AR5	0.025			0.042					0.07
	FASST	*0.049*			*0.033*	*0.020*				*0.10*
NO_x	AR5	-0.245			0.14		-0.040			-0.14
	FASST	*-0.167*			*0.13*	*-0.068*	*-0.040*			*-0.15*
NH_3	AR5						-0.070	0.01		-0.06
	FASST						*-0.091*			*-0.09*
BC	AR5		0.60							0.60
	FASST		*0.15*							*0.15*
OC	AR5			-0.29						-0.29
	FASST			*-0.24*						*-0.24*
SO_2	AR5							-0.41		-0.21
	FASST							*-0.37*		*-0.37*
INDIRECT AEROSOLS	AR5								-0.45	-0.45
	FASST								*-0.81*	*-0.81*

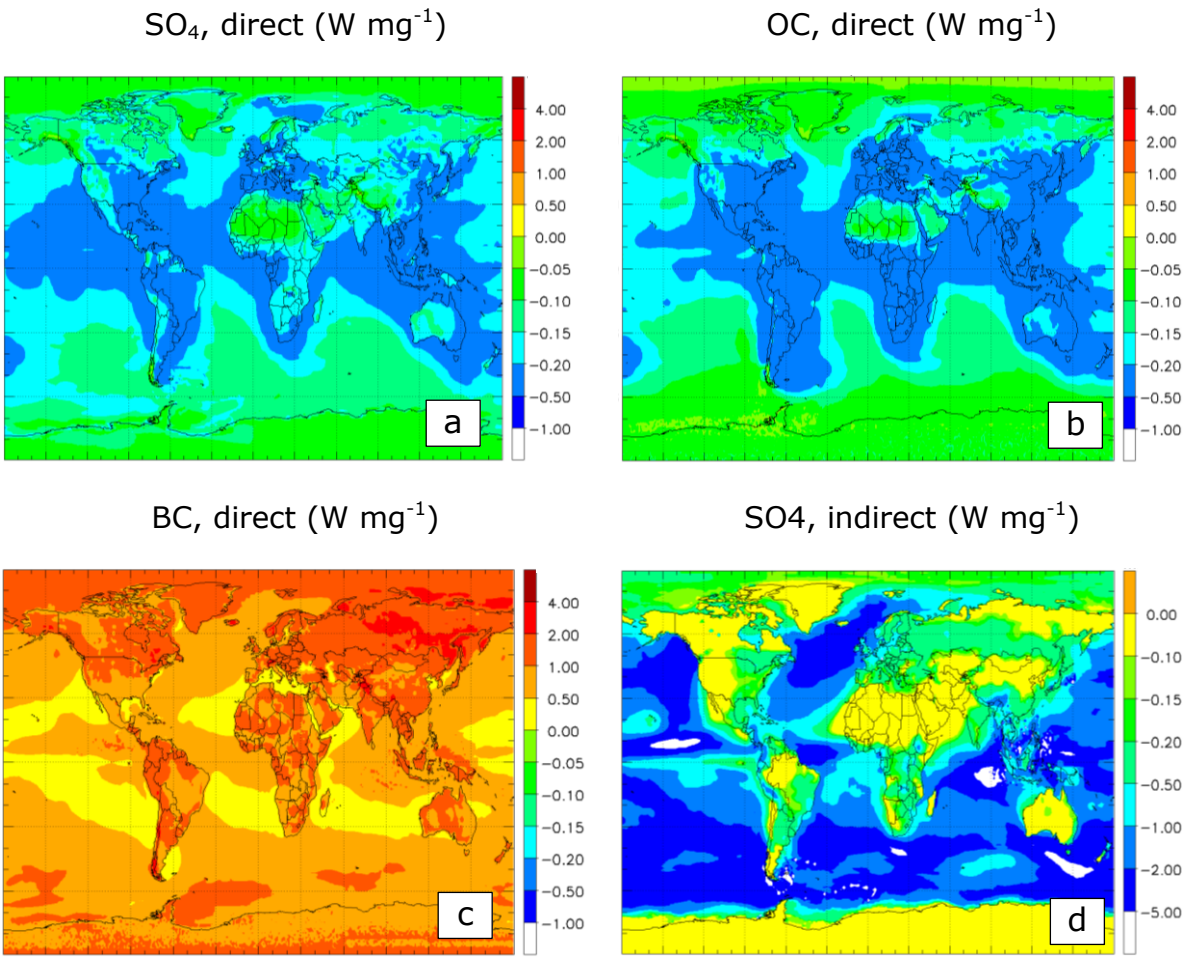

Figure S6.1: Annual average radiative forcing efficiencies (Watt per mg column burden) for SO_4, Particulate Organic Matter, Black carbon, and the indirect forcing associated with SO_4

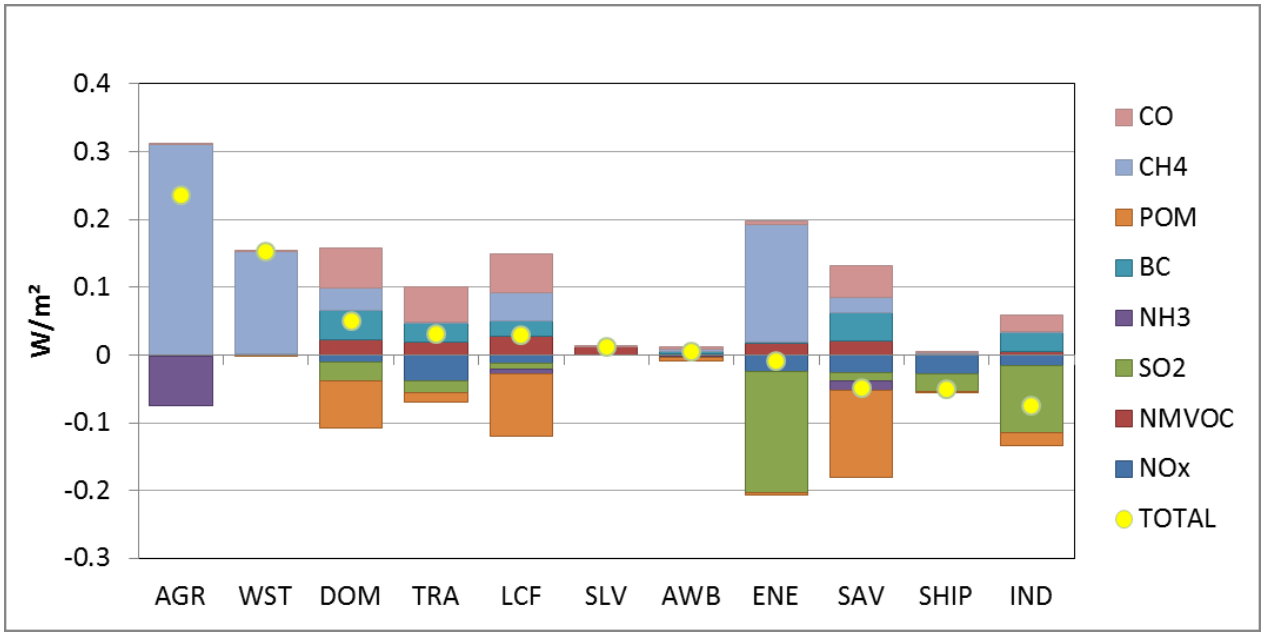

Figure S6.2 TM5-FASST break-down of direct radiative forcing by sector by emitted component, based on RCP year 2000 emission inventory by sector.

S7 Supplemental Tables and Figures to Section 3.1 - Validation against the full TM5 model: additivity and linearity

Table S7.1 Statistical metrics describing the correspondence between the linearized FASST and TM5 computed secondary $PM_{2.5}$ upon -80% and 100% emission perturbation in its precursors (SO_2, NO_x, NH_3 and combined SO_2 + NO_x). Statistics are calculated over all 1°x1° grid cells in each region.

	FASST MEAN ($\mu g\ m^{-3}$)		TM5 MEAN ($\mu g\ m^{-3}$)		NMB[(a)] (%)		MB[(b)]		$R^{2(c)}$	
Region	-80%	100%	-80%	100%	-80%	100%	-80%	100%	-80%	100%
	Precursor: SO_2									
EUR	5.4	7.6	5.2	7.4	2.5	1.9	0.13	0.14	1.00	1.00
USA	3.2	5.1	3.1	5.0	2.5	2.1	0.08	0.10	1.00	1.00
JPN	4.8	5.5	4.8	5.5	0.3	0.4	0.02	0.02	1.00	1.00
CHN	7.0	10.3	6.8	10.0	3.3	2.7	0.22	0.28	1.00	1.00
IND	9.9	14.7	9.8	14.5	1.0	1.4	0.10	0.20	1.00	1.00
	Precursor: NO_x									
EUR	5.4	7.5	5.3	7.1	2.8	5.0	0.15	0.36	0.99	1.00
USA	3.6	4.6	3.4	4.4	4.5	4.9	0.15	0.21	1.00	1.00
JPN	4.8	5.5	4.7	5.3	2.2	3.2	0.11	0.17	1.00	1.00
CHN	7.7	9.5	7.6	9.2	1.4	2.9	0.11	0.26	1.00	1.00
IND	11.5	12.8	11.5	12.9	-0.3	-0.6	-0.04	-0.08	1.00	1.00
	Precursor: NH_3									
EUR	5.2	7.7	4.8	7.6	9.5	2.1	0.45	0.16	0.98	0.99
USA	3.4	4.8	3.2	4.6	4.9	3.8	0.16	0.17	0.99	1.00
JPN	4.7	5.6	4.7	5.5	1.6	1.8	0.07	0.10	1.00	1.00
CHN	7.7	9.4	7.4	9.2	3.6	3.2	0.26	0.30	1.00	1.00
IND	11.9	12.3	11.7	12.2	1.6	0.7	0.18	0.08	1.00	1.00
	Precursor: SO_2+NO_x									
EUR	4.4	8.8	4.0	8.1	9.5	7.7	0.38	0.63	0.98	1.00
USA	2.7	5.7	2.5	5.3	9.6	7.7	0.24	0.40	0.98	1.00
JPN	4.5	5.8	4.4	5.6	2.5	4.1	0.11	0.23	1.00	1.00

[(a)] Normalized Mean Bias = $\left(\overline{FASST - TM5}\right)/\overline{TM5}$

[(b)] Mean Bias = $\left(\overline{FASST - TM5}\right)$

[(c)] Correlation coefficient

$\bar{Y}$ = average of all grid cells in region

Table S7.2: Statistical metrics describing the correspondence between the linearized FASST and TM5 computed O_3 exposure metric 6mDMA1 upon -80% and 100% emission perturbation in its precursors (NMVOC, NO_x and combined NO_x + NMVOC), relative to the RCP2000 base scenario. Statistics are calculated over all 1°x1° grid cells in each region.

	FASST MEAN (ppb)		TM5 MEAN (ppb)		NMB[(a)] (%)		MB[(b)] (ppb)		$R^{2(c)}$	
Region	-80%	100%	-80%	100%	-80%	100%	-80%	100%	-80%	100 %
Precursor: NMVOC										
EUR	47.8	51.1	47.6	50.7	0.4	1.0	0.2	0.5	0.99	0.99
USA	47.5	50.1	47.4	49.8	0.3	0.5	0.1	0.3	1.00	1.00
JPN	50.6	52.6	50.5	52.4	0.3	0.5	0.1	0.3	1.00	1.00
CHN	50.5	52.5	50.1	52.0	0.8	1.0	0.4	0.5	1.00	0.99
IND	53.7	55.6	53.4	55.2	0.5	0.7	0.3	0.4	1.00	1.00
Precursor: NO_x										
EUR	46.6	52.6	44.8	50.5	4.1	4.2	1.9	2.1	0.98	0.99
USA	44.1	54.3	41.8	52.0	5.4	4.5	2.3	2.3	0.94	0.99
JPN	50.4	52.9	48.8	51.2	3.2	3.5	1.6	1.8	0.92	0.95
CHN	47.0	56.8	45.3	54.7	3.8	3.8	1.7	2.1	0.97	0.95
IND	47.3	63.6	44.9	61.0	5.3	4.3	2.4	2.7	0.95	0.99
Precursor: NO_x + NMVOC										
EUR	45.3	54.3	44.2	53.1	2.4	2.3	1.1	1.2	0.99	1.00
USA	43.1	55.6	41.6	53.8	3.7	3.2	1.5	1.7	0.96	1.00
CHN	46.3	57.7	45.3	56.6	2.2	2.0	1.0	1.1	0.99	0.99
IND	46.5	64.6	45.0	63.0	3.5	2.6	1.6	1.6	0.98	1.00

[(a)] Normalized Mean Bias = $\left(\overline{FASST - TM5}\right)/\overline{TM5}$

[(b)] Mean Bias = $\left(\overline{FASST - TM5}\right)$

[(c)] Correlation coefficient

$\bar{Y}$ = average of all grid cells in region

Table S7.3: Statistical metrics describing the correspondence between the linearized FASST and TM5 computed O_3 crop exposure metric AOT40 upon -80% and 100% emission perturbation in its precursors (NMVOC, NO_x and combined NO_x + NMVOC), relative to the RCP2000 base scenario. Statistics are calculated over all 1°x1° grid cells in each region.

	FASST MEAN (ppm.h)		TM5 MEAN (ppm.h)		NMB[(a)] (%)		MB[(b)] (ppm.h)		$R^{2(c)}$	
Region	-80%	100%	-80%	100%	-80%	100 %	-80%	100%	-80%	100%
Precursor: NMVOC										
EUR	6.7	9.2	6.5	9.0	2.2	3.1	0.1	0.3	0.99	0.99
USA	9.5	11.8	9.4	11.6	1.2	2.3	0.1	0.3	1.00	1.00
JPN	10.0	11.4	9.9	11.2	1.0	2.0	0.1	0.2	1.00	1.00
CHN	9.0	10.5	8.7	10.1	3.2	4.0	0.3	0.4	1.00	0.99
IND	8.5	9.8	8.3	9.5	2.7	3.3	0.2	0.3	1.00	1.00
Precursor: NO_x										
EUR	5.7	10.4	4.7	9.1	22.7	14.5	1.1	1.3	0.97	0.99
USA	6.0	16.3	4.3	14.2	39.2	14.7	1.7	2.1	0.90	0.99
JPN	9.9	11.5	9.0	10.4	10.4	10.8	0.9	1.1	0.97	0.97
CHN	6.7	13.4	6.2	12.1	8.3	10.3	0.5	1.3	0.98	0.97
IND	4.7	14.7	3.8	13.0	22.0	13.1	0.8	1.7	0.94	0.98
Precursor: NO_x + NMVOC										
EUR	4.6	11.8	3.6	9.6	27	23	1.0	2.2	0.97	0.99
USA	4.9	17.6	3.7	14.3	35	23	1.3	3.2	0.92	0.99
CHN	6.0	14.2	5.4	12.1	12	18	0.6	2.2	0.99	0.99
IND	4.0	15.4	3.3	12.7	21	22	0.7	2.7	0.96	0.99

[(a)] Normalized Mean Bias = $\left(\overline{FASST - TM5}\right)/\overline{TM5}$

[(b)] Mean Bias = $\left(\overline{FASST - TM5}\right)$

[(c)] Correlation coefficient

$\bar{Y}$ = average of all grid cells in region

Table S7.4: Statistical metrics describing the correspondence between the linearized FASST and TM5 computed O_3 crop exposure metric M12 upon -80% and 100% emission perturbation in its precursors (NMVOC, NO_x and combined NO_x + NMVOC), relative to the RCP2000 base scenario. Statistics are calculated over all 1°x1° grid cells in each region.

	FASST MEAN (ppb)		TM5 MEAN (ppb)		NMB[(a)] (%)		MB[(b)] (ppb)		$R^{2(c)}$	
Region	-80%	100%	-80%	100%	-80%	100 %	-80%	100%	-80%	100%
Precursor: NMVOC										
EUR	43.0	45.0	42.3	45.2	1.6	-0.5	0.7	-0.2	0.98	0.98
USA	45.5	47.8	45.3	47.5	0.3	0.6	0.1	0.3	1.00	1.00
JPN	47.2	48.8	47.1	48.5	0.3	0.5	0.1	0.2	1.00	1.00
CHN	45.3	47.0	44.9	46.5	0.8	1.0	0.4	0.5	1.00	1.00
IND	46.3	47.8	46.1	47.4	0.6	0.7	0.3	0.3	1.00	1.00
Precursor: NO_x										
EUR	42.3	45.9	40.7	44.3	3.8	3.6	1.6	1.6	0.97	0.98
USA	42.2	51.9	40.1	49.7	5.2	4.3	2.1	2.2	0.91	0.99
JPN	48.4	47.3	47.3	46.0	2.3	2.8	1.1	1.3	0.97	0.97
CHN	42.6	50.3	41.2	48.6	3.6	3.6	1.5	1.7	0.97	0.96
IND	42.1	53.0	40.2	50.9	4.9	4.2	2.0	2.1	0.95	0.98
Precursor: NO_x + NMVOC										
EUR	41.0	47.5	40.1	46.6	2.1	2.0	0.9	0.9	0.98	0.99
USA	41.3	53.0	39.9	51.5	3.5	3.0	1.4	1.5	0.93	0.99
CHN	42.0	51.0	41.2	50.2	1.9	1.7	0.8	0.9	0.99	0.99
IND	41.6	53.7	40.3	52.5	3.1	2.3	1.2	1.2	0.98	0.99

[(a)] Normalized Mean Bias = $\left(\overline{FASST - TM5}\right)/\overline{TM5}$

[(b)] Mean Bias = $\left(\overline{FASST - TM5}\right)$

[(c)] Correlation coefficient

$\bar{Y}$ = average of all grid cells in region

$PM_{2.5}$ additivity of simultaneous SO_2 + NO_x -20% emission perturbation responses

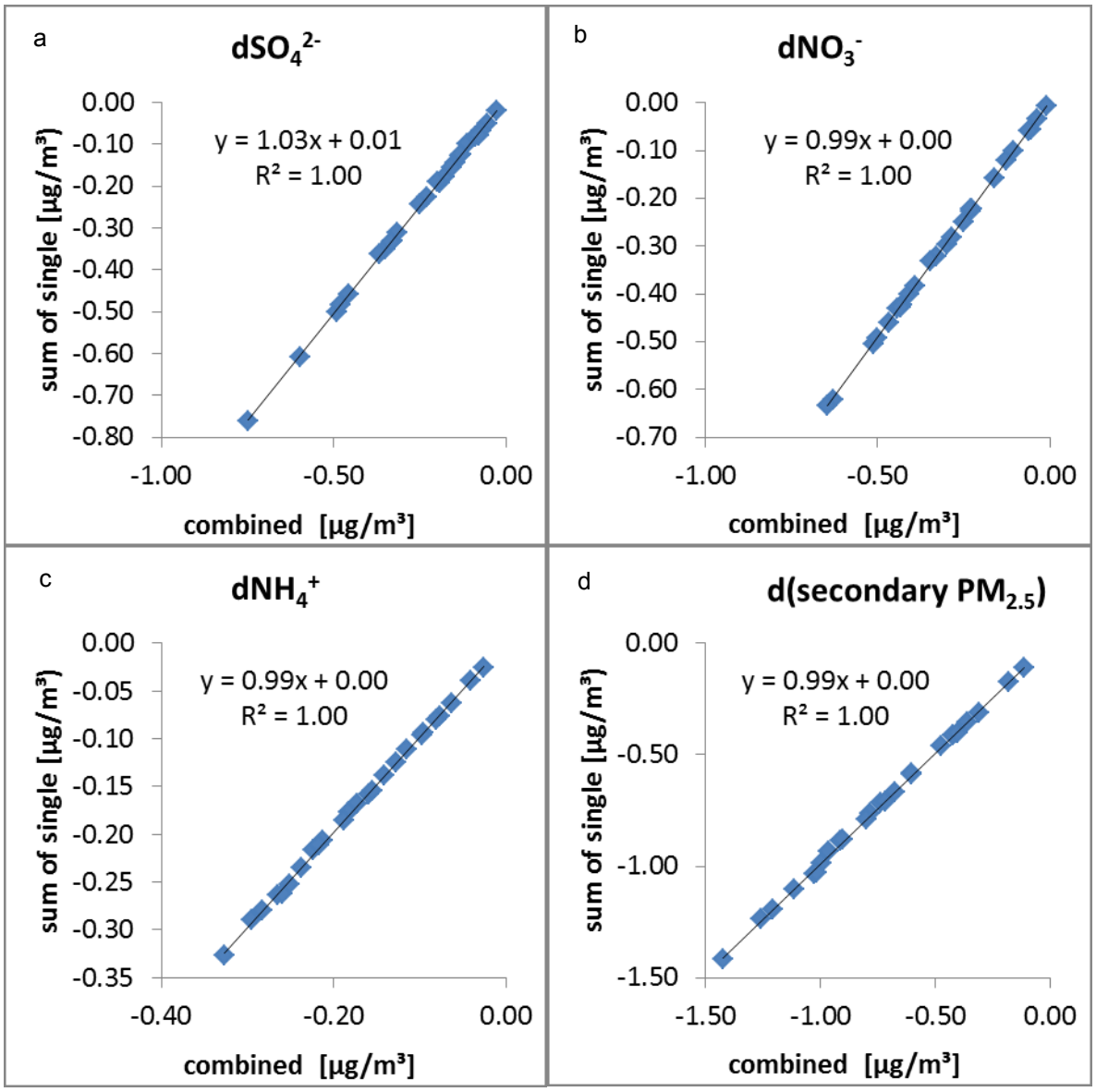

Figure S7.1 Secondary $PM_{2.5}$ species response to SO_2 and NO_x -20% emission perturbations. Y-axis: summed individual perturbations (P2 + P3) X-axis: response to combined perturbation (P1). All results are obtained with TM5-CTM. (a): sulfate (b) nitrate (c) ammonium (d) sum of all 3 components

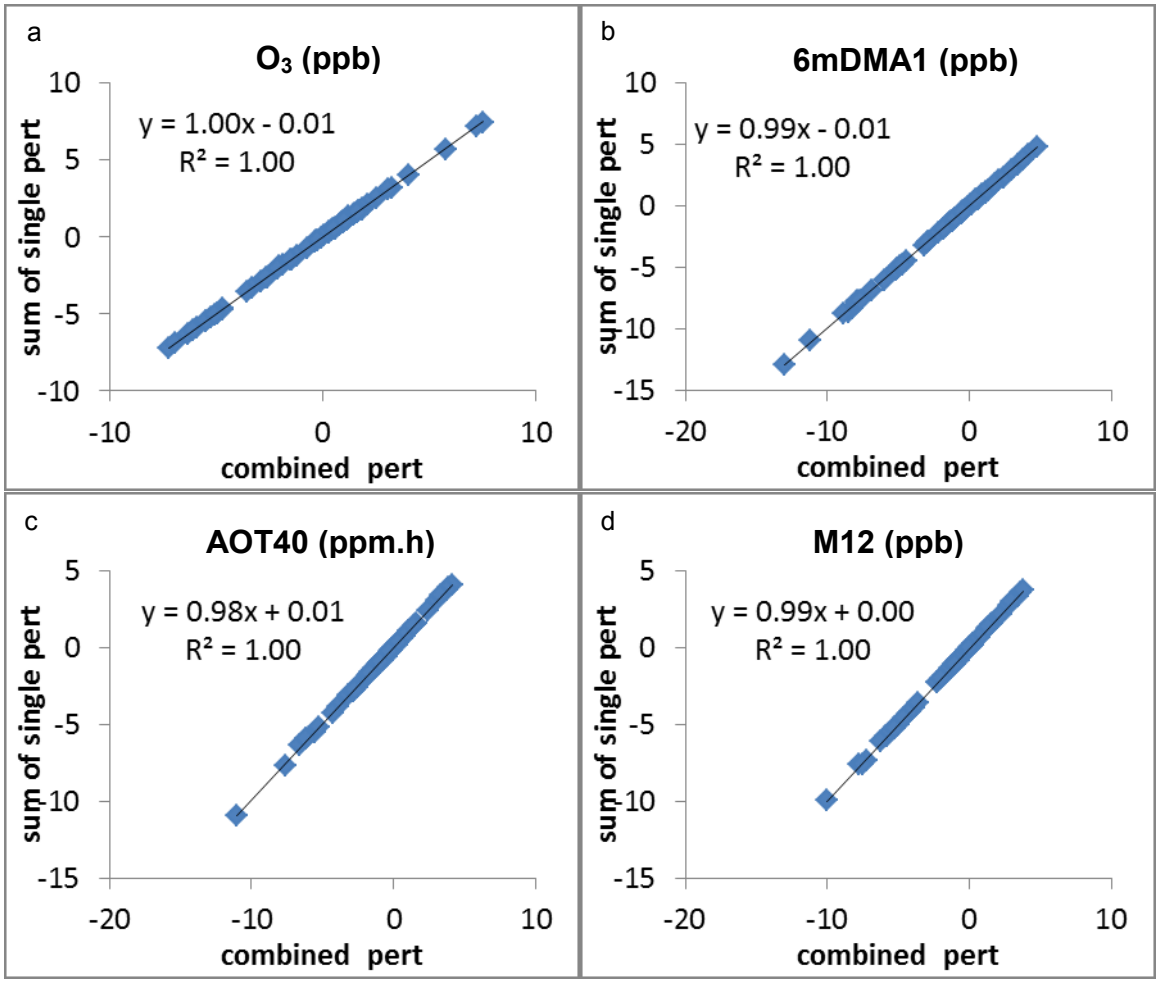

Figure S7.2 TM5 O_3 (a) and O_3 metrics 6mDMA1 (b), AOT40 (c) and M12 (d) responses to simultaneous SO_2 and NO_x perturbations including the -80%, -20% and +100% perturbation outcomes for the limited set of source regions. Y-axis: calculated as the sum of the individual responses; X-axis: evaluated from simultaneous perturbation.

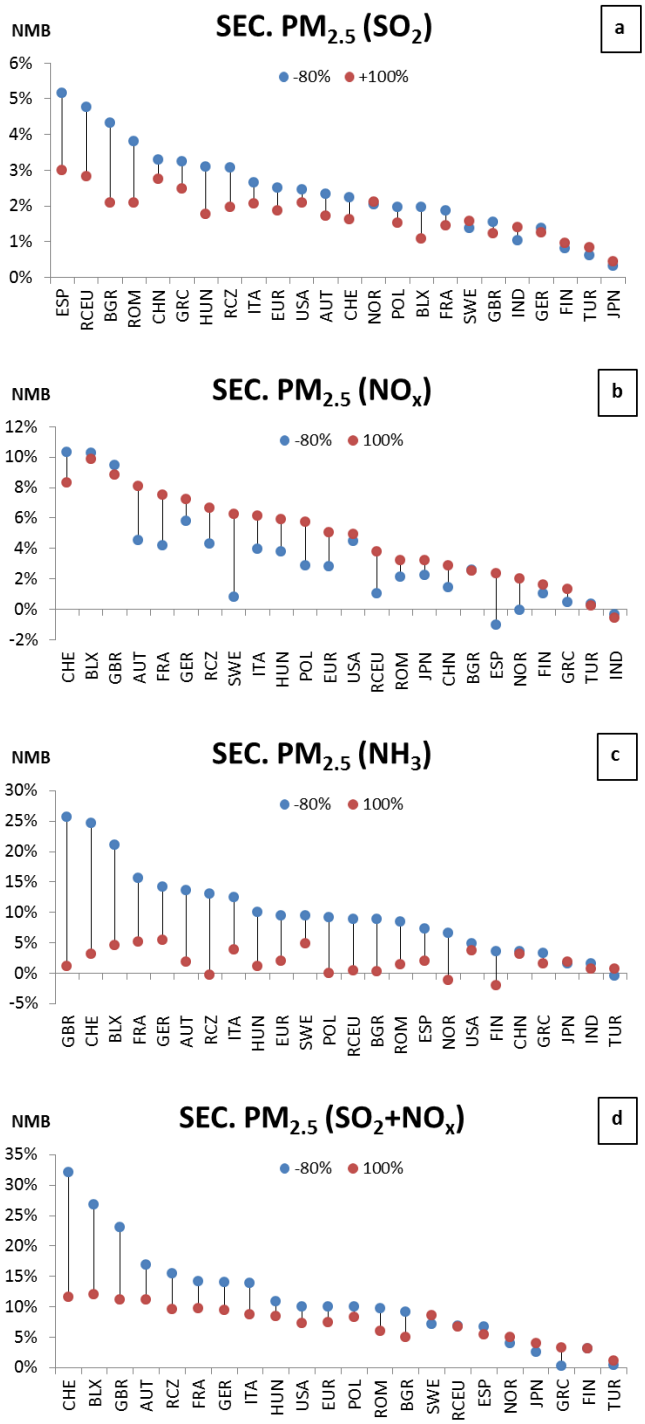

Figure S7.3 Relative deviation (Normalized Mean Bias) between the linearized FASST and TM5 computed regional mean absolute secondary $PM_{2.5}$ upon -80% and 100% emission perturbation in precursors (a) SO_2, (b) NO_x (c) NH_3, (d) SO_2 + NO_x. Statistics are calculated over all 1°x1° grid cells in each region.

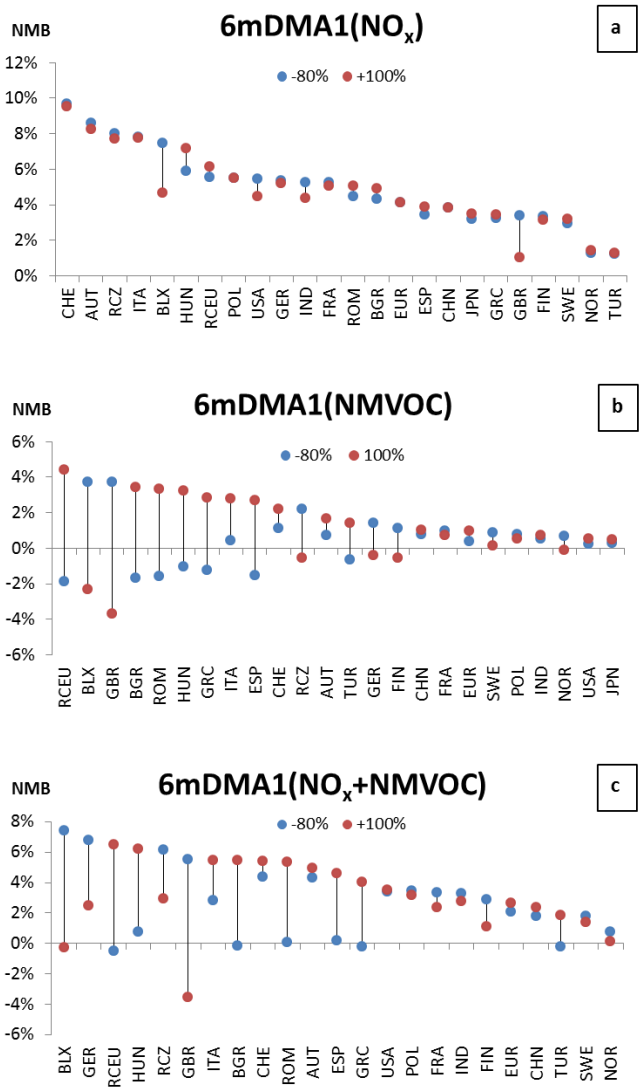

Figure S7.4 Relative deviation (Normalized Mean Bias) between the linearized FASST and TM5 computed regional mean ozone exposure metric 6mDMA1 upon -80% and 100% emission perturbation in precursors NO_x and NMVOC. Statistics are calculated over all 1°x1° grid cells in each region. (a) NO_x only perturbation (b) NMVOC only perturbation (c) combined NO_x + NMVOC perturbation

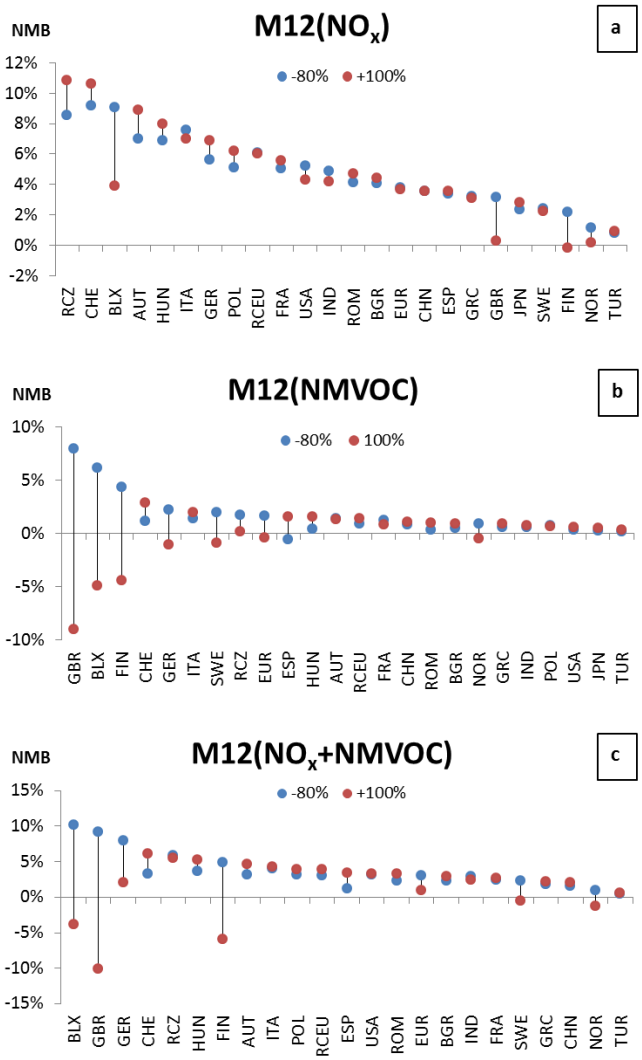

Figure S7.5 Relative deviation (Normalized Mean Bias) between the linearized FASST and TM5 computed regional mean crop ozone exposure metric M12 upon -80% and 100% emission perturbation in precursors NO_x and NMVOC. Statistics are calculated over all 1°x1° grid cells in each region. (a) NO_x only perturbation (b) NMVOC only perturbation (c) combined NO_x + NMVOC perturbation

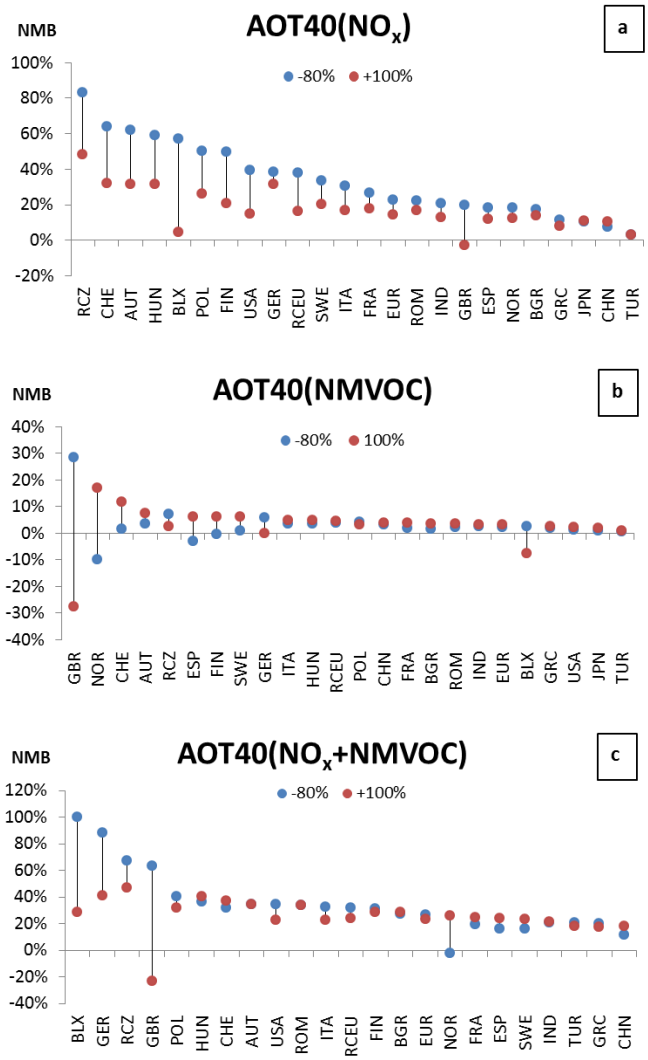

Figure S7.6 Relative deviation (Normalized Mean Bias) between the linearized FASST and TM5 computed regional mean crop ozone exposure metric AOT40 upon -80% and 100% emission perturbation in precursors NO_x and NMVOC. Statistics are calculated over all 1°x1° grid cells in each region. (a) NO_x only perturbation (b) NMVOC only perturbation (c) combined NO_x + NMVOC perturbation

S8 Supplemental information to Section 3.2 - TM5-FASST_v0 versus TM5 for future emission scenarios

S8.1 Major features of the Global Energy Assessment scenarios used in the validation study

The GEA scenarios (Riahi, Dentener et al. 2012), consistent with similar long-term climate outcomes as the RCPs, are implemented in the MESSAGE model (Messner and Strubegger 1995; Riahi, Gruebler et al. 2007) and include more detailed representation of short-term air quality legislations from the GAINS model (Amann et al., 2011). A number of air pollutants are included in the scenario (SO_2, NO_x, CO, VOCs, BC, OC, total primary $PM_{2.5}$) air pollutants and are available at 0.5^o x 0.5^o resolution based on inventory data described in Lamarque et al. (2010), and an exposure-driven algorithm for the downscaling of the regional air-pollutant emissions projections. The GEA scenarios have been used to estimate global health impacts of outdoor air pollution (Rao et al., 2012, 2013) as well as for regional impacts analysis (Colette et al., 2012, 2013). We evaluate following pair:

1. FLE-2030 (Fixed Legislation scenario): This is a scenario with no improvement in air quality legislations beyond 2005. It thus serves to indicate a scenario with failure in terms of implementation of future air quality and climate policies and is used as a worst-case scenario, defining an upper boundary for the range of plausible air pollutant emission scenarios until 2030. In the literature this kind of scenarios is also referred to as Frozen legislation, or no-further-controls (NFC).
2. MIT-2030 (MITigation scenario): This scenario, consistent with long-term climate outcomes of the RCP2.6, assumes stringent climate mitigation policies consistent with a target of 2^oC global warming by the end of the century (2100), combined with stringent air quality legislations (SLE). Thus the MIT-2030 scenario provides a best-case scenario, defining the lower boundary of pollutant emission strengths. We evaluate the outcome in the year 2030.

Table S8.1: Regional relative emission changes for the test scenarios MIT2030 and FLE2030 compared to the year 2000 RCP base scenario used for the 20% perturbation simulations. Region legend: see table S2.2

	BC	NH_3	NO_x	POM	SO_2	NMVOC	$PM_{2.5}$
			MIT2030				
EAS	-51%	+27%	-38%	-54%	-72%	-43%	+109%
SEA	-46%	+10%	-33%	-45%	-49%	-31%	-20%
SAS+RSAS	-46%	+34%	-8%	-75%	-19%	-27%	-15%
EUR	-89%	+17%	-83%	-80%	-93%	-72%	-56%
NAM	-70%	+21%	-82%	-31%	-85%	-62%	-11%
AFR+RSA	-30%	+33%	-40%	-29%	-49%	-30%	-24%
RUS	-51%	+30%	-60%	-24%	-69%	-28%	-13%
MAM+CAM	-44%	+46%	-51%	-26%	-29%	-29%	-18%
AUS+PAC	-16%	+30%	-45%	-7%	-73%	-18%	+4%
GLOBAL	**-47%**	**+25%**	**-48%**	**-35%**	**-69%**	**-37%**	**-5%**
			FLE2030				
EAS	+109%	+30%	+109%	+33%	+66%	+47%	+590%
SEA	+67%	+12%	+181%	+11%	+140%	+46%	+56%
SAS+RSAS	+152%	+37%	+407%	+73%	+292%	+136%	+181%
EUR	-26%	+19%	-29%	-16%	-13%	-35%	+52%
NAM	-26%	+24%	-44%	-13%	-21%	-34%	+39%
AFR+RSA	+71%	+36%	+33%	+23%	+107%	+76%	+29%
RUS	-13%	+30%	+14%	-17%	+10%	+8%	+20%
MAM+CAM	-17%	+46%	+10%	-23%	+34%	+26%	-4%
AUS+PAC	-5%	+30%	-22%	-4%	-11%	-4%	+10%
GLOBAL	**+47%**	**+27%**	**+25%**	**+7%**	**+42%**	**+35%**	**+95%**

Table S8.2 Absolute regional population-weighted mean anthropogenic $PM_{2.5}$ concentrations (total, primary and secondary components) for the high (FLE2030) and low (MIT2030) emission scenarios described in section 3.2, computed with the full chemical transport model TM5 and the reduced-form model TM5-FASST_v0.

	MIT2030					
	Total $PM_{2.5}$ (μg/m³)		Primary $PM_{2.5}$ (μg/m³)		Secondary $PM_{2.5}$ (μg/m³)	
REGION	FASST	TM5	FASST	TM5	FASST	TM5
EAS	10.1	8.5	7.4	5.9	2.8	2.6
SEA	9.5	7.5	6.7	4.7	2.8	2.8
SAS+RSAS	5.8	5.3	3.6	2.5	2.1	2.7
EUR	4.0	2.1	1.1	0.7	2.9	1.4
NAM	2.8	2.2	1.6	1.3	1.3	0.9
AFR+RSA	4.6	4.3	2.7	2.6	1.9	1.7
RUS	2.6	2.1	1.2	1.0	1.4	1.0
MAM+CAM	4.4	4.3	3.6	3.4	0.8	0.9
AUS+PAC	1.4	1.3	0.9	0.8	0.5	0.5
	FLE2030					
	Total $PM_{2.5}$ (μg/m³)		Primary $PM_{2.5}$ (μg/m³)		Secondary $PM_{2.5}$ (μg/m³)	
REGION	FASST	TM5	FASST	TM5	FASST	TM5
EAS	30.2	27.5	22.3	19.5	7.9	7.9
SEA	28.0	27.8	15.1	13.6	12.8	14.2
SAS+RSAS	19.4	22.3	9.8	9.3	9.6	13.0
EUR	9.2	8.7	3.4	2.8	5.8	5.9
NAM	4.7	4.2	2.2	1.6	2.5	2.6
AFR+RSA	8.6	9.4	4.3	5.0	4.3	4.3
RUS	5.8	5.7	2.7	2.3	3.1	3.4
MAM+CAM	5.0	4.9	3.8	3.6	1.2	1.3
AUS+PAC	1.6	1.6	0.9	0.8	0.7	0.8

Table S8.3 Absolute regional population-weighted mean annual O_3 and m6DMA1 for the high (FLE2030) and low (MIT2030) emission scenarios described in section 3.2, computed with the full chemical transport model TM5 and the reduced-form model TM5-FASST_v0.

	MIT2030			
	Annual mean O_3 (ppb)		Ozone exposure metric 6mDMA1 (ppb)	
REGION	FASST	TM5	FASST	TM5
EAS	37	36	50	46
SEA	35	35	49	45
SAS+RSAS	38	37	53	50
EUR	34	33	49	43
NAM	31	29	43	39
AFR+RSA	31	30	48	45
RUS	29	28	40	37
MAM+CAM	23	22	32	31
AUS+PAC	22	22	29	27
	FLE2030			
	Total $PM_{2.5}$ ($\mu g/m^3$)		Primary $PM_{2.5}$ ($\mu g/m^3$)	
REGION	FASST	TM5	FASST	TM5
EAS	48	44	62	58
SEA	57	50	78	70
SAS+RSAS	57	52	79	75
EUR	35	36	54	52
NAM	34	34	49	47
AFR+RSA	37	37	57	55
RUS	32	32	46	45
MAM+CAM	26	26	38	36
AUS+PAC	24	24	31	30

Table S8.4: Regional and global mortalities from anthropogenic $PM_{2.5}$ exposure from TM5 and FASST in the 2 test scenarios

	FLE2030			MIT2030			FLE2030-MIT2030		
	TM5	FASST	NMB	TM5	FASST	NMB	TM5	FASST	NMB
EUR	4.20E+05	4.41E+05	5%	1.96E+05	2.80E+05	43%	2.24E+05	1.61E+05	-28%
NAM	1.27E+05	1.41E+05	11%	7.23E+04	1.04E+05	43%	5.50E+04	3.73E+04	-32%
China+	2.39E+06	2.48E+06	4%	1.27E+06	1.57E+06	23%	1.12E+06	9.16E+05	-18%
India+	1.94E+06	1.94E+06	0%	1.03E+06	1.15E+06	11%	9.04E+05	7.98E+05	-12%
Russia	9.27E+04	9.98E+04	8%	5.54E+04	6.83E+04	23%	3.74E+04	3.14E+04	-16%
Brazil	4.99E+04	6.05E+04	21%	4.29E+04	5.50E+04	28%	7.00E+03	5.42E+03	-22%
RSEAS	3.89E+05	4.08E+05	5%	2.34E+05	2.82E+05	21%	1.56E+05	1.26E+05	-19%
GLOBAL	6.30E+06	6.47E+06	3%	3.43E+06	4.10E+06	19%	2.87E+06	2.37E+06	-17%

Table S8.5: As Table S8.4, but now for O_3 mortalities

	FLE2030			MIT2030			FLE2030-MIT2030		
	TM5	FASST	NMB	TM5	FASST	NMB	TM5	FASST	NMB
EUR	7.12E+04	73936.71	4%	6.08E+04	69702.68	15%	1.04E+04	4.23E+03	-59%
NAM	5.52E+04	59163	7%	4.41E+04	53964.9	22%	1.11E+04	5.20E+03	-53%
China+	4.95E+05	525405.9	6%	3.86E+05	435405.3	13%	1.09E+05	9.00E+04	-17%
India+	8.36E+05	914410	9%	5.23E+05	566520	8%	3.13E+05	3.48E+05	11%
Russia	1.31E+04	13365.9	2%	1.08E+04	12010	11%	2.26E+03	1.36E+03	-40%
Brazil	1.83E+04	19420	6%	1.56E+04	17285	11%	2.75E+03	2.14E+03	-22%
RSEAS	1.30E+05	147008.8	13%	1.02E+05	122161.1	20%	2.83E+04	2.48E+04	-12%
GLOBAL	2.02E+06	2.17E+06	7%	1.47E+06	1.63E+06	11%	5.50E+05	5.38E+05	-2%

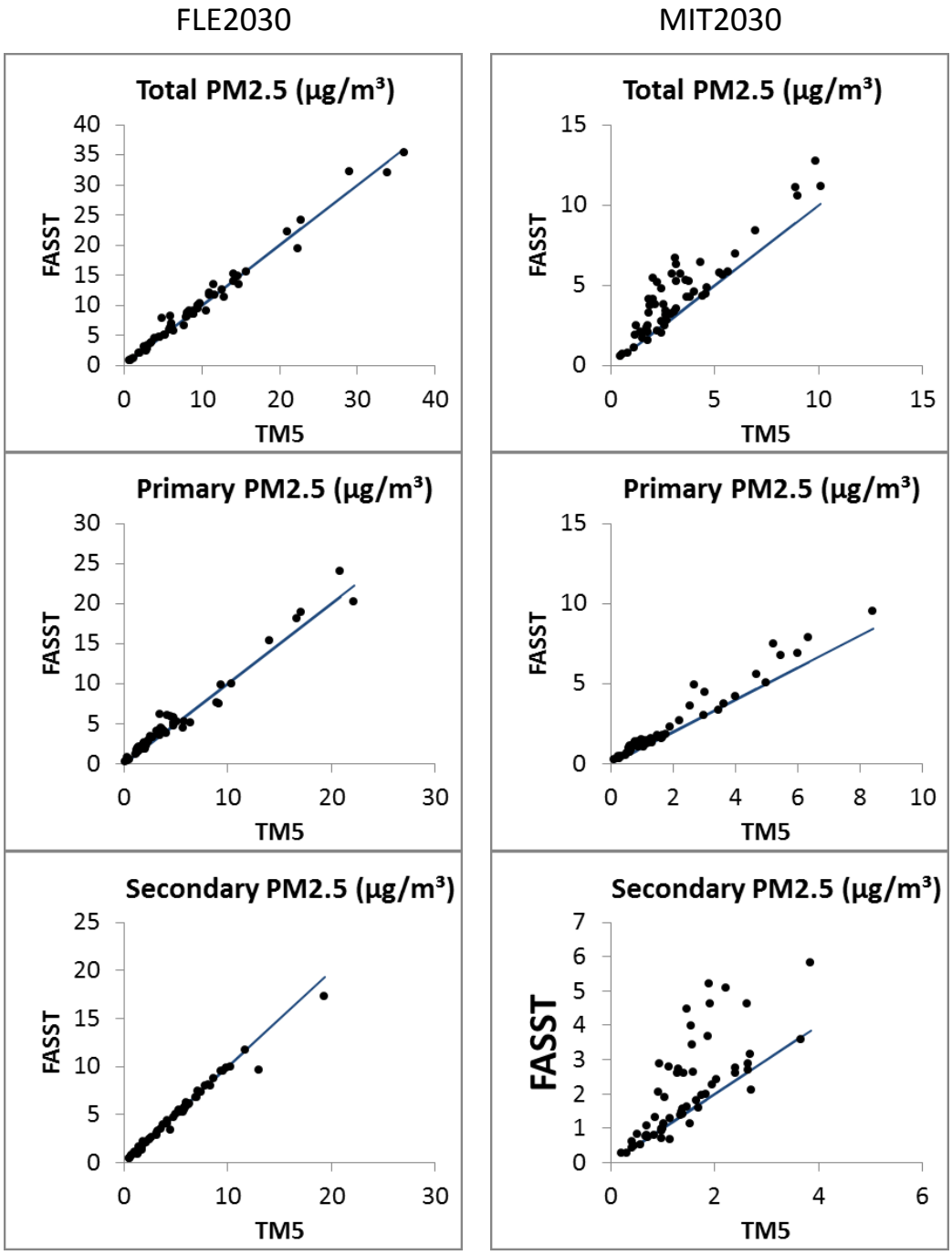

Figure S8.1 TM5-FASST vs. TM5_CTM anthropogenic $PM_{2.5}$ for GEA scenarios FLE2030 (left hand panels) and MIT-2030 (right hand panels), and break-down for the primary (middle panels) and secondary (lower panels) fractions. Each point represents the population-weighted mean over a FASST source region. The full line represents the 1:1 relation.

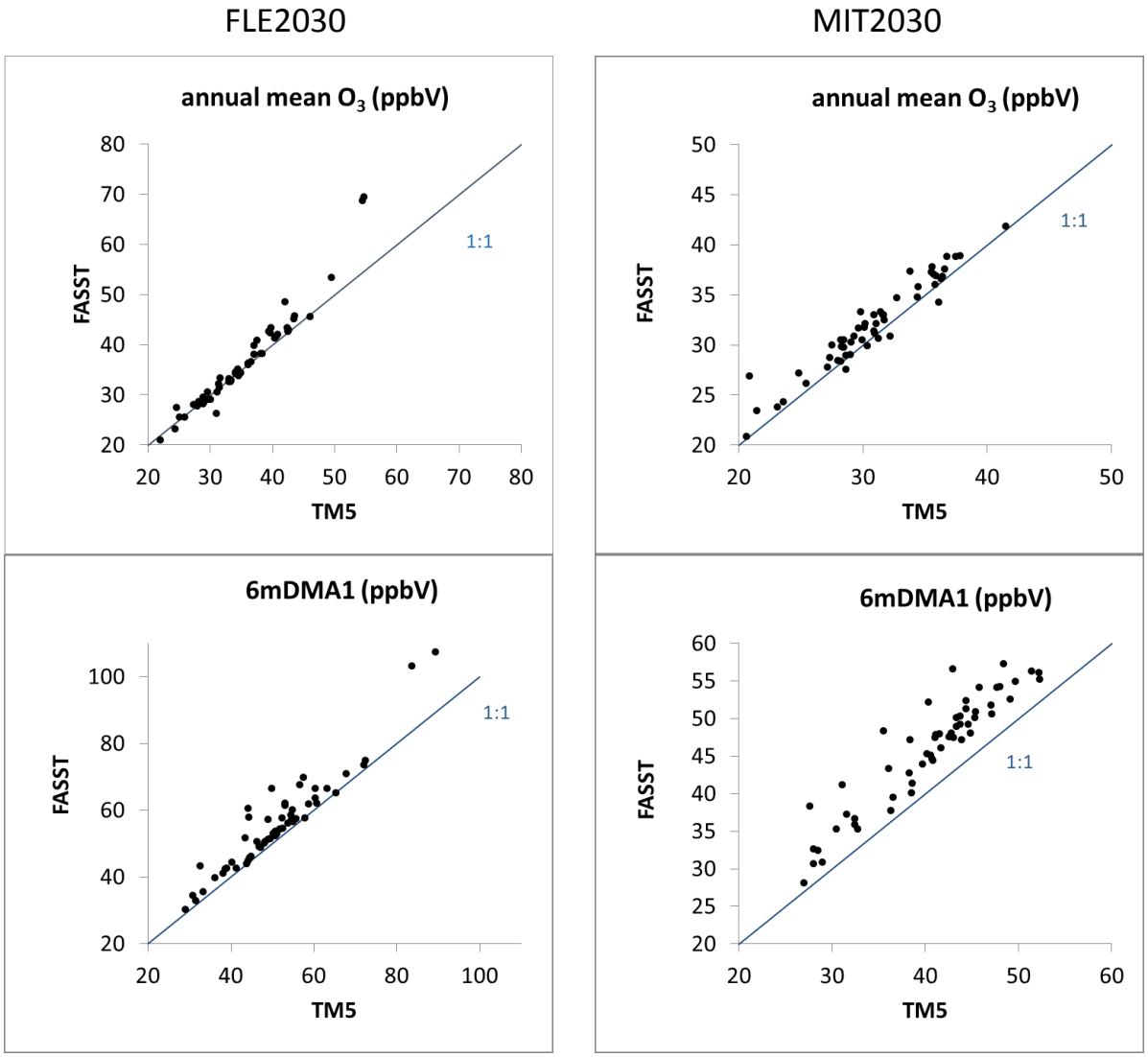

Figure S8.2 TM5-FASST versus TM5-CTM annual mean ozone (upper panels) and exposure metric 6mDMA1 (lower panels) for GEA scenarios FLE2030 (left hand panels) and MIT-2030 (right hand panels). Each point represents the population-weighted mean over a FASST source region. The full line represents the 1:1 relation

S9 Supplemental figures to section 3.3.5 - Health impacts in future scenarios: intercomparison with ACCMIP model ensemble

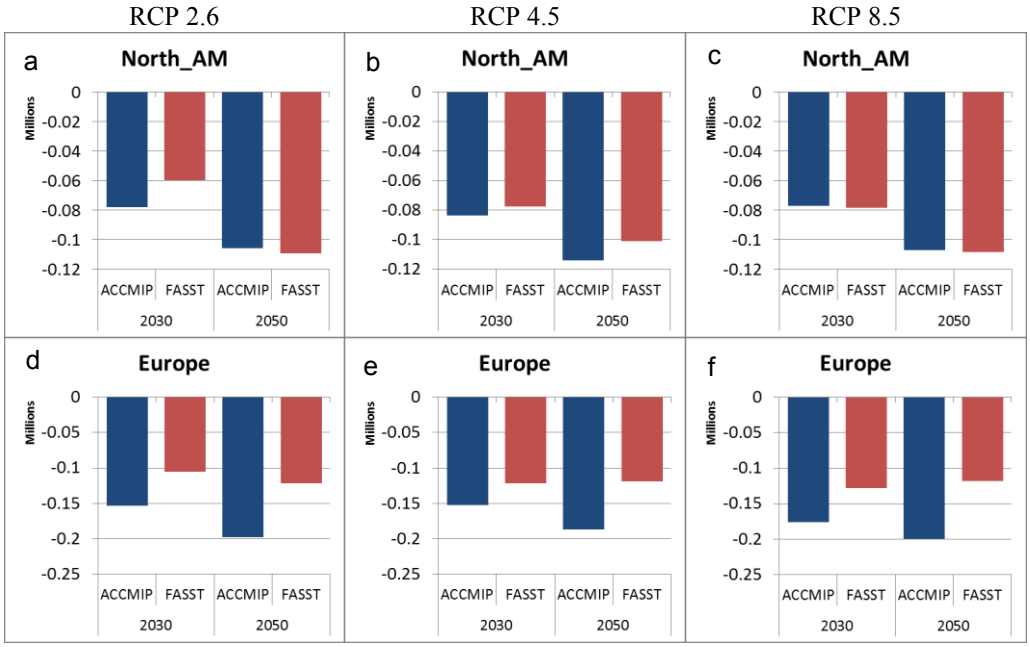

Figure S9.1: Mortality burden (million deaths) from $PM_{2.5}$ in 2030 and 2050 for RCP scenarios RCP 2.6 (a, d). RCP 4.5 (b, e) and RCP8.5 (c, f) relative to exposure to year 2000 concentrations, for North America (a to c) Europe and Europe (d to f). Blue bars: Mean of ACCMIP model ensemble results (Silva et al., 2016). Red bars: TM5-FASST.

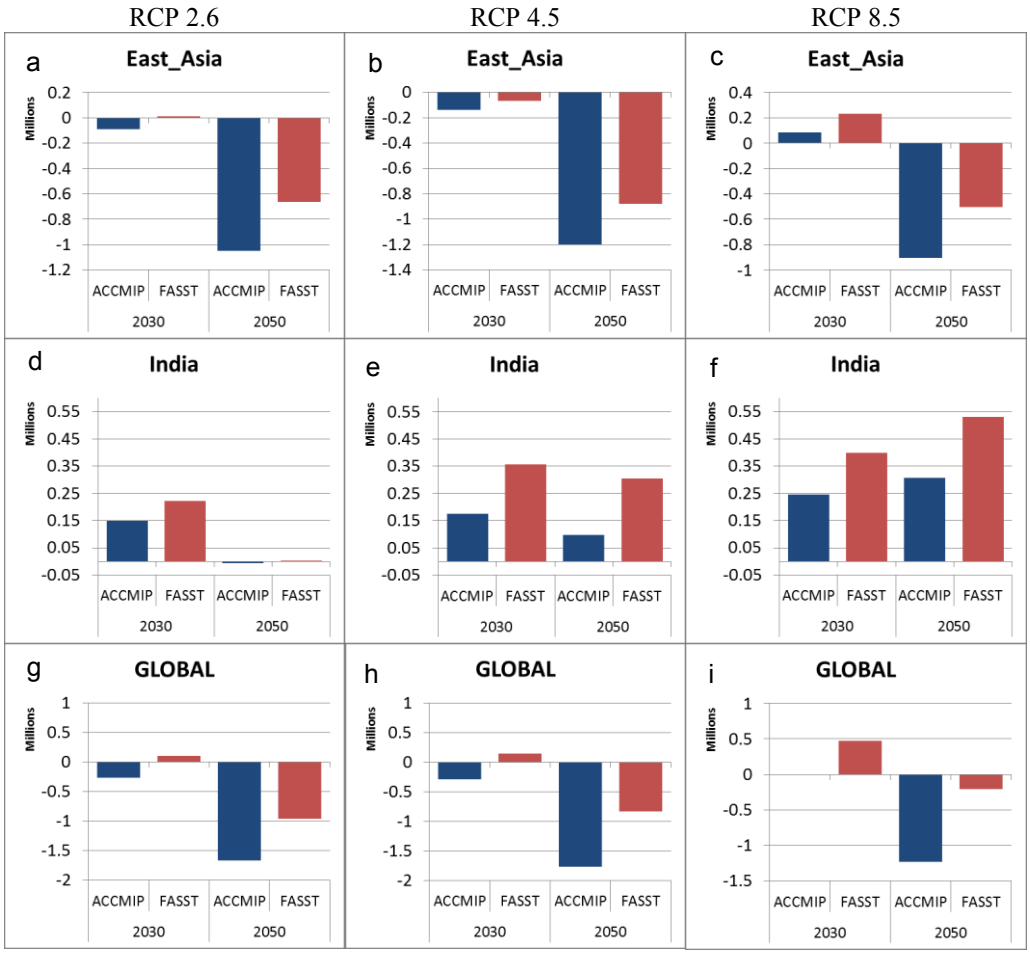

Figure S9.2: As in Fig. S9.1, now for regions East Asia (a to c), India (d to f) and the globe (g to i)

Supplemental Information - References

Amann, M., Bertok, I., Borken-Kleefeld, J., Cofala, J., Heyes, C., Höglund-Isaksson, L., Klimont, Z., Nguyen, B., Posch, M., Rafaj, P., Sandler, R., Schöpp, W., Wagner, F. and Winiwarter, W.: Cost-effective control of air quality and greenhouse gases in Europe: Modeling and policy applications, Environ. Model. Softw., 26(12), 1489–1501, doi:10.1016/j.envsoft.2011.07.012, 2011.

Andersson, C., Langner, J. and Bergström, R.: Interannual variation and trends in air pollution over Europe due to climate variability during 1958–2001 simulated with a regional CTM coupled to the ERA40 reanalysis, Tellus B, 59(1), 77–98, doi:10.1111/j.1600-0889.2006.00196.x, 2007.

Bergamaschi, P., Krol, M., Dentener, F., Vermeulen, A., Meinhardt, F., Graul, R., Ramonet, M., Peters, W. and Dlugokencky, E. J.: Inverse modelling of national and European CH4 emissions using the atmospheric zoom model TM5, Atmospheric Chem. Phys., 5(9), 2431–2460, 2005.

Brauer, M., Amann, M., Burnett, R. T., Cohen, A., Dentener, F., Ezzati, M., Henderson, S. B., Krzyzanowski, M., Martin, R. V., Van Dingenen, R., Van Donkelaar, A. and Thurston, G. D.: Exposure assessment for estimation of the global burden of disease attributable to outdoor air pollution, Environ. Sci. Technol., 46(2), 652–660, doi:10.1021/es2025752, 2012.

Brauer, M., Freedman, G., Frostad, J., Van, D., Martin, R. V., Dentener, F., Dingenen, R. V., Estep, K., Amini, H., Apte, J. S., Balakrishnan, K., Barregard, L., Broday, D., Feigin, V., Ghosh, S., Hopke, P. K., Knibbs, L. D., Kokubo, Y., Liu, Y., Ma, S., Morawska, L., Sangrador, J. L. T., Shaddick, G., Anderson, H. R., Vos, T., Forouzanfar, M. H., Burnett, R. T. and Cohen, A.: Ambient Air Pollution Exposure Estimation for the Global Burden of Disease 2013, Environ. Sci. Technol., 50(1), 79–88, doi:10.1021/acs.est.5b03709, 2016.

Burnett, R. T., Pope, C. A., III, Ezzati, M., Olives, C., Lim, S. S., Mehta, S., Shin, H. H., Singh, G., Hubbell, B., Brauer, M., Anderson, H. R., Smith, K. R., Balmes, J. R., Bruce, N. G., Kan, H., Laden, F., Prüss-Ustün, A., Turner, M. C., Gapstur, S. M., Diver, W. R. and Cohen, A.: An Integrated Risk Function for Estimating the Global Burden of Disease Attributable to Ambient Fine Particulate Matter Exposure, Environ. Health Perspect., doi:10.1289/ehp.1307049, 2014.

CIESIN: Gridded Population of the World Version 3 (GPWv3), [online] Available from: http://sedac.ciesin.columbia.edu/gpw (Accessed 12 September 2012), 2005.

Cohen, A. J., Brauer, M., Burnett, R., Anderson, H. R., Frostad, J., Estep, K., Balakrishnan, K., Brunekreef, B., Dandona, L., Dandona, R., Feigin, V., Freedman, G., Hubbell, B., Jobling, A., Kan, H., Knibbs, L., Liu, Y., Martin, R., Morawska, L., Pope, C. A., III, Shin, H., Straif, K., Shaddick, G., Thomas, M., van Dingenen, R., van Donkelaar, A., Vos, T., Murray, C. J. L. and Forouzanfar, M. H.: Estimates and 25-year trends of the global burden of disease attributable to ambient air pollution: an analysis of data from the Global Burden of Diseases Study 2015, The Lancet, 389(10082), 1907–1918, doi:10.1016/S0140-6736(17)30505-6, 2017.

Colette, A., Granier, C., Hodnebrog, ø., Jakobs, H., Maurizi, A., Nyiri, A., Rao, S., Amann, M., Bessagnet, B., D'Angiola, A., Gauss, M., Heyes, C., Klimont, Z., Meleux, F., Memmesheimer, M., Mieville, A., Rouïl, L., Russo, F., Schucht, S., Simpson, D., Stordal, F., Tampieri, F. and Vrac, M.: Future air quality in Europe: A multi-model assessment of projected exposure to ozone, Atmospheric Chem. Phys., 12(21), 10613–10630, doi:10.5194/acp-12-10613-2012, 2012.

Colette, A., Bessagnet, B., Vautard, R., Szopa, S., Rao, S., Schucht, S., Klimont, Z., Menut, L., Clain, G., Meleux, F., Curci, G. and Rouïl, L.: European atmosphere in 2050, a regional air quality and climate perspective under CMIP5 scenarios, Atmospheric Chem. Phys., 13(15), 7451–7471, doi:10.5194/acp-13-7451-2013, 2013.

Crippa, M., Janssens-Maenhout, G., Dentener, F., Guizzardi, D., Sindelarova, K., Muntean, M., Van Dingenen, R. and Granier, C.: Forty years of improvements in European air quality: Regional policy-industry interactions with global impacts, Atmospheric Chem. Phys., 16(6), 3825–3841, doi:10.5194/acp-16-3825-2016, 2016.

Dana, M. T. and Hales, J. M.: Statistical aspects of the washout of polydisperse aerosols, Atmospheric Environ. 1967, 10(1), 45–50, 1976.

De Meij, A., Krol, M., Dentener, F., Vignati, E., Cuvelier, C. and Thunis, P.: The sensitivity of aerosol in Europe to two different emission inventories and temporal distribution of emissions, Atmospheric Chem. Phys., 6(12), 4287–4309, 2006.

Dentener, F., Drevet, J., Lamarque, J. F., Bey, I., Eickhout, B., Fiore, A. M., Hauglustaine, D., Horowitz, L. W., Krol, M., Kulshrestha, U. C., Lawrence, M., Galy-Lacaux, C., Rast, S., Shindell, D., Stevenson, D., Van Noije, T., Atherton, C., Bell, N., Bergman, D., Butler, T., Cofala, J., Collins, B., Doherty, R., Ellingsen, K., Galloway, J., Gauss, M., Montanaro, V., Müller, J. F., Pitari, G., Rodriguez, J., Sanderson, M., Solmon, F., Strahan, S., Schultz, M., Sudo, K., Szopa, S. and Wild, O.: Nitrogen and sulfur deposition on regional and global scales: A multimodel evaluation, Glob. Biogeochem. Cycles, 20(4), GB4003, doi:10.1029/2005GB002672, 2006.

Dentener, F., Keating, T., Akimoto, H., Pirrone, N., Dutchak, S., Zuber, A., Convention on Long-range Transboundary Air Pollution, United Nations and UNECE Task Force on Emission Inventories and Projections, Eds.: Hemispheric transport of air pollution 2010: prepared by the Task Force on Hemispheric Transport of Air Pollution acting within the framework of the Convention on Long-range Transboundary Air Pollution, United Nations, New York ; Geneva., 2010.

van Donkelaar, A., Martin, R. V., Brauer, M., Hsu, N. C., Kahn, R. A., Levy, R. C., Lyapustin, A., Sayer, A. M. and Winker, D. M.: Global Estimates of Fine Particulate Matter using a Combined Geophysical-Statistical Method with Information from Satellites, Models, and Monitors, Environ. Sci. Technol., 50(7), 3762–3772, doi:10.1021/acs.est.5b05833, 2016.

Fenech, S., Doherty, R. M., Heaviside, C., Vardoulakis, S., Macintyre, H. L. and O'Connor, F. M.: The influence of model spatial resolution on simulated ozone and fine particulate matter for Europe: implications for health impact assessments, Atmospheric Chem. Phys., 18(8), 5765–5784, doi:10.5194/acp-18-5765-2018, 2018.

Fenn, R. W., Clough, S. A., Gallery, W. O., Good, R. E., Kneizys, F. X., Mill, J. D., Rothman, L. S., Shettle, E. P. and Volz, F. E.: Optical and infrared properties of the atmosphere, in Handbook of Geophysics and the Space Environment, vol. 18, pp. 1–27, Air Force Geophys. Lab., Hanscom Air Force Base, Bedford, Mass., 1985.

Fiore, A. M., Jacob, D. J., Field, B. D., Streets, D. G., Fernandes, S. D. and Jang, C.: Linking ozone pollution and climate change: The case for controlling methane, Geophys. Res. Lett., 29(19), 25–1, 2002.

Fiore, A. M., West, J. J., Horowitz, L. W., Naik, V. and Schwarzkopf, M. D.: Characterizing the tropospheric ozone response to methane emission controls and the benefits to climate and air quality, J. Geophys. Res. Atmospheres, 113(8), doi:10.1029/2007JD009162, 2008.

Fiore, A. M., Dentener, F. J., Wild, O., Cuvelier, C., Schultz, M. G., Hess, P., Textor, C., Schulz, M., Doherty, R. M., Horowitz, L. W., MacKenzie, I. A., Sanderson, M. G., Shindell, D. T., Stevenson, D. S., Szopa, S., Van Dingenen, R., Zeng, G., Atherton, C., Bergmann, D., Bey, I., Carmichael, G., Collins, W. J., Duncan, B. N., Faluvegi, G., Folberth, G., Gauss, M., Gong, S., Hauglustaine, D., Holloway, T., Isaksen, I. S. A., Jacob, D. J., Jonson, J. E., Kaminski, J. W., Keating, T. J., Lupu, A., Marmer, E., Montanaro, V., Park, R. J., Pitari, G., Pringle, K. J., Pyle, J. A., Schroeder, S., Vivanco, M. G., Wind, P., Wojcik, G., Wu, S. and Zuber, A.: Multimodel estimates of intercontinental source-receptor relationships for ozone pollution, J. Geophys. Res. Atmospheres, 114(D4), doi:10.1029/2008JD010816, 2009.

Forouzanfar, M. H., Afshin, A., Alexander, L. T., Biryukov, S., Brauer, M., Cercy, K., Charlson, F. J., Cohen, A. J., Dandona, L., Estep, K., Ferrari, A. J., Frostad, J. J., Fullman, N., Godwin, W. W., Griswold, M., Hay, S. I., Kyu, H. H., Larson, H. J., Lim, S. S., Liu, P. Y., Lopez, A. D., Lozano, R., Marczak, L., Mokdad, A. H., Moradi-Lakeh, M., Naghavi, M., Reitsma, M. B., Roth, G. A., Sur, P. J., Vos, T., Wagner, J. A., Wang, H., Zhao, Y., Zhou, M., Barber, R. M., Bell, B., Blore, J. D., Casey, D. C., Coates, M. M., Cooperrider, K., Cornaby, L., Dicker, D., Erskine, H. E., Fleming, T., Foreman, K., Gakidou, E., Haagsma, J. A., Johnson, C. O., Kemmer, L., Ku, T., Leung, J., Masiye, F., Millear, A., Mirarefin, M., Misganaw, A., Mullany, E., Mumford, J. E., Ng, M., Olsen, H., Rao, P., Reinig, N., Roman, Y., Sandar, L., Santomauro, D. F., Slepak, E. L., Sorensen, R. J. D., Thomas, B. A., Vollset, S. E., Whiteford, H. A., Zipkin, B., Murray, C. J. L., Mock, C. N., Anderson, B. O., Futran, N. D., Anderson, H. R., Bhutta, Z. A., Nisar, M. I., Akseer, N., Krueger, H., Gotay, C. C., Kissoon, N., Kopec, J. A., Pourmalek, F., Burnett, R., Abajobir, A. A., Knibbs, L. D., Veerman, J. L., Lalloo, R., Scott, J. G., Alam, N. K. M., Gouda, H. N., Guo, Y., McGrath, J. J., Charlson, F. J., Erskine, H. E., Jeemon, P., Dandona, R., Goenka, S., Kumar, G. A., et al.: Global, regional, and national comparative risk assessment of

79 behavioural, environmental and occupational, and metabolic risks or clusters of risks, 1990–2015: a systematic analysis for the Global Burden of Disease Study 2015, The Lancet, 388(10053), 1659–1724, doi:10.1016/S0140-6736(16)31679-8, 2016.

Fry, M. M., Naik, V., West, J. J., Schwarzkopf, M. D., Fiore, A. M., Collins, W. J., Dentener, F. J., Shindell, D. T., Atherton, C., Bergmann, D., Duncan, B. N., Hess, P., MacKenzie, I. A., Marmer, E., Schultz, M. G., Szopa, S., Wild, O. and Zeng, G.: The influence of ozone precursor emissions from four world regions on tropospheric composition and radiative climate forcing, J. Geophys. Res. Atmospheres, 117(7), doi:10.1029/2011JD017134, 2012.

Ganzeveld, L. and Lelieveld, J.: Dry deposition parameterization in a chemistry general circulation model and its influence on the distribution of reactive trace gases, J. Geophys. Res., 100(D10), 20,999-21,012, 1995.

GEA: Global Energy Assessment - Toward a Sustainable Future, Cambridge University Press, Cambridge, UK and New York, NY, USA and the International Institute for Applied Systems Analysis, Laxenburg, Austria. [online] Available from: www.globalenergyassessment.org, 2012.

Gery, M. W., Whitten, G. Z., Killus, J. P. and Dodge, M. C.: A photochemical kinetics mechanism for urban and regional scale computer modeling, J. Geophys. Res., 94(D10), 12,925-12,956, 1989a.

Gery, M. W., Edmond, R. D. and Whitten, G. Z.: Potential effects of stratospheric ozone depletion and global temperature rise on urban photochemistry, Stud. Environ. Sci., 35(C), 365–375, doi:10.1016/S0166-1116(08)70604-6, 1989b.

Guelle, W., Balkanski, Y. J., Dibb, J. E., Schulz, M. and Dulac, F.: Wet deposition in a global size-dependent aerosol transport model 2. Influence of the scavenging scheme on 210Pb vertical profiles, surface concentrations, and deposition, J. Geophys. Res. Atmospheres, 103(D22), 28875–28891, 1998.

Hertel, O., Berkowicz, R., Christensen, J. and Hov, Ø.: Test of two numerical schemes for use in atmospheric transport-chemistry models, Atmospheric Environ. Part Gen. Top., 27(16), 2591–2611, doi:10.1016/0960-1686(93)90032-T, 1993.

Hoek, G., Krishnan, R. M., Beelen, R., Peters, A., Ostro, B., Brunekreef, B. and Kaufman, J. D.: Long-term air pollution exposure and cardio- respiratory mortality: a review, Environ. Health, 12, 43, doi:10.1186/1476-069X-12-43, 2013.

Houweling, S., Dentener, F. and Lelieveld, J.: The impact of nonmethane hydrocarbon compounds on tropospheric photochemistry, J. Geophys. Res. Atmospheres, 103(3339), 10673–10696, 1998.

Huijnen, V., Williams, J., van Weele, M., van Noije, T., Krol, M., Dentener, F., Segers, A., Houweling, S., Peters, W., de Laat, J., Boersma, F., Bergamaschi, P., van Velthoven, P., Le Sager, P., Eskes, H., Alkemade, F., Scheele, R., Nédélec, P. and Pätz, H.-W.: The global chemistry transport model TM5: description and evaluation of the tropospheric chemistry version 3.0, Geosci. Model Dev., 3(2), 445–473, doi:10.5194/gmd-3-445-2010, 2010.

IHME: Global Burden of Disease Study 2010 (GBD 2010) - Ambient Air Pollution Risk Model 1990 - 2010 | GHDx, [online] Available from: http://ghdx.healthdata.org/record/global-burden-disease-study-2010-gbd-2010-ambient-air-pollution-risk-model-1990-2010 (Accessed 8 November 2016), 2011.

Jerrett, M., Burnett, R. T., Arden, P. I., Ito, K., Thurston, G., Krewski, D., Shi, Y., Calle, E. and Thun, M.: Long-term ozone exposure and mortality, N. Engl. J. Med., 360(11), 1085–1095, doi:10.1056/NEJMoa0803894, 2009.

Jeuken, A., Veefkind, J. P., Dentener, F., Metzger, S. and Robles, G.: Simulation of the aerosol optical depth over Europe for August 1997 and a comparison with observations, J. Geophys. Res. Atmospheres, 106(D22), 28295–28311, 2001.

Kirschke, S., Bousquet, P., Ciais, P., Saunois, M., Canadell, J. G., Dlugokencky, E. J., Bergamaschi, P., Bergmann, D., Blake, D. R., Bruhwiler, L., Cameron-Smith, P., Castaldi, S., Chevallier, F., Feng, L., Fraser, A., Heimann, M., Hodson, E. L., Houweling, S., Josse, B., Fraser, P. J., Krummel, P. B., Lamarque, J.-F.,

Langenfelds, R. L., Le Quéré, C., Naik, V., O'Doherty, S., Palmer, P. I., Pison, I., Plummer, D., Poulter, B., Prinn, R. G., Rigby, M., Ringeval, B., Santini, M., Schmidt, M., Shindell, D. T., Simpson, I. J., Spahni, R., Steele, L. P., Strode, S. A., Sudo, K., Szopa, S., van der Werf, G. R., Voulgarakis, A., van Weele, M., Weiss, R. F., Williams, J. E. and Zeng, G.: Three decades of global methane sources and sinks, Nat. Geosci., 6(10), 813–823, doi:10.1038/ngeo1955, 2013.

Kitous, A., Keramidas, K., Vandyck, T., Saveyn, B., Van Dingenen, R., Spadaro, J. and Holland, M.: Global Energy and Climate Outlook 2017: How climate policies improve air quality, Joint Research Centre, Luxembourg: Publications Office of the European Union., 2017.

Krewski, D., Jerrett, M., Burnett, R. T., Ma, R., Hughes, E. and Shi, Y.: Extended Follow-Up and Spatial Analysis of the American Cancer Society Study Linking Particulate Air Pollution and Mortality., Research Report, Health Effects Institute, Boston., 2009.

Krol, M., Houweling, S., Bregman, B., van den Broek, M., Segers, A., van Velthoven, P., Peters, W., Dentener, F. and Bergamaschi, P.: The two-way nested global chemistry-transport zoom model TM5: algorithm and applications, Atmos Chem Phys, 5(2), 417–432, doi:10.5194/acp-5-417-2005, 2005.

Kuylenstierna, J. C. I., Zucca, M. C., Amann, M., Cardenas, B., Chambers, B., Klimont, Z., Hicks, K., Mills, R., Molina, L., Murray, F., Pearson, P., Sethi, S., Shindell, D., Sokona, Y., Terry, S., Vallack, H., Van Dingenen, R., Williams, M., Wilson, C. and Zusman, E.: Near-term climate protection and clean air benefits: Actions for controlling short-lived climate forcers, Report, United Nations Environment Programme, Nairobi, Kenya. [online] Available from: http://researchrepository.murdoch.edu.au/id/eprint/15325/ (Accessed 10 January 2017), 2011.

Lamarque, J., Bond, T., Eyring, V., Granier, C., Heil, A., Klimont, Z., Lee, D., Liousse, C., Mieville, A., Owen, B., Schultz, M., Shindell, D., Smith, S., Stehfest, E., Van Aardenne, J., Cooper, O., Kainuma, M., Mahowald, N., McConnell, J., Naik, V., Riahi, K. and van Vuuren, D.: Historical (1850-2000) gridded anthropogenic and biomass burning emissions of reactive gases and aerosols: methodology and application, Atmospheric Chem. Phys., 10, 7017–7039, doi:10.5194/acp-10-7017-2010, 2010.

Li, J., Wong, J. G. D., Dobbie, J. S. and Chýlek, P.: Parameterization of the optical properties of sulfate aerosols, J. Atmospheric Sci., 58(2), 193–209, 2001.

Li, Y., Henze, D. K., Jack, D. and Kinney, P. L.: The influence of air quality model resolution on health impact assessment for fine particulate matter and its components, Air Qual. Atmosphere Health, 9(1), 51–68, doi:10.1007/s11869-015-0321-z, 2016.

Lim, S. S., Vos, T., Flaxman, A. D., Danaei, G., Shibuya, K., Adair-Rohani, H., Amann, M., Anderson, H. R., Andrews, K. G., Aryee, M., Atkinson, C., Bacchus, L. J., Bahalim, A. N., Balakrishnan, K., Balmes, J., Barker-Collo, S., Baxter, A., Bell, M. L., Blore, J. D., Blyth, F., Bonner, C., Borges, G., Bourne, R., Boussinesq, M., Brauer, M., Brooks, P., Bruce, N. G., Brunekreef, B., Bryan-Hancock, C., Bucello, C., Buchbinder, R., Bull, F., Burnett, R. T., Byers, T. E., Calabria, B., Carapetis, J., Carnahan, E., Chafe, Z., Charlson, F., Chen, H., Chen, J. S., Cheng, A. T.-A., Child, J. C., Cohen, A., Colson, K. E., Cowie, B. C., Darby, S., Darling, S., Davis, A., Degenhardt, L., Dentener, F., Des Jarlais, D. C., Devries, K., Dherani, M., Ding, E. L., Dorsey, E. R., Driscoll, T., Edmond, K., Ali, S. E., Engell, R. E., Erwin, P. J., Fahimi, S., Falder, G., Farzadfar, F., Ferrari, A., Finucane, M. M., Flaxman, S., Fowkes, F. G. R., Freedman, G., Freeman, M. K., Gakidou, E., Ghosh, S., Giovannucci, E., Gmel, G., Graham, K., Grainger, R., Grant, B., Gunnell, D., Gutierrez, H. R., Hall, W., Hoek, H. W., Hogan, A., Hosgood III, H. D., Hoy, D., Hu, H., Hubbell, B. J., Hutchings, S. J., Ibeanusi, S. E., Jacklyn, G. L., Jasrasaria, R., Jonas, J. B., Kan, H., Kanis, J. A., Kassebaum, N., Kawakami, N., Khang, Y.-H., Khatibzadeh, S., Khoo, J.-P., Kok, C., et al.: A comparative risk assessment of burden of disease and injury attributable to 67 risk factors and risk factor clusters in 21 regions, 1990-2010: A systematic analysis for the Global Burden of Disease Study 2010, The Lancet, 380(9859), 2224–2260, doi:10.1016/S0140-6736(12)61766-8, 2012.

Lund Myhre, C. E. and Nielsen, C. J.: Optical properties in the UV and visible spectral region of organic acids relevant to tropospheric aerosols, Atmos Chem Phys, 4(7), 1759–1769, doi:10.5194/acp-4-1759-2004, 2004.

Malley, C. S., Henze, D. K., Kuylenstierna, J. C. I., Vallack, H., Davila, Y., Anenberg, S. C., Turner, M. C. and Ashmore, M.: Updated Global Estimates of Respiratory Mortality in Adults ≥30Years of Age Attributable to Long-Term Ozone Exposure., Environ. Health Perspect., 125(8), 087021, doi:10.1289/EHP1390, 2017.

Nemesure, S., Wagener, R. and Schwartz, S. E.: Direct shortwave forcing of climate by the anthropogenic sulfate aerosol: Sensitivity to particle size, composition, and relative humidity, J. Geophys. Res. Atmospheres, 100(D12), 26105–26116, doi:10.1029/95JD02897, 1995.

van Noije, T. P. C., Eskes, H. J., Dentener, F. J., Stevenson, D. S., Ellingsen, K., Schultz, M. G., Wild, O., Amann, M., Atherton, C. S., Bergmann, D. J., Bey, I., Boersma, K. F., Butler, T., Cofala, J., Drevet, J., Fiore, A. M., Gauss, M., Hauglustaine, D. A., Horowitz, L. W., Isaksen, I. S. A., Krol, M. C., Lamarque, J.-F., Lawrence, M. G., Martin, R. V., Montanaro, V., Müller, J.-F., Pitari, G., Prather, M. J., Pyle, J. A., Richter, A., Rodriguez, J. M., Savage, N. H., Strahan, S. E., Sudo, K., Szopa, S. and van Roozendael, M.: Multi-model ensemble simulations of tropospheric NO2 compared with GOME retrievals for the year 2000, Atmos Chem Phys, 6(10), 2943–2979, doi:10.5194/acp-6-2943-2006, 2006.

OECD: The Economic Consequences of Outdoor Air Pollution, OECD Publishing. [online] Available from: http://www.oecd-ilibrary.org/environment/the-economic-consequences-of-outdoor-air-pollution_9789264257474-en (Accessed 10 January 2017), 2016.

Penner, J. E., Chuang, C. C. and Grant, K.: Climate forcing by carbonaceous and sulfate aerosols, Clim. Dyn., 14(12), 839–851, doi:10.1007/s003820050259, 1998.

Peters, W.: Toward regional-scale modeling using the two-way nested global model TM5: Characterization of transport using SF $_6$, J. Geophys. Res., 109(D19), doi:10.1029/2004JD005020, 2004.

Petersen, A. C., Spee, E. J., Van, D. and Hundsdorfer, W.: An evaluation and intercomparison of four new advection schemes for use in global chemistry models, J. Geophys. Res. Atmospheres, 103(D15), 19253–19269, 1998.

Pope, C. A., III, Burnett, R. T., Thun, M. J., Calle, E. E., Krewski, D., Ito, K. and Thurston, G. D.: Lung Cancer, Cardiopulmonary Mortality, and Long-term Exposure to Fine Particulate Air Pollution, JAMA, 287(9), 1132–1141, doi:10.1001/jama.287.9.1132, 2002.

Prather, M., Ehhalt, D., Dentener, F., Derwent, R., Dlugokencky, E., Holland, E., Isaksen, I., Katima, J., Kirchhoff, V., Matson, P., Midgley, P., Wang, M., Berntsen, T., Bey, I., Brasseur, G., Buja, L., Pitari, G. and Et, A.: Chapter 4: Atmospheric Chemistry and Greenhouse Gases, Cambridge University Press. [online] Available from: https://ricerca.univaq.it/handle/11697/24359#.WItxbn0XGao (Accessed 27 January 2017), 2001.

Punger, E. M. and West, J. J.: The effect of grid resolution on estimates of the burden of ozone and fine particulate matter on premature mortality in the United States, Air Qual. Atmosphere Health, 6(3), doi:10.1007/s11869-013-0197-8, 2013.

Rao, S., Chirkov, V., Dentener, F., Van Dingenen, R., Pachauri, S., Purohit, P., Amann, M., Heyes, C., Kinney, P., Kolp, P., Klimont, Z., Riahi, K. and Schoepp, W.: Environmental Modeling and Methods for Estimation of the Global Health Impacts of Air Pollution, Environ. Model. Assess., 17(6), 613–622, doi:10.1007/s10666-012-9317-3, 2012.

Rao, S., Pachauri, S., Dentener, F., Kinney, P., Klimont, Z., Riahi, K. and Schoepp, W.: Better air for better health: Forging synergies in policies for energy access, climate change and air pollution, Glob. Environ. Change, 23(5), 1122–1130, doi:10.1016/j.gloenvcha.2013.05.003, 2013.

Rao, S., Klimont, Z., Leitao, J., Riahi, K., Van Dingenen, R., Reis, L. A., Katherine Calvin, Dentener, F., Drouet, L., Fujimori, S., Harmsen, M., Luderer, G., Chris Heyes, Strefler, J., Tavoni, M. and Vuuren, D. P. van: A multi-model assessment of the co-benefits of climate mitigation for global air quality, Environ. Res. Lett., 11(12), 124013, doi:10.1088/1748-9326/11/12/124013, 2016.

Rao, S., Klimont, Z., Smith, S. J., Van Dingenen, R., Dentener, F., Bouwman, L., Riahi, K., Amann, M., Bodirsky, B. L., van Vuuren, D. P., Aleluia Reis, L., Calvin, K., Drouet, L., Fricko, O., Fujimori, S., Gernaat, D., Havlik, P., Harmsen, M., Hasegawa, T., Heyes, C., Hilaire, J., Luderer, G., Masui, T., Stehfest, E., Strefler, J., van der Sluis, S. and Tavoni, M.: Future air pollution in the Shared Socio-economic Pathways, Glob. Environ. Change, 42, 346–358, doi:10.1016/j.gloenvcha.2016.05.012, 2017.

Riahi, K., Dentener, F., Gielen, D., Grubler, A., Jewell, J., Klimont, Z., Krey, V., McCollum, D., Pachauri, S., Rao, S., van Ruijven, B., van Vuuren, D. P. and Wilson, C.: The Global Energy Assessment - Chapter 17 - Energy Pathways for Sustainable Development, in Global Energy Assessment - Toward a Sustainable Future, pp. 1203–1306, Cambridge University Press, Cambridge, UK and New York, NY, USA and the International Institute for Applied Systems Analysis, Laxenburg, Austria. [online] Available from: www.globalenergyassessment.org, 2012.

Russell, G. L. and Lerner, J. A.: A New Finite-Differencing Scheme for the Tracer Transport Equation, J. Appl. Meteorol., 20(12), 1483–1498, doi:10.1175/1520-0450(1981)020<1483:ANFDSF>2.0.CO;2, 1981.

Shindell, D. T., Chin, M., Dentener, F., Doherty, R. M., Faluvegi, G., Fiore, A. M., Hess, P., Koch, D. M., MacKenzie, I. A., Sanderson, M. G., Schultz, M. G., Schulz, M., Stevenson, D. S., Teich, H., Textor, C., Wild, O., Bergmann, D. J., Bey, I., Bian, H., Cuvelier, C., Duncan, B. N., Folberth, G., Horowitz, L. W., Jonson, J., Kaminski, J. W., Marmer, E., Park, R., Pringle, K. J., Schroeder, S., Szopa, S., Takemura, T., Zeng, G., Keating, T. J. and Zuber, A.: A multi-model assessment of pollution transport to the Arctic, Atmos Chem Phys, 8(17), 5353–5372, doi:10.5194/acp-8-5353-2008, 2008.

Silva, R. A., West, J. J., Lamarque, J. F., Shindell, D. T., Collins, W. J., Dalsoren, S., Faluvegi, G., Folberth, G., Horowitz, L. W., Nagashima, T., Naik, V., Rumbold, S. T., Sudo, K., Takemura, T., Bergmann, D., Cameron-Smith, P., Cionni, I., Doherty, R. M., Eyring, V., Josse, B., MacKenzie, I. A., Plummer, D., Righi, M., Stevenson, D. S., Strode, S., Szopa, S. and Zengast, G.: The effect of future ambient air pollution on human premature mortality to 2100 using output from the ACCMIP model ensemble, Atmospheric Chem. Phys., 16(15), 9847–9862, doi:10.5194/acp-16-9847-2016, 2016.

Sloane, C. S.: Optical properties of aerosols—comparison of measurements with model calculations, Atmospheric Environ. 1967, 17(2), 409–416, doi:10.1016/0004-6981(83)90059-8, 1983.

Textor, C., Schulz, M., Guibert, S., Kinne, S., Balkanski, Y., Bauer, S., Berntsen, T., Berglen, T., Boucher, O., Chin, M., Dentener, F., Diehl, T., Easter, R., Feichter, H., Fillmore, D., Ghan, S., Ginoux, P., Gong, S., Grini, A., Hendricks, J., Horowitz, L., Huang, P., Isaksen, I., Iversen, I., Kloster, S., Koch, D., Kirkevåg, A., Kristjansson, J. E., Krol, M., Lauer, A., Lamarque, J. F., Liu, X., Montanaro, V., Myhre, G., Penner, J., Pitari, G., Reddy, S., Seland, Ø., Stier, P., Takemura, T. and Tie, X.: Analysis and quantification of the diversities of aerosol life cycles within AeroCom, Atmos Chem Phys, 6(7), 1777–1813, doi:10.5194/acp-6-1777-2006, 2006.

The World Bank, The International Cryosphere Climate Initiative: On Thin Ice, Washington DC. [online] Available from: http://iccinet.org/thinicepubfinal, 2013.

Toon, O. B., Pollack, J. B. and Khare, B. N.: The optical constants of several atmospheric aerosol species: Ammonium sulfate, aluminum oxide, and sodium chloride, J. Geophys. Res., 81(33), 5733–5748, doi:10.1029/JC081i033p05733, 1976.

Turner, M. C., Jerrett, M., Pope, C. A., Krewski, D., Gapstur, S. M., Diver, W. R., Beckerman, B. S., Marshall, J. D., Su, J., Crouse, D. L. and Burnett, R. T.: Long-Term Ozone Exposure and Mortality in a Large Prospective Study, Am. J. Respir. Crit. Care Med., 193(10), 1134–1142, doi:10.1164/rccm.201508-1633OC, 2016.

UN DESA: World Population Prospects: The 2008 Revision Database., Working Paper, United Nations Department of Economic and Social Affairs (UN DESA), New York., 2009.

UNEP and CCAC: Integrated Assessment of Short-Lived Climate Pollutants for Latin America and the Caribbean: improving air quality while mitigating climate change. Summary for decision makers., United Nations Environmenal Programme, Nairobi, Kenya. [online] Available from: http://www.ccacoalition.org/sites/default/files/resources/UNEP_Assessment%20A%20SINGLE.pdf (Accessed 14 December 2017), 2016.

Van Dingenen, R., Dentener, F. J., Raes, F., Krol, M. C., Emberson, L. and Cofala, J.: The global impact of ozone on agricultural crop yields under current and future air quality legislation, Atmos. Environ., 43(3), 604–618, doi:10.1016/j.atmosenv.2008.10.033, 2009.

Vignati, E., Karl, M., Krol, M., Wilson, J., Stier, P. and Cavalli, F.: Sources of uncertainties in modelling black carbon at the global scale, Atmospheric Chem. Phys., 10(6), 2595–2611, 2010.

Wehrli, C.: Solar Spectral Irradiance: Wehrli 1985 AM0 Spectrum, Wehrli 1985 AM0 Spectr. [online] Available from: http://rredc.nrel.gov/solar/spectra/am0/wehrli1985.new.html (Accessed 18 December 2017), 1985.

van der Werf, G. R., Randerson, J. T., Collatz, G. J., Louis Giglio, Kasibhatla, P. S., Arellano, A. F., Olsen, S. C. and Kasischke, E. S.: Continental-Scale Partitioning of Fire Emissions During the 1997 to 2001 El Niño/La Niña Period, Science, 303(5654), 73–76, doi:10.1126/science.1090753, 2004.

West, J. J., Fiore, A. M., Naik, V., Horowitz, L. W., Schwarzkopf, M. D. and Mauzerall, D. L.: Ozone air quality and radiative forcing consequences of changes in ozone precursor emissions, Geophys. Res. Lett., 34(6), doi:10.1029/2006GL029173, 2007.

WHO: Health risks of air pollution in Europe – HRAPIE project - Recommendations for concentration – response functions for cost – benefit analysis of particulate matter, ozone and nitrogen dioxide, WHO Regional Office for Europe, Copenhagen, Denmark. [online] Available from: http://www.euro.who.int/__data/assets/pdf_file/0006/238956/Health_risks_air_pollution_HRAPIE_project.pdf (Accessed 3 January 2018), 2013.

Wild, O. and Prather, M. J.: Excitation of the primary tropospheric chemical mode in a global three-dimensional model, J. Geophys. Res. Atmospheres, 105(D20), 24647–24660, 2000.

Wild, O. and Prather, M. J.: Global tropospheric ozone modeling: Quantifying errors due to grid resolution, J. Geophys. Res. Atmospheres, 111(D11), doi:10.1029/2005JD006605, 2006.

van Zelm, R., Preiss, P., van Goethem, T., Van Dingenen, R. and Huijbregts, M.: Regionalized life cycle impact assessment of air pollution on the global scale: Damage to human health and vegetation, Atmos. Environ., 134, 129–137, doi:10.1016/j.atmosenv.2016.03.044, 2016.